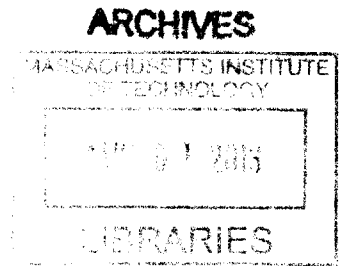# A Multi-dimensional Microfluidic Platform Recapitulating Chemotactic and Morphogenic Chemical Gradients

by:
Ovid C. Amadi

B.S. Mechanical Engineering
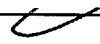Massachusetts Institute of Technology, 2007

SUBMITTED TO THE DIVISION OF HEALTH SCIENCES AND TECHNOLOGY IN
PARTIAL FULFILLMENT OF THE REQUIREMENTS FOR THE DEGREE OF

DOCTOR OF PHILOSOPHY IN MEDICAL ENGINEERING
AT THE
MASSACHUSETTS INSTITUTE OF TECHNOLOGY

JUNE 2013

©2013 Ovid C. Amadi. All rights reserved.

Signature of Author: _____
Division of Health Sciences and Technology
May 29, 2013

Certified by: _____
Richard T. Lee, MD
Professor of Medicine, Harvard Medical School
Thesis Supervisor

Accepted by: _____
Emery N. Brown, MD, PhD
Director, Harvard-MIT Program in Health Sciences and Technology
Professor of Computational Neuroscience and Health Sciences and Technology

Thesis Committee:

Richard T. Lee, MD - Supervisor
Professor of Medicine
Harvard Medical School
Director, Brigham Regenerative Medicine Center

Roger D. Kamm, PhD - Chair
Cecil and Ida Green Distinguished Professor of Biological and Mechanical
Engineering
Massachusetts Institute of Technology

Richard N. Mitchell, MD, PhD
Professor of Pathology and Health Sciences and Technology
Harvard Medical School

A Multi-dimensional Microfluidic Platform Recapitulating Chemotactic and Morphogenic Chemical Gradients

by:
Ovid C. Amadi

Submitted to the Division of Health Sciences and Technology on May 29, 2013
in partial fulfillment of the requirements for the degree of
Doctor of Philosophy in Medical Engineering

ABSTRACT

The requirement that individual cells be able to communicate with one another over a range of length scales is a fundamental prerequisite for the evolution of multi-cellular organisms. Often diffusible chemical molecules originate from a source and span the distance between cells in order to establish a line of communication - where the meaning of the signal is a function of both spatial and temporal chemical concentrations. In the case of chemotaxis, cells respond to concentration gradients to establish directionality. In the case of morphogenesis, cells respond to the magnitude of the local concentration field to regulate gene expression. Presented here is an *in vitro* platform, applicable in the contexts of chemotaxis and morphogenesis, where cells may be exposed to dynamic chemical concentration fields while cultured in a 3-dimensional macromolecular matrix. In the first-generation system, cells are exposed to a one-dimensional gradient – constant along the two orthogonal axes. The second-generation system produces two orthogonally oriented gradients intersecting in a 2-dimensional field. These platforms were able to stimulate chemotaxis – both of cultured mammalian cells and emanating from murine skeletal muscle explants. Further, as a developmental tool, we were able to probe the role of Wnt signaling during Sonic Hedgehog based patterning of the vertebrate ventral neural tube. Using the presumptive enhancer for the p3 progenitor domain gene Nkx2.2, our findings indicate that such an enhancer would both negatively and positively regulate Nkx2.2 expression in response to Wnt signaling. However we found that the net effect of positive Wnt signaling - in the context of the cross-repressive interactions between various neural tube transcription factors (Nkx2.2, Olig2, and Pax6) - is inhibition of Nkx2.2 expression and p3 progenitor domain specification. On the basis of our new model, we postulate that the two opposing influences of Wnt on Sonic hedgehog signaling have distinct but dependent functions: first to inhibit Sonic Hedgehog signaling in the dorsal neural tube and secondly to prevent oscillatory behavior at the dorsal p3 boundary.

ACKNOWLEDGEMENTS

TABLE OF CONTENTS

CHAPTER ONE: INTRODUCTION

The earliest forms of life, prokaryotic organisms, were composed of a single cell encompassing the genetic, structural, metabolic and regulatory components within a singular plasma membrane. Even at this early stage, survival required individual responses to pertinent stimuli including the acquisition of nutrients. The plasma membrane effectively isolated cellular components from the external environment, yet at the same time interaction with this environment was a necessity. Functionalized membranes, with extracellular receptors whose transmembrane domains relayed signals intracellularly, provided a mechanism for chemically sampling the local environment. Thus cells gained the ability to recognize and respond to soluble molecules beyond the confines of the plasma membrane.

The binding of a soluble ligand (L) to its cognate receptor (R) often, though not always, initiates receptor activation and downstream signaling. Given forward and reverse rate constants of k_f and k_r, respectively, the formation of ligand-receptor complex (LR) formation is governed by the following first order kinetics.

$$L + R \underset{k_r}{\overset{k_f}{\Leftrightarrow}} LR$$
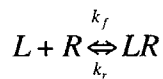
$$\frac{dLR}{dt} = k_f[L][R] - k_r[LR]$$

Receptor activation is a balance between binding and unbinding as dictated by the relative concentration of free ligand, free receptor, and receptor-ligand pairs. Both the rate and ultimate extent of ligand binding are not binary functions – ON in the presence of ligand and OFF in the absence of ligand – rather there exists a graded response over a range of ligand concentrations.

Given this basic paradigm of ligand receptor interaction, both single and multicellular organisms have evolutionarily developed multiple classes of cellular responses, each initiated by a ligand-receptor interaction. In the first class, the cellular response is a continuous and gradual function of ligand concentration. Such

is the case of how the binding of insulin to its tyrosine kinase receptor yields a concentration dependent increase in the glucose transporter expression (Wang, Moller et al. 1989). Expanding the ligand-receptor binding process to encompass the more general phenomenon of protein-protein binding reveals additional means of refining this concentration dependence. Enzyme catalysis as described by Michaelis-Menten kinetics accelerates reactions that, in the absence of an enzyme, are thermodynamically unfavorable. Further, the cooperative binding of oxygen to hemoglobin exemplifies the dependence of binding affinity on ligand concentration.

Chemotaxis, the directed migration of a cell in response to a concentration gradient, represents a second class of responses where the critical ligand property is not its concentration at a given point, but instead the variability of its concentration in space. In response, cells migrate toward regions of higher ligand concentration. Morphogenesis represents the third class of cellular responses to a soluble signal. During morphogenesis or tissue patterning, qualitatively different cell phenotypes are adopted in response to different concentrations of a ligand or morphogen. In a sense, this is similar to the first class of insulin-like responses in that the independent variable is ligand concentration. However, the dependent variable, cell phenotype, is a discrete rather than continuous function of ligand concentration. The presence of various ligand densities and hence concentration gradients suggests a chemotaxis-like context. Indeed, while morphogen gradients are present, individual cells respond to the magnitude of the local concentration. The challenge then, to both the evolutionarily ambitious species and the researcher is to understand how a continuous input – ligand concentration – can be biologically transformed into qualitatively unique patterns of gene expression at each successive ligand concentration regime. In doing so, an introduction to biological gradients is pertinent.

1.1 - Biological Gradients

A differentiable scalar or vector-valued function is uniquely defined in space and time and has similarly defined partial derivatives. These partial derivatives specify the magnitude and direction of the function's variability at any point given an incremental change along one of four dimensions (three orthonormal spatial vectors and time). In biological systems such a function might represent temperature, charge, pH, or molecular concentration.

In mammals, global temperature regulation is a metabolic requirement, but at the cellular level small, but relevant temperature variations may exist. Such temperature differences, also experienced by simpler organisms, may give rise to thermotaxis – migration in response to a temperature gradient. Thermotaxis was first described in the orientation and growth of pseudoplasmodia in the slime mold *Dictyostelium discoideum* in response to a temperature gradient of 0.05°C/cm (Bonner, Clarke et al. 1950). *C. elegans* grown at 20°C and subsequently placed in a gradient from 13°C - 27°C will directionally migrate up or down the gradient toward their growth temperature (Hedgecock and Russell 1975). In *E. coli* motility is temperature dependent and results in a migratory response analogous to chemotaxis (Maeda, Imae et al. 1976). Thermotaxis has also been observed in mammalian cells. Initially demonstrated in polymorphonuclear leukocytes (Kessler, Jarvik et al. 1979; Mizuno, Kawasaki et al. 1992), thermotaxis has most recently been studied in spermatozoa (Bahat, Tur-Kaspa et al. 2003). Unlike *d. discoideum* and *c. elegans*, spermatozoa can only respond to positive temperature gradients which guide them down the oviduct toward the fertilization site. The temperature gradient in the female reproductive system is transient, increasing for several hours during ovulation to a magnitude of ~0.1°C/cm (Bahat and Eisenbach 2006).

Electrochemical gradients formed by the separation of positively and negatively charged molecules are a ubiquitous means of storing and communicating

information. The propagation of action potentials in neurons and excitation-contraction coupling in cardiac muscle are dependent on ion concentration gradients and selective membrane permeability which confer a resting potential in most living cells. In the axon of a neuron, for example, the concentrations of potassium and sodium are high and low, respectively, relative to the extracellular environment, and the cell is polarized with a negative membrane potential. This electrical gradient is maintained by an impermeable membrane that prevents equilibration of the charge separation. Indeed in a physiological saline solution, the charge relaxation time is on the order of 0.07ns (Weiss 1996). The rapid propagation of action potentials results from voltage gated ion channels that permit the flow of ions down their electrochemical gradient, initiating membrane depolarization and repolarization (Hodgkin and Huxley 1952). In cardiac muscle, cardiomyocytes become depolarized in response to an action potential due to the voltage sensitive increase in L-type calcium channel permeability. Ryanodine receptors respond to this calcium influx by releasing addition calcium into the cytosol from the sarcoplasmic reticulum. This calcium induced calcium release stimulates sarcomere contraction (Fabiato 1983).

A special subtype of electrochemical gradients where the spatially distributed species are hydrogen ions – single protons whose concentration determines pH. During aerobic respiration in bacteria and mitochondria the energy released by the reduction of molecular oxygen powers a series of proton pumps that externally concentrate H^+ ions against its electrochemical gradient. In mitochondria protons accumulate in the intermembrane space between the internal and external lipid bilayers. The enzyme ATP synthase couples the diffusion of H^+ ions back into the mitochondrial matrix with the production of ATP, thus converting the potential energy of the proton electrochemical gradient into a transferrable form of energy currency (Babcock and Wikstrom 1992).

Molecular or chemical concentration gradients, of which electrochemical gradients are sub-type, represent a large class of biological gradients. Soluble chemical

gradients allow individual cells to assess the local environment and communicate between near or distant neighbors. In order to function over any given length-scale molecules must originate from a source and be transported to a sink/destination. The physical principles governing mass transport allow researchers to model and predict chemical gradients both *in vitro* and *in vivo*.

Diffusion is the random motion of molecules resulting from inter-molecular collisions and the transfer of thermal energy. These collisions, occurring at a rate of trillions per second, can be modeled as a random walk in which a single molecule is displaced along a unit vector **Δr**, randomly oriented, in a time Δt. This random walk continues with each successive step randomly oriented. After a time t the mean square displacement of the molecule will indicate its net displacement from its initial position, and represents the mobility of the particular solute molecule in a particular solvent. This mobility - a function of solute, solvent, pressure, and temperature - is the diffusion coefficient D_{ij} of the solute i in solvent j.

Adolph Fick observed experimentally the flux of a solute across a plane is proportional to the concentration difference across the boundary. The constant of proportionality is the diffusion coefficient and generalized to three dimensions.

$$\bar{N} = -D\nabla C + \bar{v}C$$

where $\bar{N}$ is the solute flux of units moles/m²s, C is the concentration of the solute as a function of time and space and v is the bulk solvent velocity. The negative sign indicates that when the concentration is increasing along a vector, the flux of solute will occur in the opposite direction. That is, molecules diffuse down concentration gradients - from regions of high concentration to regions of low concentration. The first term in the equation represents solute diffusion while the second term represents advection of the solute due to fluid flow in the solvent.

Consider a control volume in space with a fixed boundary. The rate of accumulation of solute in the volume is the sum of net flux across the boundary and the net rate of

production within the control volume. Conservation of mass yields the following mass transport relation:

$$\frac{\partial C}{\partial t} = D\nabla^2 C - \nabla(\vec{v}C) + R$$

where and R is the net rate of solute production/degradation. This relationship neglects electrochemical drift effects which are important in context of charged solute and solvent molecules. Both chemotaxis and morphogenesis rely on gradient formation and mass transport phenomenon as governed by this mass transport relation.

1.1.1 – Chemotaxis

Chemotaxis is the directed migration of a cell in response to a soluble gradient. Prokaryotes are unable to sense gradients across the length scale of a typical cell (1-2 μm). Instead, they rely on a series of uni-directional random walks, powered by flagellum or pili. Each persistent random walk is interrupted by a tumble - non-directional movement that results in the cell orienting itself in a new direction for a successive random walk. Higher chemoattractant concentrations decrease the frequency of tumbles, producing more persistent random walks. As the cell moves up a concentration gradient the random walk in that direction persists, whereas movement away from the concentration source yields increased tumbling and re-orientation. In this manner, bacteria randomly sample various locations and their movement becomes less interrupted and more "directed" in regions of greater chemoattractant concentration (Berg 1988).

1.1.1.1 – Motility, Directional Sensing, and Polarity

Eukaryotic cells, an order of magnitude larger than bacteria, are capable of sensing and responding to concentration gradients exhibiting concentration differences as low as 2% between the front and back ends of the cell. Motility, directional sensing, and polarity together characterize the process of chemotaxis (Swaney, Huang et al.

2010). *D. discoideum* and leukocytes have been studied extensively, and share many genetic and cellular mechanisms in spite of their divergence more than 800 million years ago (Baldauf, Roger et al. 2000). In the absence or at baseline levels of a pro-motility factor, cells randomly and frequently (~1/min) produce pseudopodia as actin polymerization extends these feet-like projections of the cytoplasm away from the cell border. Pseudopodia may attach to the adjacent substrate followed by acto-myosin mediated contraction and translocation of the cell in the direction of the pseudopod. Alternatively, pseudopodia may be retracted without cell movement and a subsequent pseudopod will extend in a new direction. Thus, at baseline, cells exhibit some motility or ability to move randomly and intermittently (Van Haastert and Devreotes 2004). A non-directional increase in motility in response to a chemical stimulus is termed chemokinesis and must be distinguished from directed chemotaxis.

Directional sensing involves the extra- and intra-cellular signaling cascades that interpret chemoattractant concentrations at multiple locations along the plasma membrane. Chemotaxis is often initiated by ligand binding of G-protein coupled receptors on the cell membrane. Via Ras proteins, G-proteins activate phosphatidylinositol 3-kinases (PI3Ks) which leads to accumulation of phosphatidylinositol tri-phosphate (PIP$_3$) near the plasma membrane (Huang, Iijima et al. 2003). Activation occurs rapidly and uniformly along the plasma membrane and to a magnitude proportional to the chemoattractant concentration. The Local Excitation Global Inhibition model suggests that although activation occurs locally as a function of local receptor occupancy, inhibition occur globally in response to the mean chemoattractant concentration surrounding the cell (Parent and Devreotes 1999). Thus, regions of the cell adjacent to higher concentrations (leading end) will experience a local activation that exceeds the global inhibition signal, and regions adjacent to lower concentrations (trailing end) will experience an activation that is exceeded by the inhibition signal. The presence of PI3K and PIP$_3$ is sustained at the front end of the cell, whereas phosphatase and tensin homolog (PTEN), a negative regulator of PIP$_3$, accumulates in the rear. In addition to modulating the excitatory

signal that enables direction sensing, the inhibition mechanism is also responsible for adaptation in the presence of a uniform concentration field and uniform cellular activation. In this context, however, the global inhibition is sufficient to globally attenuate the positive signal. The precise mode of global inhibition has not yet been clarified, but sustained G-protein activation has been observed in the presence of a uniform gradient. Ras activation, however, is not – indicating that adaptation and global inhibition may lie upstream of Ras and downstream to the G-protein (Zhang, Charest et al. 2008).

Polarity describes the elongation of the cell body and functionalization of the front and rear ends of a cell in a concentration gradient. Following PIP_3 accumulation at the front-end, actin polymerization and the repeated formation of pseudopodia in the direction of the increasing gradient are thought to be dependent on Rac proteins and Cdc42 (Van Haastert and Devreotes 2004). In addition to extension at the leading edge, translocation of the cell body requires myosin-II mediated contraction at the trailing edge. Generally, rear-end localization is achieved by chemoattractant-receptor dependent maintenance of myosin-II phosphorylation and subsequent de-polymerization at the front end (Steimle, Yumura et al. 2001; Xu, Wang et al. 2003).

1.1.1.2 – Extracellular Matrix Interactions

Adhesion at the leading edge and contraction at the trailing edge require optimally tuned interactions with extracellular matrix (ECM) molecules. Integrins are a heterodimeric class of membrane receptors that signal intracellularly in addition to binding ECM components such as collagens, fibronectin, laminins, and vitronectin (Humphries, Byron et al. 2006). Focal adhesion complexes connect ECM-bound integrins to the cytoskeleton thereby permitting bi-directional force transmission. Contractile forces generated within the cell induce unbinding at the trailing edge, while the cell is anchored at the leading edge. Thus the adhesion strength between the cell and the substrate must be sufficiently moderate so as to be ruptured during

retraction and sufficiently strong to maintain attachment in the front. Indeed migration speed is maximum at an intermediate range of cell-substrate adhesiveness (Palecek, Loftus et al. 1997).

While various ECM components may be arranged or patterned in either a 2-dimensional or 3-dimensional environment, cells respond differently in each context (Elsdale and Bard 1972; Cukierman, Pankov et al. 2001). Cells cultured on a 2D substrate tend to flatten and spread out, adopting a bottom to top polarity that is not common in non-epithelial cells types. Epithelial cells and fibroblasts form wide flat lamellipodia at the leading edge rather than pseudopodia, indicative of an adaptation suitable for migration along a planar surface (Schneider and Haugh 2006). Recent studies have revealed a diverse and complex array of context-dependent adhesion mechanisms, motility patterns, and intracellular regulators during 3D migration (Friedl, Sahai et al. 2012). 3D migration exhibits multiple types of extracellular adhesions including fibrillar adhesions, focal complexes, 3D-matrix adhesions, nascent adhesions, podosomes, and invadopodia – in addition to focal adhesions (Harunaga and Yamada 2011). The traditional balance between actin polymerization, acto-myosin contraction, and rear retraction (Lauffenburger and Horwitz 1996) does not always exist in 3D. Cells may migrate by contraction-induced propulsion of blunt cylindrical processes called lobopodia. Lobopodia based migration does not require PIP_3 polarization or actin and myosin localization. Rather contraction of the cytoskeleton increases intra-cellular pressure and traction forces near the rear-end of the cell allow the cell to push itself forward through the matrix (Petrie, Gavara et al. 2012).

Beyond presenting ECM components in an additional dimension, 3D matrices introduce additional variables associated with matrix formation. Randomly oriented ECM molecules create a porous structure through which cells must either navigate or degrade depending on the ratio of pore size to the diameter of the minimally deformable nucleus. 2D substrates are generally stiff or non-deformable whereas 3D matrices exist over a range of significantly more elastic moduli. A typical 1-2

16

mg/ml collagen gel has a Young's modulus of only 50 Pa, whereas typical plastics such as polystyrene have a modulus on the order of 1 GPa (Grinnell and Petroll 2010). Cells themselves are also relatively compliant with moduli on the order of 2Pa. Matrix cross-linking as well as large deformation (approaching macromolecular contour lengths) of structural ECM components may produce strain-stiffening as the modulus increases in response to strain. This non-linear elastic behavior has been shown to influence the transition from lamellipodia to lobopodia based migration (Petrie, Gavara et al. 2012).

1.1.1.3 – Chemokines and Context Diversity of Migration

Differences exhibited during 2-dimensional vs. 3-dimensional migration and the various mechanisms of motility only partial encompass the variability present during chemotaxis *in vivo*. For instance, in addition to protrusion, amoeboid, or run and tumble based migration of individual cells, migration may occur collectively. Collective migration is characterized by the maintenance of cell-cell junctions, the generation of traction forces by coordinated cytoskeletal protrusion and contraction, and the modification of the local environment either through matrix degradation or the deposition of a basement membrane (Friedl and Gilmour 2009). Epithelial cells, bound both to one another and an underlying basement membrane, often migrate collectively as is the case during wound healing.

The prevalence of chemotaxis in several *in vivo* contexts is uniquely catalogued by the role of chemokines. Chemokines are low molecular weight chemotactic cytokines that stimulate migration of immune cells, epithelial cells, and endothelial cells. More than 40 chemokine ligands in addition to 18 corresponding G-protein coupled receptors have been identified in mammals. The utilization of chemokines is pervasive, modulating diverse cell populations in biological processes including immune function, inflammation, autoimmune disorders, wound repair/regeneration, angiogenesis, tumor metastasis, and embryonic development.

Each of these phenomena is only partially dependent on chemokine activity, further highlighting the abundance of unique implementations of gradient-based migration that have evolved to date.

1.1.2 –Tissue Patterning and Morphogenesis

During development, a single fertilized egg is fated to give rise to the entire heterogeneous population of cells in the adult organism. New cells eventually mature, differentiate, and together self-organize into functional tissues and organs. The instructions that specify the appropriate magnitude and location of each cell type are contained within the genome of the first undifferentiated and pluripotent cell. Over the past 100 years, the process by which cell fates are determined as a function of positional location has been described with increasing detail and accuracy. The progression occurred in stages, first recognizing the significance of induction, followed by gradients, thresholds, and diffusion (Rogers and Schier 2011).

Scientists initially postulated that the organization of undifferentiated cells into functionalized tissues must be dependent on cell-cell communication. Through this interaction, one cell could induce a second cell to adopt a particular phenotype and gene expression profile. Although the concept of induction represented a significant first step, the question of how a cell could induce multiple cell fates within a single tissue remained unanswered. Still in the early years of the early 20th century, Thomas Hunt Morgan proposed that a spatial gradient in the presence of a *substance* could underlie embryological tissue patterning (Rogers and Schier 2011). However, it was not until the idea that thresholds exist between the maximum and minimum gradient values and that the spatial locations of these thresholds separate adjacent regions of unique target cell induction that the first model of tissue pattern formation was described. In the late 1960's Wolpert's French flag model described how an inducing cell produced a concentration gradient within a field of responding

18

cells (Wolpert 1969). The concentration at each position within the field, relative to the magnitude of the various thresholds, conferred positional information at that point. However, a cell's realization of its positional identity, rather than the signal from the inducing cell, determined cell fate. A few years later, the idea that molecular diffusion from a source to a sink could create stable concentration gradients set the stage for the discovery and characterization of actual tissue patterning systems (Crick 1970).

Before describing the various mechanisms through which tissues create and interpret morphogen gradients, a brief overview of various classic systems will provide the basis for future examples. In the *Drosophila* blastoderm, a syncytium of early progenitors, Bicoid exists as an intracellular gradient specifying anterior-posterior positioning (Driever and Nusslein-Volhard 1988). Bicoid mRNA is found at the most anterior region producing an exponentially decreasing gradient of the Bicoid transcription/translation factor – the first morphogen gradient to be described in the literature (Driever and Nusslein-Volhard 1988). Dorsal, also forming an intra-nuclear gradient, is required for patterning along the dorsal-ventral axis (Roth, Stein et al. 1989). The first extracellular morphogen gradient identified in *Drosophila* is Dpp, a member of the TGF-β family, which patterns, among others, both the dorsal-ventral axis in the embryo (Ferguson and Anderson 1992) and the wing imaginal disc (Lecuit, Brook et al. 1996).

The Wingless(Wg)/Wnt, Hedgehog, fibroblast growth factor (Fgf), and retinoic acid (RA) morphogen systems specify various tissue patterns throughout embryogenesis in *Drosophila* and humans. One illustrative example of multiple morphogen gradients coordinated patterning of a complex structure is the vertebrate limb (Benazet and Zeller 2009). The limb bud is patterned along 3 axes – dorsal-ventral, anterior-posterior, and proximal-distal. The distal tip of the limb bud, predominantly naïve mesenchymal cells, forms a thin epithelial structure - the apical ectodermal ridge – where Fgf production controls proximodistal patterning (Niswander, Tickle et al. 1993). Distal cell types are dependent on prolonged Fgf

exposure, whereas RA synthesized in the proximal limb bud flank specifies proximal cell fates. Thus opposing Fgf and RA gradients synergistically determine proximodistal spatial identities (Mercader, Leonardo et al. 2000). In the distal limb bud, anteroposterior patterning, including the specification of individual digits, is controlled by the posteriorly positioned zone of polarizing activity, where the morphogen sonic hedgehog diffuses anteriorly to pattern along this axis (Riddle, Johnson et al. 1993).

A diffusing chemical signal presents many challenges in ensuring the proper orientation and arrangement of inducible cell types. Indeed noise and embryo-to-embryo anatomical and genetic variations may lead to gradient disruption and defective patterning. Thus various mechanisms have evolved to control the formation and interpretation of gradients. Traditionally, gradient formation is thought to be governed by a synthesis-diffusion-clearance mechanism, where diffusion occurs between a productive source location and a destructive sink location (Kicheva, Pantazis et al. 2007). While generally true, variations on this theme exist. In *Xenopus* embryos, the production of BMP antagonists in a uniform BMP field produces a spatial gradient (Ben-Zvi, Shilo et al. 2008). Similarly, in the hindbrain of zebrafish an RA gradient is produced, without a localized source, by its spatially varied enzymatic degradation (White, Nie et al. 2007). In the mouse tail bud, Fgf8 mRNA is produced posteriorly, followed by cell division and selective mRNA destruction yielding maximal Fgf8 protein production at the most proximal locations (Dubrulle and Pourquie 2004).

During the diffusion phase of the synthesis-diffusion-clearance paradigm, modifications to the diffusing molecule itself as well as the diffusion route may regulate gradient formation. Post-translational modification of morphogen proteins may affect diffusivity by limiting or expanding the range of signaling. The addition of cholesterol and palmitic acid to newly synthesized hedgehog molecules promotes oligomerization into complexes capable of controlled long range signaling and association with plasma membranes at the cell surface (Gallet, Ruel et al. 2006).

Such lipoproteins may also be transported by extracellular plasma membrane vesicles or experience enhanced signaling capabilities through increased association with cell surface plasma membranes (Eaton 2008). Extracellular matrix components, specifically negatively charged heparan sulfate proteoglycans (HSPGs) may bind morphogens and alter gradients accordingly (Yan and Lin 2009). HSPGs may concentrate morphogens close to the cell membrane promoting receptor interaction, sometimes functioning as a co-receptor as well (Tsuda, Kamimura et al. 1999). Interestingly, binding to HSPG's may limit morphogen diffusion to regions adjacent to the source or promote long-range spreading (Vyas, Goswami et al. 2008; Yu, Burkhardt et al. 2009). Although extra-cellular diffusion is the main mechanism of morphogen gradient formation, endocytosis-based *inter*-cellular trafficking (transcytosis) has been shown to mediate the spread of Dpp (Entchev, Schwabedissen et al. 2000). In addition to transporting morphogens, cells may respond to and modulate morphogen gradients through various feedback mechanisms. Feedback may increase receptor expression and ligand sequestration at the cell surface or through endocytosis and degradation as with sonic hedgehog and its receptor patched-1 (Incardona, Lee et al. 2000). Nodal signaling, of the TGF-β family, results in the expression of its soluble inhibitor in order to limit its spatial expansion (Chen and Schier 2002).

The transduction and interpretation of morphogen gradients that results in concentration based gene expression incorporate a diverse array of regulatory schemes to achieve specific patterning requirements. Transduction of a morphogen signal from an extracellular presence to concentration dependent intracellular activity is often linearly dependent on the absolute number of occupied receptors. In *Xenopus*, a threefold change in the number of bound Activin receptors (regardless of the total number of receptors at the cell surface) results in a threefold change in the nuclear transcriptional regulator Smad2 (Shimizu and Gurdon 1999) and a transition from low to high threshold gene expression (Dyson and Gurdon 1998).

Translating small fold changes in the concentrations into intracellular morphogen effectors is achieved through differential DNA binding affinities and various types of combinatorial regulation. Broadly, target genes with low affinity binding sites require higher morphogen concentrations for expression whereas genes with high affinity binding are expressed at lower concentrations (Driever, Thoma et al. 1989). Binding affinity alone does not account for the diversity of expression patterns found in even the simplest embryos. Rather combinatorial regulation, where the morphogen effector in conjunction with additional transcriptional activators and repressors interact with cis-regulatory enhancer elements, determines target gene expression (Ashe and Briscoe 2006). In a feed-forward loop, a morphogen effector induces the expression of a second activator, and together both proteins induce expression of the target gene. In a positive feedback loop, the target gene is initially induced by the morphogen effector alone and subsequent expression is augmented through self-induction by the target gene and the morphogen. Cross-repression allows differential expression of two target genes A and B by the same morphogen as gene A is inhibited by gene B and gene B is inhibited by gene A. In a reciprocal-repressor gradient, the morphogen establishes an inverse gradient of its repressor such that the repressor activity is high where activator activity is low and vice versa. The ratio of activator to repressor determines gene expression of target genes.

The reproducibility of tissue patterning is dependent upon four concepts: precision/sharpening, corrections, robustness, and scaling. Many of the above strategies for gradient interpretation contribute to sharp boundaries separating regions of differential gene expression and the precise mechanisms that sharpen each type of morphogen boundary is unclear. Error correction following the mis-expression of a target gene outside its proper domain, may be achieved through re-specification where the cell adopts the gene expression profile of its neighbors (Standley, Zorn et al. 2001), rearrangement, where the cell repositions itself within its proper domain (Wijgerde, McMahon et al. 2002), or simply by cell death (Namba, Pazdera et al. 1997). Robustness refers to the proper interpretation of gradients in the presence perturbations such as stochastic variations in concentration or signal

transduction. Feedback contributes greatly to robustness by filtering out noise or regulating concentration based clearance mechanisms to account for altered morphogen production rates (Eldar, Dorfman et al. 2002). A fascinating property of morphogen gradients is the ability to properly pattern tissues, with appropriate proportioning, in embryos of multiple sizes, particularly as diffusion time scales with the square of diffusion length. The exact mechanisms of scaling are not entirely identified but one model, the expansion-repression model, concludes that an expander protein that expands the signaling range of a morphogen by increasing its diffusivity or decreasing its degradation will naturally scale a morphogen gradient if the morphogen also inhibits expression of the expander (Ben-Zvi and Barkai 2010). This feedback topology is analogous to an integral-feedback controller, where the controlled variable is the length of the morphogen gradient, the desired output is a full-length gradient where the expander is not produced, and the error is the region where the expander is produced. The time integral of expander accumulation lengthens the gradient, reducing the error.

1.1.2.1 - Neural Tube

Many of the morphogen gradient properties discussed above are present in the vertebrate neural tube, an embryological structure that develops into the central nervous system: the brain and spinal cord. In the early embryo, the three germ layers – ectoderm (dorsal), mesoderm, and endoderm (ventral) – are formed during gastrulation. The dorsal mesoderm directs the ectoderm to form the neural plate medially. These cells, up to 50% of the ectoderm, adopt a distinctive columnar shape. The neural plate elongates along the anteroposterior axis and narrows mediolaterally. Bilaterally the neural plate is bound by a neural plate border region and pre-epidermis non-neural ectoderm. Folding of the neural plate begins as midline neural plate cells are anchored to the ventrally positioned notochord. The neural plate border regions begin to rise dorsally and converge medially, forming the two neural folds dorsal the medial neural groove. The two neural folds fuse and

in some species, cells at this location become neural crest cells which migrate throughout the embryo forming many cell types including peripheral neurons and melanocytes (Gilbert 2000). The hollow neural tube, oriented along the anteroposterior axis, is open at either extreme and bordered by epidermis forming surface ectoderm dorsally, the notochord ventrally, and mesoderm laterally.

Failure of the neural plate to properly fuse into the neural tube results in a class of congenital anomalies known as neural tube defects (Wallingford, Niswander et al. 2013). The prevalence of neural tube defects remains high in developed countries (1 in 2000 births in the United States) despite recent advances in prevention and treatment. Neural tube defects are broadly classified into three categories according to the location along the anteroposterior axis where neural tube closure is incomplete. Anterior/cranial defects are referred to as anencephaly. Anencephaly is typically a lethal condition characterized by severe cerebral malformations as well as the absence of the cerebellum. Posterior/caudal defects are referred to as spina bifida and allow the protrusion of spinal cord tissue from the vertebrae. These defects are more common than anencephaly and compatible with life given proper treatment. Finally, the lethal and relatively rare condition of craniorachischisis results from incomplete closure of the neural tube along the entire anteroposterior axis.

Patterning of the neural tube occurs along its anteroposterior/cranocaudal and dorsoventral axes, as the brain develops cranially and the spinal cord caudally. Pseudostratified neuroepithelia line the inner surface of the neural tube which features a polarized elliptical cross-section with a dorsoventral major axis. The dorsal aspect produces sensory spinal neurons while the ventral region gives rise to motor spinal neurons. The dorsoventral patterning of the neural tube has been studied extensively and serves as one of the prototypical examples of complex morphogen regulation, particularly within the ventral neural tube where sonic hedgehog is a key morphogen.

1.1.2.2 - Sonic Hedgehog and the Ventral Neural Tube

Sonic hedgehog (Shh) functions as a morphogen in the ventral neural tube, conferring positional information sufficient for patterning distinct neural progenitor domains along the inner lumen of the neural tube (Jessell 2000). Each domain is defined by the expression of a unique combination of homeodomain and basic helix-loop-helix transcription factors, Figure 1.2.1. Together these transcriptional regulators result in the formation of distinct neuronal subtypes from progenitors in each domain. The Shh gradient develops over time and decreases dorsally from a maximum concentration at the ventral midline. Progenitor specification does not occur uniformly, rather induction of each domain is dependent on the magnitude and duration of Shh exposure. Thus genes induced by the lowest levels of Shh are specified first throughout the ventral neural tube, with increasingly Shh dependent genes restricted to progressively more ventral positions. Two to three fold increases in Shh concentration are sufficient to transition from induction of a given Shh dependent progenitor domain to a more ventral domain (Roelink, Porter et al. 1995). The patterning process begins with formation of the extracellular Shh gradient, followed by cell-level signal transduction leading to transcriptional regulation of target genes.

Sonic hedgehog is initially produced by the notochord just ventral to the ventral midline of the neural tube (Echelard, Epstein et al. 1993). Notochord derived Shh induces a second signal center, the floor plate, at the ventral midline which also secretes Shh protein (Marti, Bumcrot et al. 1995). Visualization of the Shh gradient reveals an exponentially decaying ligand distribution along the dorsoventral axis (Chamberlain, Jeong et al. 2008) that increases in time at each position along the DV axis while maintaining the same overall profile. Shh forms distinct apically restricted punctae within the neural tube lumen in close association with basal bodies of primary cilia, Figure 1.2.2.

Diffusion of Shh is regulated by post-translational modifications at the source, extracellular matrix components within the target field, and plasma membrane proteins expressed by target cells. Newly translated Shh precursors are cholesterol modified at the C-terminus (Porter, Young et al. 1996) and palmitoylated at the N-terminus (Pepinsky, Zeng et al. 1998). Fully-processed Shh molecules form high molecular weight complexes that are secreted via a mechanism dependent on the transmembrane protein Disp1 (Chen, Li et al. 2004). These lipid modifications affect the diffusivity of secreted Shh as well as its activity. Heparan sulfate proteoglycans, distributed throughout the neural tube, bind Shh and likely contribute to gradient regulation through local accumulation of the ligand (Rubin, Choi et al. 2002).

Two classes of membrane associated proteins interact with Shh in order to regulate its extracellular distribution and intracellular transduction. Hedgehog interacting protein-1 (Hhip1) and the Shh receptor patched-1 (Ptch1) sequester Shh, preventing diffusion and limiting ligand levels at more dorsal positions (Jeong and McMahon 2005). Additionally, the bound Ptch1-Shh complex undergoes endocytosis followed by Shh degradation (Incardona, Gruenberg et al. 2002). Ptch1 and Hhip1 are up-regulated by Shh signaling and represent a negative feedback pathway that limits the local transduction and spatial extent of Shh signaling. The second class of transmembrane proteins - including Cdo, Boc, and Gas1 - are generally inhibited by and promote Shh signaling in a cell autonomous manner (Tenzen, Allen et al. 2006; Allen, Tenzen et al. 2007). It is not known whether these binding-partners function solely by concentrating Shh ligand at the cell surface, but, together with the opposing actions of Ptch1 and Hhip1, they confer a degree of robustness to the Shh system in the presence of protein level fluctuations. In the presence of very low levels of Shh signaling, Cdo, Boc, and Gas1 are more highly expressed and may augment Shh activity. Conversely, these genes are down-regulated in the presence of very high levels of Shh and increased expression of Ptch1 and Hhip1 may serve as a signal attenuator.

In the absence of Shh, Ptch1 inhibits the transmembrane protein smoothened (Smo), Figure 1.2.2. Transduction of the Shh signal, in vertebrates, begins the binding of Ptch1 at the apical primary cilium (Ribes and Briscoe 2009). Bound Ptch1 does not inhibit Smo thereby permitting its accumulation in the primary cilium and initiation of downstream signal transduction (Murone, Rosenthal et al. 1999). Smo signaling, however, is necessary and sufficient to completely effect Shh dependent events in target cells. Smo null embryos lack all the progenitor domains ventral to the p1 domain (Wijgerde, McMahon et al. 2002), and expression of a dominant active Smo transcript cell-autonomously induces ventral phenotypes (Hynes, Ye et al. 2000). Similarly, small molecule agonists and antagonists of Smo increase and decrease, respectively, the extent of Shh induced gene expression (Frank-Kamenetsky, Zhang et al. 2002).

Signaling events initiated by Smo culminate in the modulation of three zinc-finger-containing transcription factors – Gli1, Gli2, and Gli3 (Matise and Joyner 1999). Gli proteins may function as transcriptional repressors (GliR) or activators (GliA) depending on the degree of Shh stimulation, although Gli1 is thought to function exclusively as an activator, Gli2 primarily as an activator, and Gli3 primarily as a repressor. In each cell there exists a competition between GliR and GliA, the net result of which determines the degree of Shh gene induction (Jacob and Briscoe 2003). Thus the extracellular Shh gradient is transduced into an intracellular Gli activity gradient (Stamataki, Ulloa et al. 2005). In the absence of Shh, GliR dominates due to Gli2 degradation and proteolytic cleavage of Gli3 into its repressor form Gli3R (Meyer and Roelink 2003; Pan, Bai et al. 2006). Such repression suppresses Shh dependent genes prior to Shh gradient formation ventrally and in dorsal tissues where the Shh gradient is maximally decayed. In the presence of Shh, the cleavage of Gli3 is inhibited and Gli3R levels are reduced. Elimination of Gli3R is sufficient to roughly induce the p1, p2, and pMN domains (Persson, Stamataki et al. 2002). Specification of the most ventral domains, p3 and FP, require additional GliA in addition to diminished Gli3R activity. The high level of Shh signaling in these domains prevents the degradation of Gli2, inhibits expression of Gli3 entirely, and

promotes the expression of Gli1 (Dai, Akimaru et al. 1999; Pan, Bai et al. 2006). Hence, the balance of Gli activity, dominated by Gli2 and Gli1, is tilted toward Shh target gene activation.

Both the concentration and duration of Shh exposure determine the strength of intracellular Gli activity in target cells. A temporal adaptation model suggests that exposure to Shh decreases a target cell's sensitivity to continued stimulation (Dessaud, Yang et al. 2007). Initially, Shh induces a strong GliA signal; however, negative feedback will require greater and greater concentrations of Shh to maintain this level of Gli activity. In the presence of a constant Shh concentration, GliA activity will decrease until it ceases entirely. Larger Shh concentrations will sustain GliA activity for longer periods of time, whereas lower concentrations will wane quickly. The duration of Gli activity then is proportional to Shh concentration, and the time integral of Gli activity determines the extent to which Shh may induce gene expression.

The Shh morphogen gradient functions within a larger gene regulatory network (GRN) in which cross-repressive interactions between Shh target genes contribute to domain specification and boundary sharpening (Dessaud, McMahon et al. 2008; Lek, Dias et al. 2010). Other soluble proteins including members of the BMP and Wnt families are also expressed in the neural tube, contributing to patterning in both the dorsal and ventral neural tube (Liu and Niswander 2005; Ulloa and Marti 2010).

1.2 – Figures

Shh Gradient		
	p0	Pax6, Irx3, Dbx2, Dbx1
	p1	Pax6, Irx3, Nkx6.2, Dbx2
	p2	Pax6, Irx3, Nkx6.1
	pMN	Olig2, Nkx6.1, Pax6
	p3	Nkx2.2, Nkx6.1
	FP	Foxa2, Nkx6.1
	VENTRAL MIDLINE	

Figure 1.2.1 – Progenitor Domains in the Ventral Neural Tube
Six progenitor domains are found in the ventral neural tube, each expressing a unique set of transcription factors that determine cell identity. Shh acts as a morphogen, decreasing dorsally from a maximum concentration at the ventral midline and assigning positional identities to in the floor plate (FP), p3, pMN, p2, p1, and p0 domains. Dorsal to the p0 domain exist a series of dorsal progenitor domains, primarily implicated in sensory perception, in which Shh does not function as a morphogen.
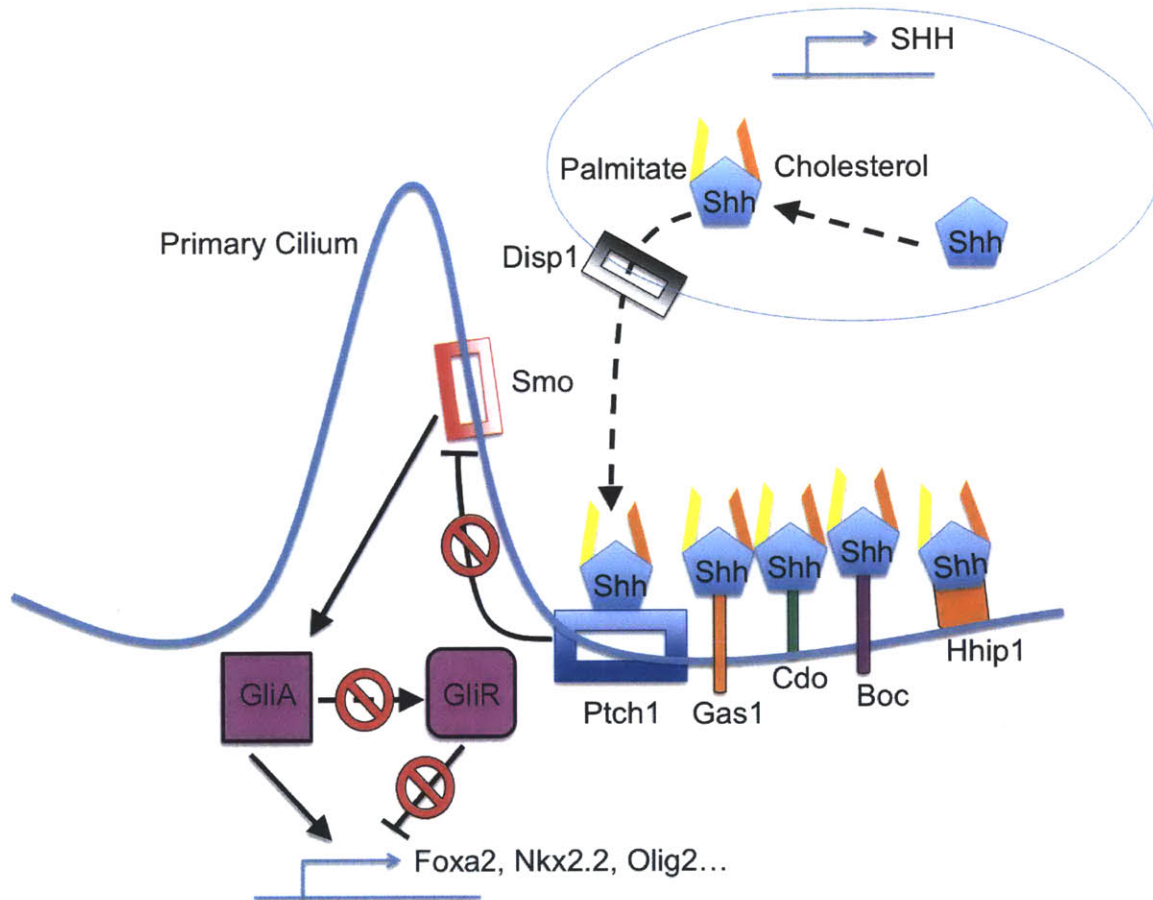
Figure 1.2.2 - Sonic Hedgehog Signaling Pathway
In the absence of Shh, patched1 inhibits smoothened which allows Gli
transcription factors to be expressed in and processed into repressor
forms. The binding of Shh to patched1 relieves the inhibition of
smoothened which then localizes to the primary cilium where it
inhibits the processing of Gli3 into its repressor form, prevents the
degradation of Gli2, and up-regulates Gli1 expression. Each of these
changes increases GliA function while decreasing GliR. GliA goes on to
positively regulate the expression of ventral transcription factors such
as Foxa2 (FP), Nkx2.2 (p3), and Olig2 (pMN).

CHAPTER TWO: RC MICROFLUIDIC BIOREACTOR

2.1 – Introduction

Many important biological processes such as gastrulation and organogenesis (Montero and Heisenberg 2004; Laird, von Andrian et al. 2008), inflammation (Friedl and Weigelin 2008), and cancer metastasis (O'Hayre, Salanga et al. 2008) depend on the directed movement or transcriptional response of cells to biochemical and biophysical stimuli. In vitro systems designed to study these cellular behaviors rely on the replication of local microenvironments, including the presentation of relevant stimuli in an appropriate spatiotemporal pattern. The microenvironment may include specific cell populations, extracellular matrix components, and soluble or immobilized chemical signals. In contrast to experiments with cells grown in 2-dimensional monolayers, 3-dimensional cell culture systems allow for the construction of microenvironments characterized by preservation of native cell-cell and cell-matrix interactions (Abbott 2003). Like cellular migration (Sun, Wise et al. 2004; Even-Ram and Yamada 2005; Zaman, Kamm et al. 2005; Gabriel and John 2006; Smalley, Lioni et al. 2006; Zaman, Trapani et al. 2006; Ghibaudo, Trichet et al. 2009), a variety of cellular functions are markedly affected by 3D environments. This has prompted the development of 3D scaffolds such as hydrogels and self-assembling peptides in which cells can be seeded and cultured (Cukierman, Pankov et al. 2001; Smalley, Lioni et al. 2006; Smalley, Lioni et al. 2006; Lee, Cuddihy et al. 2008; Zhang, George et al. 2008).

Chemotaxis is the directed translocation of a cell under the influence of a soluble chemical gradient. Several methods, with varying limitations and degrees of complexity, have been developed to study cell chemotaxis. The Boyden chamber assay establishes a chemical gradient across a thin porous membrane through which cells migrate in the direction of the concentration gradient (Boyden 1962). In

the under-agarose assay, cells migrate between a coverslip and an agarose gel toward a well containing the chemical species of interest (Nelson, Quie et al. 1975). The Zigmond and Dunn chamber assays offer improved visual observation of cells migrating across a bridge between two wells, one containing the chemoattractant (Zigmond 1977; Zicha, Dunn et al. 1991). Most assays lack quantifiable or stable concentration gradients and assay migration in 2D rather than 3D, prompting recent efforts to define stable gradients in 3 dimensional geometries (Keenan and Folch 2008).

Chemical concentration gradients may decay due to transfer of solute from the source region to the sink region. In order to establish a stable linear concentration gradient between a source and sink, the two regions must be continuously maintained at maximum and minimum concentrations, respectively. This is commonly achieved by continuous flow that replenishes the source solute concentration and eliminates the growing sink concentration. In the "Y-shaped" microfluidic device, two laminar streams are combined in a microfluidic channel, and the solute diffuses between streams, creating a gradient perpendicular to the combined flow path (Lin and Butcher 2006). These gradients are formed in a channel in which cells can migrate in a 2D but not 3D environment. In another implementation of flow-maintained gradients in microfluidic channels, a hydrogel is placed between a source and sink channel through which cells migrate up the concentration gradient established across a gel (Saadi, Rhee et al. 2007; Vickerman, Blundo et al. 2008; Chung, Sudo et al. 2009; Mack, Zhang et al. 2009; Sudo, Chung et al. 2009). The maintenance of stable linear concentration gradients by continuous flow, however, is subject to a number of practical limitations. If flow characteristics in the source and sink channels are not identical, a pressure gradient will develop and the resultant fluid flow between the two channels can disrupt the concentration gradient. Fluid flow within the channel or gel induces shear stress on cells, which can independently alter the underlying biology of interest (Garanich, Pahakis et al. 2005). Fluid flow also depletes factors secreted by cells that might function as autocrine or paracrine signals. Finally, the durations of typical chemotaxis assays

range from hours to days, periods over which replenishment by continuous flow requires substantial quantities of medium and chemoattractant. While non-continuous flow devices can facilitate stable gradients by creating source and sink wells with volumes much larger than that of the gel region (Abhyankar, Toepke et al. 2008), such devices are still subject to interstitial flow induced by inadvertent fluctuations in the pressure difference between the two wells.

A simple microfluidic approach to create and maintain concentration gradients in a microfluidic device without the use of continuous flow is described here. Source and sink concentrations are maintained by creating corresponding wells whose volumes are large relative to the diffusive flux through the connecting hydrogel channel. Interstitial flow is eliminated by connecting the source and sink wells with additional channels and reservoirs that serve as a resistor-capacitor (RC) circuit. Accordingly, in the RC-Bioreactor, any pressure gradients between the source and sink are dissipated by flow through the low impedance RC network rather than through the hydrogel channel.

2.2 - Methods

2.2.1 - Design of RC-Bioreactor

The Resistor-Capacitor (RC) Bioreactor is composed of 3 regions, an experimental (source) region, a central cell (sink) region, and a control region as shown in Figure 2.4.1. The source and sink wells are separated by a hydrogel-filled channel across which the desired chemoattractant gradient is developed. The source well is connected to the source-reservoir well by a low resistance channel, and the sink well is similarly connected to the sink-reservoir well. Finally, the source-reservoir well and the sink-reservoir well are connected to each other. Solute in the source well may diffuse or be advected via two paths: either through the hydrogel channel or through the reservoir channels. The control region is a mirror image of the source region and serves as an internal control for each experiment. The control

well is connected to the sink well by a gel region but there is not a chemical gradient between the sink and control wells as they are both filled with control/untreated solutions. Thus a control gel region for direct comparison accompanies each experimental gel region on the same chip.

2.2.2 - Fabrication of RC-Bioreactor

The microfluidic devices were fabricated as described elsewhere (Vickerman, Blundo et al. 2008). Briefly, the device design was drawn using the computer aided design (CAD) software SolidWorks and DWGeditor (Dassault Systèmes SolidWorks Corp, Concord, MA). The CAD files were sent to the Stanford Microfluidics Foundry (Palo Alto, CA) for master wafer fabrication. In this process, a transparency photomask was used to cure SU-8 photoresist on a silicon wafer and produce the positive relief of the microfluidic design. The completed wafer underwent silanization in order to facilitate the removal of the replica material. Replica molds were made from liquid polydimethylsiloxane, PDMS, (Sylgard® 184 Silicone Elastomer Kit, Dow Corning, Midland, MI) that was cured at 80 °C for 2 hours. The PDMS chips were removed from the wafer and the wells were formed by punching holes with appropriately sized biopsy punches and needles. The devices were autoclaved, plasma treated (Harrick Expanded Plasma Cleaner, Harrick Plasma, Harrick, CA) and bonded to glass cover slips. Finally, devices were coated with poly-D-lysine (poly-D-lysine hydrobromide, 1mg/ml; Sigma–Aldrich, St. Louis, MO) to promote hydrogel attachment to the PDMS and glass surfaces.

2.2.3 - Loading of Collagen Hydrogel

A prepolymer collagen solution was prepared on ice by combining 10X phosphate buffered saline, 0.5N sodium hydroxide, deionized water and Rat Tail Collagen Type I (BD Biosciences, Franklin Lakes, NJ) to produce a final collagen concentration of 2 mg/ml at pH 7. As shown in Figure 2.4.1, each 1.3 mm long gel channel is connected

to a small gel filling port. Approximately 4 μL of the collagen solution were injected into each gel region through the corresponding gel filling port. Each device was subsequently placed in a humidity chamber at 37 °C for 30 min to allow for collagen gel polymerization. The humidity chambers were assembled from empty pipette tip boxes, containing sterile water. Finally, the devices were filled with PBS or appropriate cells and culture medium.

2.2.4 - Characterization of Concentration Gradients

RC-Bioreactors were filled with PBS. The PBS solution was aspirated from the source well and source reservoir. In a subset of experiments, these ports were then filled with a 25 μg/ml FITC conjugated to a 10 kDa dextran solution. Fluorescent images of the gel region were acquired every 1 hour for 24 hours or every 2 hours for a period of 12 hours daily for 6 days. The data were analyzed using MATLAB (Mathworks, Natick, MA) software. The devices were covered with a glass cover slip to prevent evaporation during the time lapse period.

A device with a gel region whose width expands with distance from the source, Figure 2.4.5 inset, was fabricated to form a non-linear concentration gradient. Similarly to the characterization of the linear device, the wells, reservoirs and channels were filled with PBS and then the source well and source reservoir were filled with a 25 μg/ml FITC conjugated 10 kDa dextran solution. Images were acquired every 2 hours for a total of 12 hours.

2.2.5 Maintenance of Concentration Gradients with Pressure Disturbances

To evaluate the dissipation of pressure gradients, pressure gradients were introduced into devices with and without the bypass channels and reservoirs connecting the source and sink wells. In the device without the bypass channels the source well was filled with a FITC-dextran solution and a gradient was allowed to

develop for 6 hours. At this time an additional 10 μl of the FITC-dextran solution was added to the source well, and images were acquired every 10 minutes for 1 hour. In the device with the bypass channels the source and source reservoir wells were filled with the FITC-dextran and the 10 μl bolus of the FITC-dextran solution was added to the source well.

In a separate experiment the source and source reservoir wells were filled with a 50 μg/ml FITC-dextran (20 kDa) and a 10 μl bolus of the FITC-dextran solution was added to the source well. Fluorescent images were taken of each well in the device before and 5 minutes after the introduction of the bolus. These images were used to calculate the average concentration in each well before and after the introduction of the bolus.

2.3 - Results & Discussion

2.3.1 – RC-Bioreactor Dynamics

In evaluating and predicting gradient formation in the RC-Bioreactor microfluidic device, the two relevant processes affecting the concentration profile are molecular diffusion and advection. Thus the governing mass transport equation is shown below:

$$\frac{\partial M}{\partial t} = -D\nabla^2 M + \vec{v} \cdot \nabla M$$

where M is the concentration, t is time, D is the diffusivity of the solute, and v is the velocity field. The first term accounts for the solute flux due to diffusion down a concentration gradient while the second term is generated by advection of the solute in a velocity field. The velocity field can be determined as a solution to the incompressible Navier-Stokes equation for the open channels. In the RC-Bioreactor, the viscous stresses are of much greater magnitude than the inertial forces, allowing

the inertial forces to be neglected in the analysis. Within the gel regions, the resistance due to the porous collagen scaffold must be included. The result is the Brinkman equation that models viscous flow through a porous material:

$$\mu \nabla^2 \bar{v} - \frac{\mu}{K} \bar{v} - \nabla P = 0$$

where μ is the dynamic viscosity of the media, K is the permeability of the hydrogel, and P is the pressure. Coupling these two equations, one can model the complete behavior of the fluid flow and mass transport in the RC-Bioreactor.

The necessity of the low impedance reservoir channels is illustrated with the finite element model in Figure 2.4.2. Here the device consists of only the source well, the sink well, and the interconnecting gel region. The source well is loaded with 1 mm of hydrostatic pressure (10 Pa), the result of adding 7.06 µl more fluid to the source well than the sink well. The simulation was performed for 1 hour with SDF-1 as the soluble molecule. Initially the concentration in the source well was 100% and the concentration in the gel region and sink well was 0%. The velocity was everywhere zero. The diffusivity of SDF-1 is 1.6×10^{-6} cm^2/s in PBS (Veldkamp, Seibert et al. 2008) which can be assumed to approximate its diffusivity in a 0.2% w/v collagen gel. The permeability, K, of the collagen gel was taken to be 1×10^{-12} m^2 (Wang and Tarbell 2000). After 1 hour the high concentration solution has been convected through the gel as a result of the increased source pressure. Under these conditions, the average velocity in the gel is 6.5 µm/s and the corresponding Peclet number (the ratio of convective to diffusive transport) is approximately 61, demonstrating the dominance of convection.

In order to prevent this convection, the low impedance reservoirs and channels were included to complete the design of the RC-Bioreactor, Figure 2.4.1. Pressure differences between the source and sink wells are dissipated through the reservoir channels much more rapidly than through the gel region. The reservoirs decrease

the change in concentration due to the exchange of fluid between the source and the sink. For instance, if there is more fluid in the source well than in the sink well, the fluid first flows to the source reservoir well, followed by the sink reservoir well, where this small volume needed to eliminate the pressure difference is diluted, before proceeding to the sink well itself. In an analogy to electrical circuits where volumetric flow rate is to electrical current as pressure gradients are to voltage drops, the RC device can be modeled as an arrangement of resistors and capacitors as shown in Figure 2.4.3. Each of the channels in the device impose resistance on fluid flow and determine the flow rate for a given pressure difference. The volumetric flow rate, Q, of a viscous fluid through a channel with a rectangular cross-section is similar to the Hagen-Poiseuille equation for laminar, viscous and incompressible flow:

$$Q = \frac{W_c H_c^3}{12 \mu L_c} \Delta P$$

where W_c, H_c, and L_c are the width, height and length of the channel, respectively and ΔP is the pressure drop along the length of channel. The resistance of the channel, R_c, is the ratio of ΔP to Q (analogous to electrical resistance as the ratio of voltage to current through a resistor) and is given by the expression.

$$R_c = \frac{12 \mu L_c}{W_c H_c^3}$$

In the gel region, the resistance to flow is dominated by the low permeability of the hydrogel. Darcy's Law governs the relationship between pressure and flow rate, their ratio yielding the resistance of the gel region, R_g.

$$Q = \frac{K W_g H_g}{\mu L_g} \Delta P \Rightarrow R_g = \frac{\mu L_g}{K W_g H_g}$$

The wells in the device store fluid volume just as a capacitor stores charge. The capacitance of a capacitor is the ratio of the charge stored in the capacitor and the voltage drop across it. In the wells the relationship between the pressure difference between the top and bottom of the well and the volume of fluid in the well is governed by hydrostatics, $\Delta P = \rho g h$, where ρ is the density of the fluid, g is the acceleration due to gravity, and h is the depth of the fluid. The depth of fluid in the well is determined by the volume of fluid in the well divided by the cross sectional area of the well. The capacitance of a well can then be defined as the ratio of volume to pressure difference,

$$\Delta P = \frac{4\rho g}{\pi D_w^2} V \Rightarrow C_w = \frac{\pi D_w^2}{4\rho g}$$

where V is the fluid volume in the well, D_w is the diameter of the well, and C_w is the capacitance of the well.

Using the values for the various dimensions in Figure 2.4.1, the resistance of each reservoir channel is 6.94×10^{10} kg/m^{4}s, whereas the resistance of the gel filled channel is 2.80×10^{13} kg/m^{4}s, more than three orders of magnitude larger than it would be if the gel were not present. The capacitance of the source and sink wells is 7.21×10^{-10} m^{4}s^2/kg and the capacitance of the source and sink reservoirs is 1.28×10^{-9} m^{4}s^2/kg. In Figure 2.4.3 one of the capacitors contains excess charge/voltage and must dissipate charge to the remaining three. There are two paths through which the current may travel, one containing the three channel resistors and the other containing the gel resistor. This process is analogous to the source well containing excess volume/pressure and dissipating this volume to the other sinks and reservoirs (neglecting the control side of the device). The channel path contains three resistors in series and four capacitors in parallel while the gel path contains one resistor and two capacitors in parallel. The solution to the characteristic equation for the voltage in each capacitor gives the time constant for the system. The time constant, τ_c, for flow through the channel path is on the order of 50 s, and

the time constant, τ_g, for flow through the gel path is 168 minutes. Thus pressure gradients are quickly equilibrated through the channel path, preventing significant source solute convection into the gel.

To confirm the time constant the velocity of suspended cells in the channel between the source and source reservoir well was measured after a 7 µl bolus was added to the source well with a microneedle injector. The measured maximum velocity was 2.03±0.2 mm/s equal to a volumetric flow rate of 0.484 µl/s. At this flow rate the time required for the volume to be distributed throughout the device is approximately 15 seconds. This confirms that dissipation of pressure gradients occurs rapidly through the bypass channels but exhibits a more rapid time constant than had been calculated. The discrepancy is likely due to the momentum of the bolus as it was injected into the well which caused the fluid in the channels to accelerate more rapidly than if the driving force was a hydrostatic pressure difference alone.

2.3.2 - Maintenance of Stable Concentration Gradients

The generation and maintenance of a stable concentration gradient between the source and sink wells is determined by the diffusion coefficient of the biomolecule of interest and the geometry of the device. In Figure 2.4.4a, a 25 µg/ml solution of a 10 kDa FITC-Dextran in PBS was loaded into the source side of the RC-Bioreactor while the sink and control regions were filled with PBS. After 2 hours a linear concentration gradient was present between the maximum concentration at the source well and the minimum concentration at the sink well. The gradient remained constant for the duration of the 24-hour experiment.

The duration of time over which the gradient will remain constant is a function of the dimensions of the source and sink wells and the hydrogel channel as well as the definition of "constant." As the solute diffuses from the source well into the sink

well, the concentration gradient will diminish and eventually vanish entirely. The flux of solute is the product of the diffusion coefficient and the gradient of the concentration field. If, for instance, a "constant" gradient is defined as a gradient in which the source and sink concentrations do not change by more than 5% (a 10% change in the gradient slope), then the gradient formed by an 8 kDa molecule would remain "constant" for more than 2 days. Similarly, the system would require approximately 21 days for concentrations in the source and sink wells to equilibrate completely. These estimates presume that the wells are perfectly mixed but are confirmed by our experimental results. In Figure 2.4.4b the slope of the concentration gradient was measured daily for a period of 6 days. During days 1 and 2 the gradient remains relatively stable. On day 3 the gradient had decayed by ~10% and by day 5 it has decayed further to 80% of the original value. The relative stability of the gradient over several days allows the schedule of medium changes in the device to be dictated by the metabolic requirements of the cells.

By changing the shape of the gel region it was possible to change the profile of the concentration gradient. In a device with an expanding gel region, Figure 2.4.5, the concentration gradient adopts a nonlinear profile, exhibiting an exponential decay with distance from the source region. The gradient developed in less than 2 hours and remained constant for the duration of the 12 hours experiment. The stability of the nonlinear gradient should be similar to that of the linear gradient. This is because the channels and wells (except for the gel region) are identical to those in the linear gradient device, and the average flux through the gel region, determined by the source and sink concentration, is similar to the flux in the gel region with the linear gradient.

2.3.3 - Sensitivity to Pressure Disruptions

A major advantage of the RC-Bioreactor is its ability to dissipate pressure gradients through the low resistance reservoir channels as opposed to transporting fluid

through the hydrogel region. Pressure gradients between the different wells or channels in a microfluidic device are often an inevitable consequence of handling the device during its operation. Fluid volumes must be precisely dispensed in and out of the device to prevent volumetric imbalances and hydrostatic pressure differences. These hydrostatic pressure differences result in fluid flow between adjacent wells. If this fluid flow occurs in the gel channel the concentration gradient will be disrupted. Pressure differences can also be caused by inadvertent tilting of the device which places one well at a higher gravitational potential relative to other wells.

While the stable concentration gradient is not affected by incidental pressure gradients created during the initial loading of the device (Figure 2.4.4), we also explored the effect of more substantial pressure gradients on the soluble profile in the hydrogel. First this process was characterized in a device without the bypass channels connecting the source and sink wells. This device contained only a source well and a control well each connected to the sink well through a gel region. The device was loaded with a 25 μg/ml solution of 10 kDa FITC-Dextran in the source well, and a linear gradient was allowed to develop for 6 hours. At that time (t = 0), an additional 10 μl bolus of dextran solution was added to the source well creating a hydrostatic pressure difference between the source and sink wells, Figure 2.4.6. The concentration profile in the gel region was immediately disrupted as the FITC-dextran solution was convected through the gel in order to eliminate the pressure gradient. The concentration gradient was almost completely abolished as the concentration became relatively constant throughout the gel. After 6 hours the concentration gradient had not returned to a linear profile confirming that the time scale to for the system to reach equilibrium is on the order of hours as estimated above.

This experiment was repeated in the RC-Bioreactor with the channels and reservoir wells connecting the source and sink wells. Both the source well and source

reservoir well were filled with the FITC-dextran solution. After the linear gradient had developed a 10μl bolus of dextran solution was added to the source well. The concentration profile in the device did change immediately, as noted by comparing the initial and *t=0* curves in Figure 2.4.7a. However only a small fraction of the additional solute was convected through the gel region, while the majority of the bolus was transported through the reservoir channels. As a result, within 10 minutes of the bolus introduction, the concentration gradient within the hydrogel has returned to a stable, linear profile.

To investigate how the flow through the bypass channels affects the concentration in the different wells the concentration in each well was measured before and after a 10μl bolus was injected into the source well and the pressure gradients were eliminated, Figure 2.4.7b. The largest concentration change occurred in the sink reservoir well which receives high concentration fluid directly from the source reservoir well. The sink well did not experience a significant concentration change because any high concentration fluid that reaches the sink well is first diluted in the sink reservoir well. This dilution also occurs with the control reservoir and control wells, and their concentrations do not change after the introduction of the bolus.

2.4 – Figures
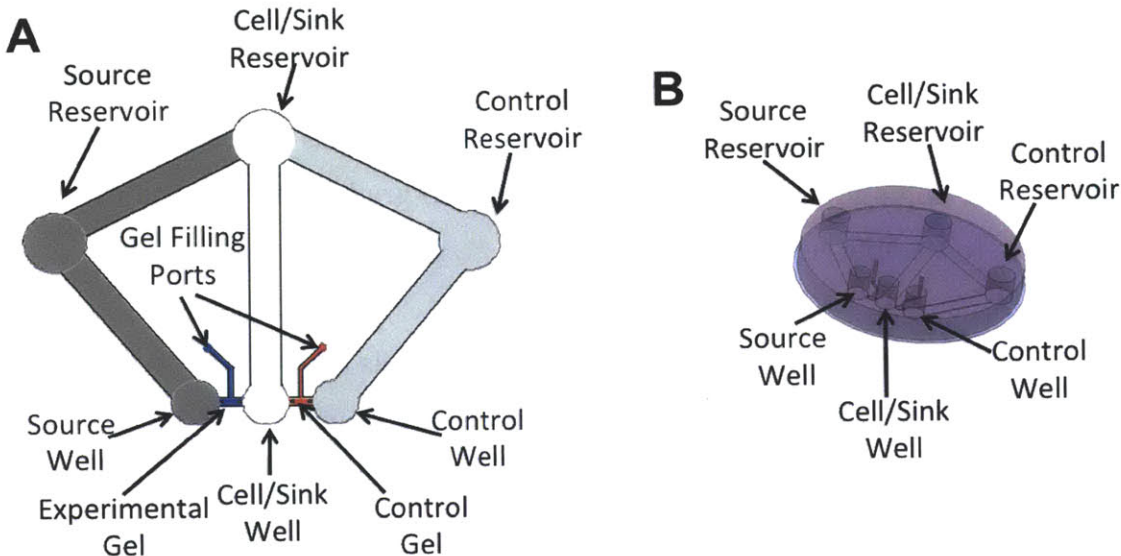
Figure 2.4.1 – RC-Bioreactor Schematic

(a) A schematic representation of the RC-Bioreactor in 2 dimensions. The unshaded channels represent the sink and sink reservoir. The dark shaded region represents the source and source reservoir/channel as well as a channel connecting the source and sink reservoirs. The lightly shaded region is the mirror image of the dark shaded source region and serves as an internal control for each experiment. The blue region is the location of the hydrogel in which the relevant concentration gradient forms, and the red region is the analogous control hydrogel. The chemical species of interest is placed in the source well and source reservoir. The remainder of the device is filled with a control solution. (b) A 3D representation of the RC-Bioreactor constructed from PDMS and bonded to a glass coverslip. The diameter of the source, sink, and control wells is 3 mm, and the diameter of the source, sink , and control reservoirs is 4 mm. The hydrogel channels are 1.5 mm long, 0.6 mm wide, and 0.120 mm tall. The remaining channels are 20 mm long, 2 mm wide, and 0.120 mm tall.
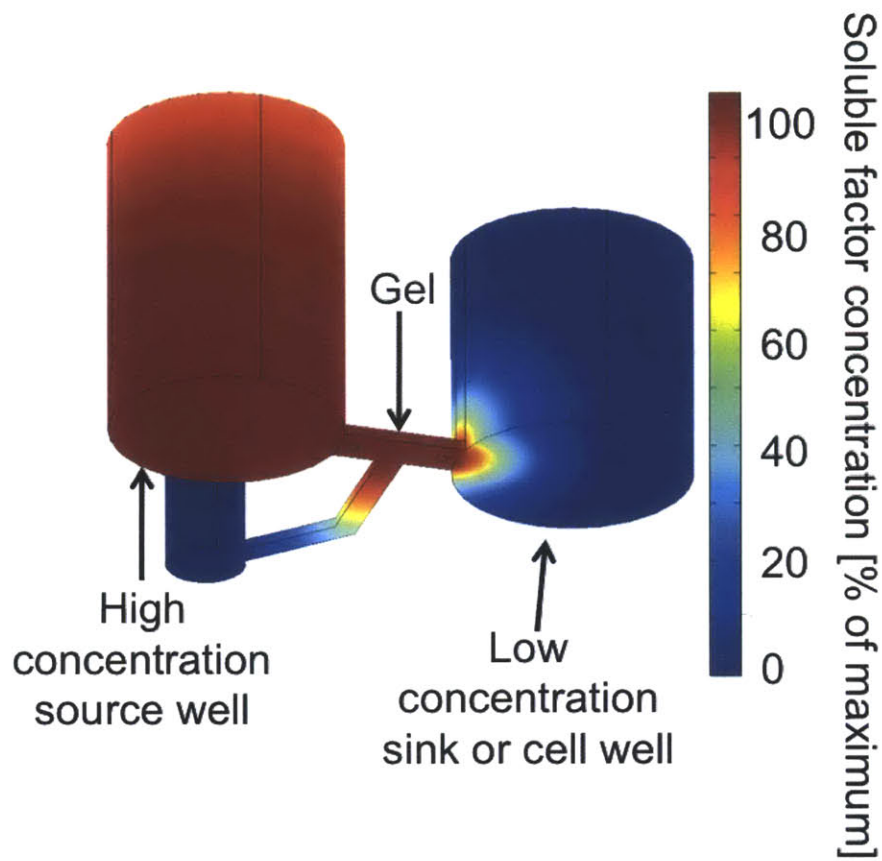
Figure 2.4.2 – Pressure Gradients Disrupt Concentration Gradients Between Source and Sink Wells

Initially the gel region and the sink well did not contain any solute. The high concentration source well was loaded with a 1mm hydrostatic pressure difference relative to the sink well. Without the low resistance circuit the pressure difference must be dissipated via fluid flow through gel region. This fluid flow is accompanied by convection of the solute into the gel. The solute is modeled as SDF-1 with a diffusivity of 1.6×10^{-6} cm^2/s and the permeability of the gel region is 1×10^{-12} m^2. The simulation was executed for 1 hour.
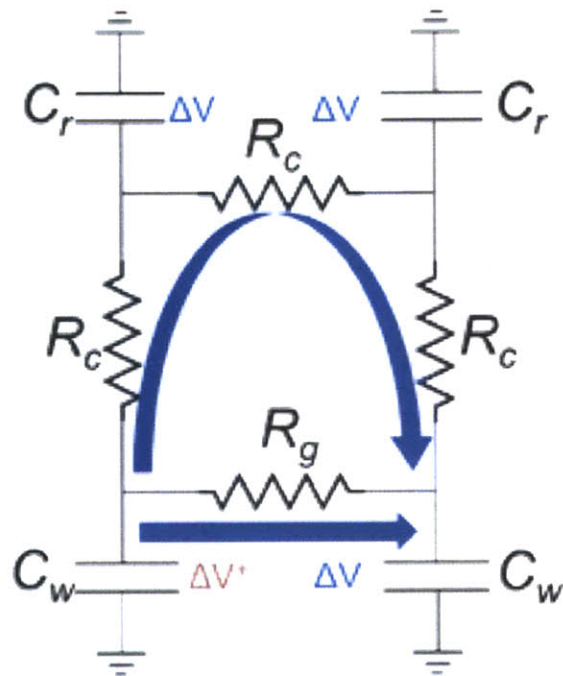
Figure 2.4.3 – Electrical Circuit Analogy
An analogous RC electrical circuit can be used to depict how the low resistance channels dissipate pressure gradients more rapidly than the high resistance gel region. . Movement of that fluid volume is volumetric flow just as the movement of charge is current. Wells store volume as capacitors store charge, and channels resist the flow of volume just as resistors resist the flow of charge. In this circuit the sink and source well capacitors are separated by the gel resistor, and voltage differences between the two capacitors will result in current through the gel resistor. The resistor and capacitor in series actually serve as a low-pass filter with a time constant on the order of hours. However by adding additional resistors and capacitors in parallel (resistors are open channels with much less resistance to fluid flow than the hydrogel filled gel channels and capacitors are wells), the signal is filtered further and provides a path with a time constant on the order of seconds through which fluid can flow in order to equalize pressures.
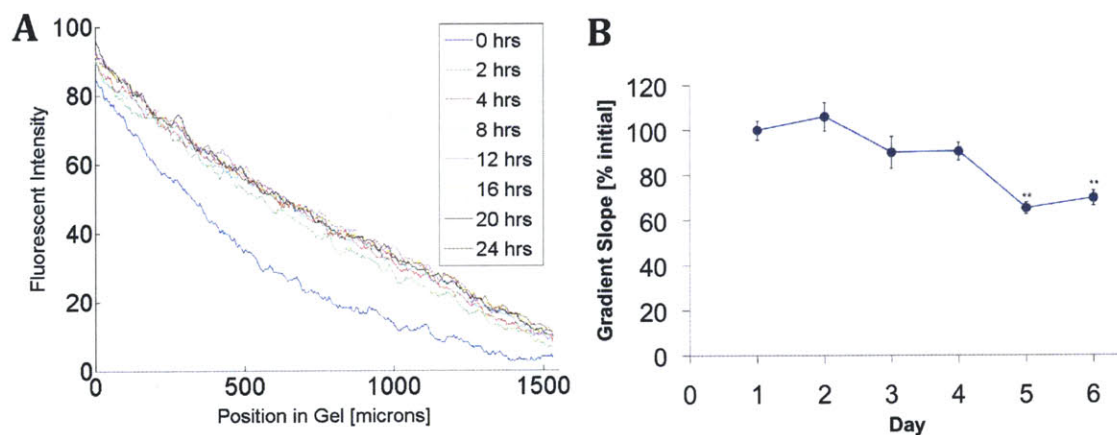
Figure 2.4.4 – Stable Concentration Gradients in the RC-Bioreactor

(A) A 10 kDa FITC-dextran molecule was used to model the diffusion of a similarly sized protein such as SDF-1. The dextran solution (25 µg/ml) was loaded into the source well and source reservoir. The sink well, control well, sink reservoir, and control reservoir were filled with PBS. The device was placed on a fluorescent microscope and images were acquired every hour (representative time points shown) for 24 hours. To prevent evaporation the device was covered with a glass cover slip during image acquisition. Within 2 hours a linear concentration profile is achieved in the gel region and maintained for the duration of the experiment. (B) The dextran gradient was tracked over the course of 6 days and the average slope of the concentration profile is shown for each day. The slope remains constant for the first 48 hours and on day 3 the slope has decayed by 10%.
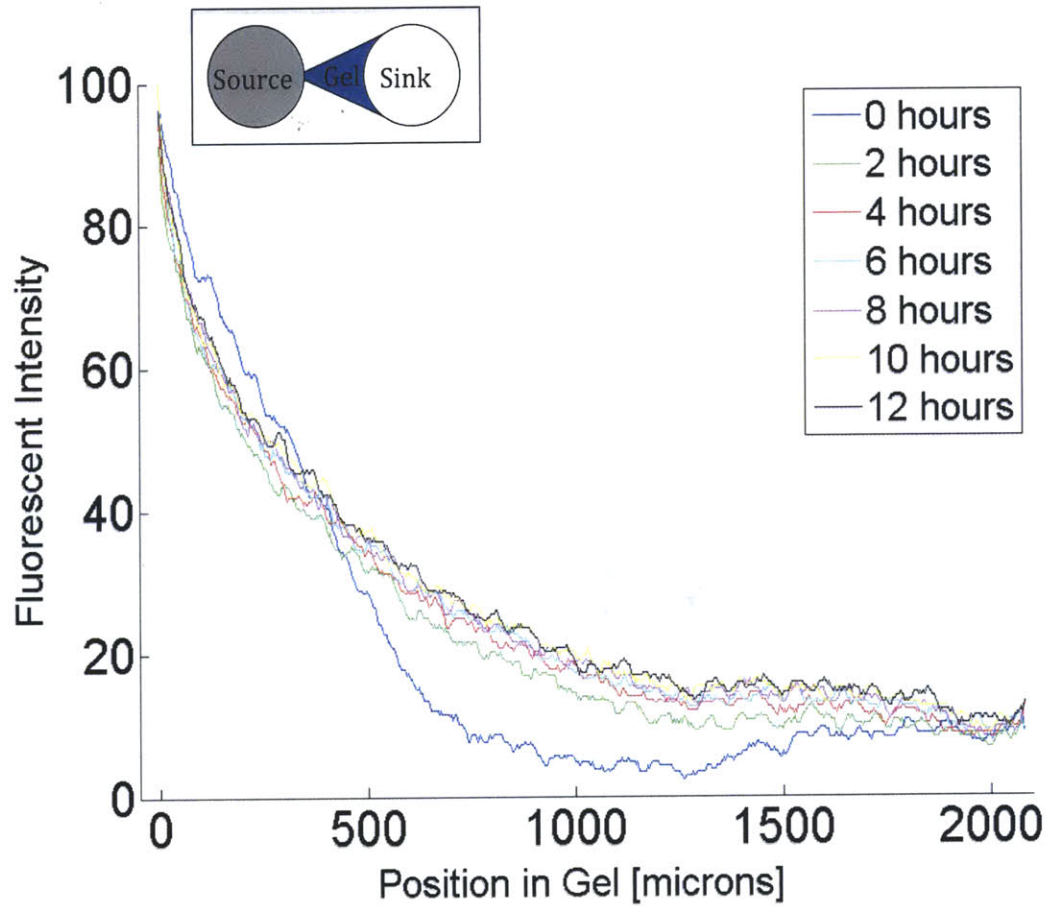
Figure 2.4.5 – Exponentially Decaying Gradient in Modified RC-Bioreactor
By changing the geometry of the gel region (as shown in the inset) a non-linear concentration profile with an exponential dependency was achieved in the RC device. Fluorescent images were acquired every 2 hours for 12 hours.
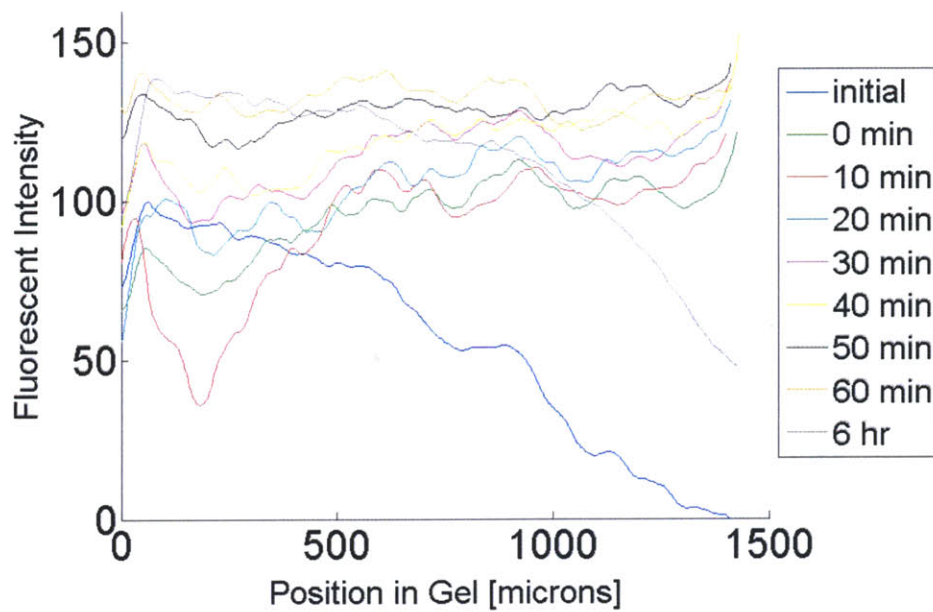
Figure 2.4.6 –Pressure Differences in the Absence of RC Bypass Channels

In a device without the low resistance bypass channels (consisting of only the source, sink, and control wells connected by 2 hydogels) a gradient was allowed to develop across the experimental gel region for 6 hours by placing a 25 μg/ml FITC-dextran solution in the source well. Then 10 μl of the dextran solution was added to the source well and the gradient was imaged every 10 minutes for an additional hour. The gradient was disrupted and after 6 hours did not return to its original profile.
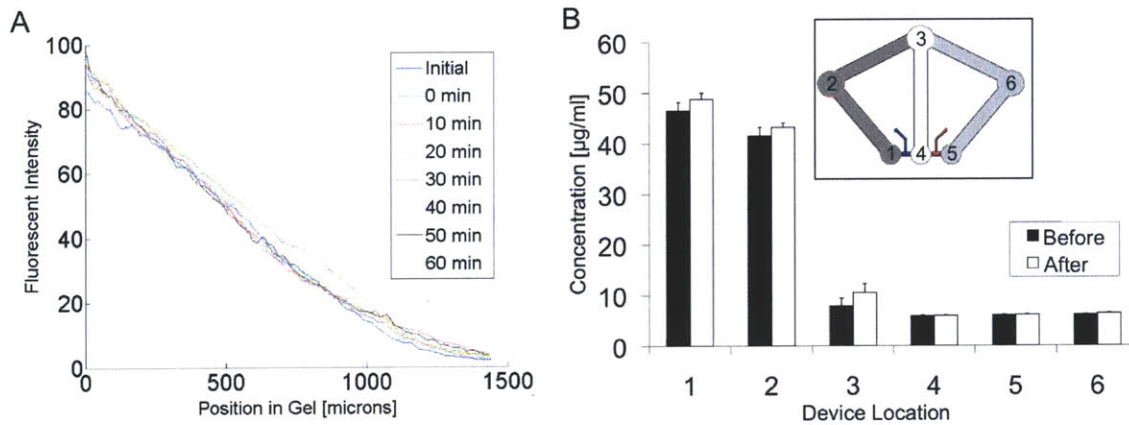
Figure 2.4.7 - Equilibration of Pressure Differences in RC-Bioreactor

(A) In the RC-Bioreactor with the bypass channels, although the concentration profile changed slightly with the addition of a 10µl bolus to the source well, within 10 minutes the gradient returned to a linear profile. Images were acquired every 10 minutes for 1 hour after the introduction of the bolus. (B) The source well and reservoir were filled with a 50 µg/ml solution of FITC-dextran and the concentrations in all of the wells and reservoirs were measured before and after the addition of a 10 µl injection into the source well. The sink reservoir (location 3) experiences the greatest concentration change while the concentrations in the sink well, control well, and control reservoir remain relatively unchanged.

CHAPTER THREE: CHEMOTAXIS IN RC BIOREACTOR

3.1 - Introduction

Previous efforts confirmed that gradient generation within the RC Bioreactor rapidly achieved linearity, decayed over a sufficiently long timescale, and exhibited resistance to hydrostatic pressure perturbations. Gradient validation enabled a series of proof-of-concept experiments to validate the system's ability to replicate chemotactic responses *in vitro*. To assert suitability in the context of multiple forms of 3-D migration, cells were chosen to represent three different classes of migration. Vascular smooth muscles cells are mesenchymal cells, typically located within extracellular matrix components capable of fibroblast-like migration. Jurkat T-lymphocytes may exhibit features of both malignant cell types and plasma cells such as the neutrophil. Finally, bovine aortic endothelial cells are noted for epithelial-basement membrane interactions and collective cell migration as in angiogenesis.

Successful chemotaxis in these cell types suggested that hypothesis based experiments without known ligand-cell chemotactic partners might be possible. Satellite cells are a population of progenitors within skeletal muscle capable of contributing to newly generated myocytes in response to tissue damage. While many pathological and traumatic processes may result in acute muscle damage, contraction induced damage, and/or inflammatory myopathies, suitable recovery often lacks complete or rapid muscle regeneration (Tabebordbar, Wang et al. 2013). The search for effective therapies targeting skeletal muscle regeneration is ongoing and satellite cells, expressing the chemokine receptor CXCR4, are a promising candidate for stimulating endogenous muscle repair (Ratajczak, Majka et al. 2003). CXCR4 and its ligand, stromal-derived factor 1 (SDF-1), are expressed in many progenitor cells and are implicated in recruitment of stem cells during development and regeneration (Miller, Banisadr et al. 2008). The SDF-1/CXCR4 axis may

represent a therapeutically relevant approach to improve skeletal muscle repair by enhancing the recruitment and/or proliferation of resident satellite cells, thus motivating the pairing of skeletal muscle tissue and SDF-1 gradients in the RC Bioreactor.

3.2 – Methods

3.2.1 Cell Migration Assays

Vascular smooth muscle cells (VSMC's) were cultured in Dulbecco's Modified Eagle Medium (DMEM) supplemented with 1% penicillin/streptomycin, 1% L-glutamine and 10% fetal bovine serum (FBS). Bovine aortic endothelial cells (BAEC's) were cultured in DMEM supplemented with 1% penicillin/streptomycin and 10% FBS. Jurkat T lymphocytes cells were cultured in suspension with RPMI-1640 medium supplemented with 1% penicillin/streptomycin and 10% FBS. Immediately after the collagen gel polymerization, devices were filled with PBS to prevent any air bubble formation around the gel region. The PBS was aspirated from the device and the sink well was filled with 40 µL of a cell suspension at a concentration of 1×10^6 cells/ml. 10 µL of media were placed in the source and control wells to create a pressure gradient and thus interstitial flow from the sink well into the source well. This flow caused the cells to accumulate on the surface of the collagen gel. The devices were incubated for 3 hours at 37 °C in order to allow the cells to adhere to the collagen surface. The medium within the source and source reservoir wells was replaced with medium supplemented with PDGF-BB (4nM), VEGF (0.1 and 1.0 nM), or SDF-1 (1.0 and 10 nM). The sink and sink reservoir wells were filled with un-supplemented control medium. To prevent evaporation without limiting gas exchange with the environment, devices were incubated in a high humidity chamber at 37 °C and media was changed daily. After 48 hours the devices were fixed with 4% paraformaldehyde and stained with DAPI. Fixing and staining were performed overnight to allow the PFA and DAPI molecules to diffuse throughout the gel region.

Images of both the experimental and control gel regions were acquired at 10X magnification.

3.2.2 Explant Migration Assay

Skeletal muscle explants were harvested from anterior tibialis muscles of C57Bl6 mice. Following euthanasia, mice were perfused with 10ml of DMEM and sterilely isolated muscles - freed of fascia, nerves and tendons - were placed on ice in DMEM as well. Mincing of tissue produced explants with diameters of approximately 1-1.5mm which were suspended in the cell/sink well of poly-d-lysine coated modified-RC-Bioreactors. Modification included the removal of the two gel region support posts adjacent to the cell well. Matrigel was injected bilaterally through the gel filling ports, flowed into the cell well and surrounded the explant. Following incubation at 37°C for 20 minutes, devices were filled with DMEM supplemented with 10% FBS, 10 mM HEPES, and 1% penicillin/streptomycin. The location of source wells and reservoirs were randomly assigned in each device and media therein was supplemented with 200 nM SDF-1. Media were changed every two days and cells were fixed and stained on day 5.

3.2.2 Data Analysis

The location of each cell in each gel region was stored and categorized into bins at 100 μm increments into the gel. With sufficient magnification individual cells could be identified manually. When cells were closely crowded and difficult to distinguish from one another the manual identification tended to underestimate the number of cells, biasing the result toward the null hypothesis. In the VSMC (N=4) migration assay the bin data for the experimental and control regions were averaged and compared using a Student T-test. In the BAEC (N=5) and Jurkat (N=4) assays, the control bin data were first subtracted from the experimental bin data from each device. The scaled data were averaged for each concentration and compared using

Student's T-test. Data were further analyzed using the Bonferroni correction for multiple comparisons.

3.3 - Results & Discussion

3.3.1 VSMC migration toward PDGF-BB

Platelet derived growth factor has been shown to induce chemotaxis of vascular smooth muscle cells in vitro (Bornfeldt KE 1994). Figure 3.4.1 shows the comparison of migration of VSMC's toward a 4.0 nM solution of PDGF-BB versus a control. The images have been reoriented such that in both the PDGF-BB and control cases, the direction of migration toward the PDGF-BB (or control) well is from left to right.

While is it clear that the response to PDGF-BB is greater than that of the control, it is difficult to comment definitively on the relative number of migrating cells and the distance these cells have migrated solely from the images. A single metric could be calculated to describe the chemotactic response but some information regarding the complete cell distribution would likely be lost. Figure 3.4.1 uses a histogram approach to compare the number of VSMC's which have migrated a given distance into the gel regions. At each distance, there were more cells present in the PDGF-BB gel region than at the corresponding distance in the control gel, achieving statistical significance in the 0-100 and the 100-200 μm ranges before the Bonferroni correction. In both cases the number of migrating cells decreased as one moved farther into the gel.

3.3.2 Jurkat T lymphocyte and endothelial cell chemotaxis

In addition to comparing migration toward a chemoattractant versus a control, we used RC-Bioreactor to quantify a dose response for a single factor. Figures 3.4.2 and

3.4.3 compare the migration of Jurkat T Lymphocytes toward a known chemoattractant SDF-1 (Hesselgesser, Liang et al. 1998) at two different concentrations, 1 nM and 10 nM, as well as the migration of bovine aortic endothelial cells to VEGF-A (Vernon and Sage 1999) at concentrations of 0.1 nM and 1 nM, respectively. Both cell types exhibited a dose-dependent chemotactic response, but cell-type differences in migratory patterns are observed. The Jurkat cells exhibited a similar response to the VSMC's in that the number of cells at each location decreases with increasing distance into the gel. In contrast, the maximal endothelial response occurs at an intermediate value, 400-600 µm. Both the high and low VEGF-A concentrations induced endothelial cells to migrate a short distance into the gel – the major difference between the responses occurring at an intermediate distance in the gel where there were markedly more cells in the high concentration case. The endothelial cells migrated as single cells and did not form tube-like structures as they entered the gel. This behavior is likely a result of the short time period in which the cells were allowed to form cell to cell contacts and organize into a monolayer before the chemotaxis assay began.

Media in the devices were replenished daily, but this process does not have a profound effect on the gradient and cell behavior for at least two reasons. First, during the brief time during which the source or sink well is empty the pressure difference will cause flow primarily through the bypass channels as was the case after the 10 µl bolus injection. Second, as shown in Figure 2.4.7, even if the gradient is disrupted during the media loading process the profile will return to a steady state value in less than 2 hours.

3.3.3 - Skeletal Muscle Tissue Explant

Although previous experiments were performed with homogenous populations of cultured and isolated cell lines, such protocols may present significant artifacts into experimental protocols. Namely isolation procedures may result in un-pure cell

populations and the physical and chemical requirements of isolation may adversely affect viability or induce undesirable cellular responses. Moreover, introducing primary cells into tissue culture conditions may result in dedifferentiation, loss of differentiation potential, or altered gene expression each of which may be inconsistent with conditions *in vivo* (Proudfoot and Shanahan 2012). The acquisition of tissue samples in a minimally aggressive manner more favorably reflects *in vivo* cell behavior and holds greater promise for therapeutic translation. Such considerations suggested that satellite cell biology, in which cells reside between skeletal muscle sarcolemma and basement membranes, would be conducive to explant culture rather than serial-digestion based isolations (Pasut, Jones et al. 2013).

Normally in the RC-Bioreactor, the ends of each gel region feature a square post extending from the glass bottom surface to the PDMS ceiling. As the pre-polymerized gel is added to the device, adhesion to the post and surface tension within the fluid present a barrier to flow beyond the confines of the gel region and into the adjoining wells. Because nutrient transport limited the size of the explant to approximately 1-2 mm^3, a single explant was incapable of positioning adjacent to the two gel regions on either side of the cell well. Placing the explant in the center of the well, however, would require cells to migrate on the 2-dimensional glass surface before entering the gel. Moreover chemotaxis would only be possible among cells adjacent to the glass surface rather than throughout the explant surface area. Eliminating the two posts proximal to the cell well allowed the pre-polymer solution, in this case the Matrigel™ basement membrane matrix, to flow beyond the gel region and bilaterally engulf the tissue explant. Modeling of the SDF-1 gradient within this continuous gel region indicated the presence of a shallow gradient adjacent to the explant (Figure 3.4.4), thus necessitating larger source well concentrations (200 nM) an order of magnitude greater than typically employed with Jurkat T-lymphocytes.

In response SDF-1 gradients, cells emanating from skeletal muscle explants preferentially migrated in the direction of an ascending SDF-1 gradient, Figure 3.4.5. Compared to the control case, in the absence of SDF-1 gradients, 50% of cells migrated to toward either gel region exhibiting a 1:1 non-preference for either direction. In the presence of 200 nM SDF-1 source gradients 66.15 ± 0.07% of cells were located outside of the explant in the direction of the SDF-1 gradient. AMD3100, a potent antagonist of CXCR4, abolished the preferential migration toward SDF-1 when included in culture media. In the presence of AMD3100 50.64 ± 0.11% of cells migrated toward SDF-1, effectively exhibiting the same 1:1 response of the control setting without SDF-1 gradients. Interestingly migrating cells adopted a tubular morphology and appeared to fuse into multinucleate bodies, indicative of myoblast fusion during myogenesis (Capers 1960). Although molecular characterization of migrating/differentiating cell is ongoing, these results confirm the chemotactic potential of SDF-1 in the context of skeletal muscle explants.
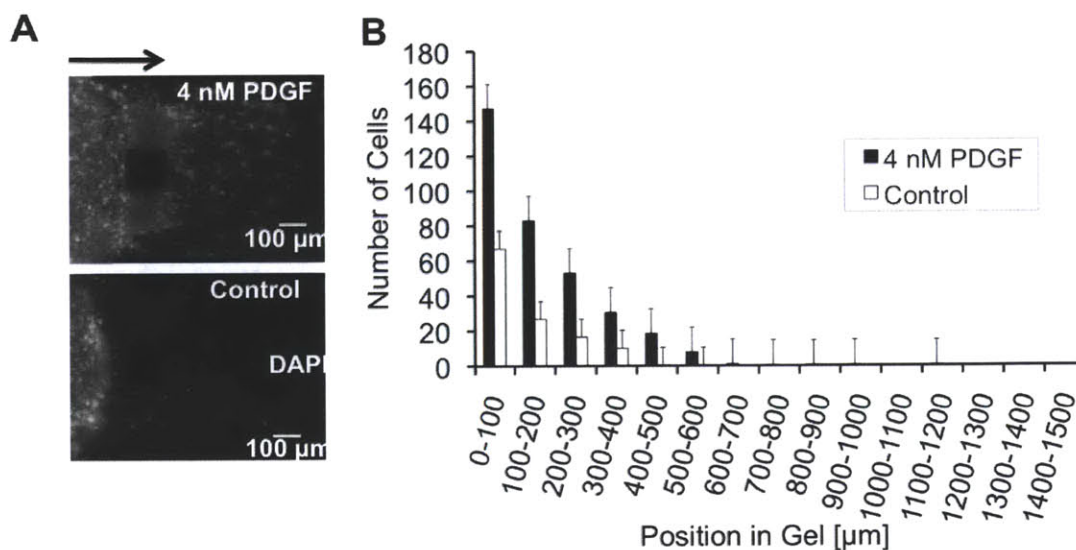
Figure 3.4.1 – Migration of Vascular Smooth Muscle Cells in RC-Bioreactor

Vascular smooth muscle cells were loaded into the sink well of the RC-Bioreactor and media supplemented with 4 nM of PDGF-BB was added to the source well and reservoir. The sink and control wells and reservoirs were filled with control media. (A) Migration of vascular smooth muscle cells from left to right toward 4 nM PDGF-BB and the matching control from a sample device. (B) Comparison of migration toward PDGF-BB vs control. The number of cells at each location decreases with increasing distance into the gel. A particularly marked difference between the PDGF and control gels is observed in the first 200 μm of the gel region. n = 4. 10X, arrows indicate direction of migration.
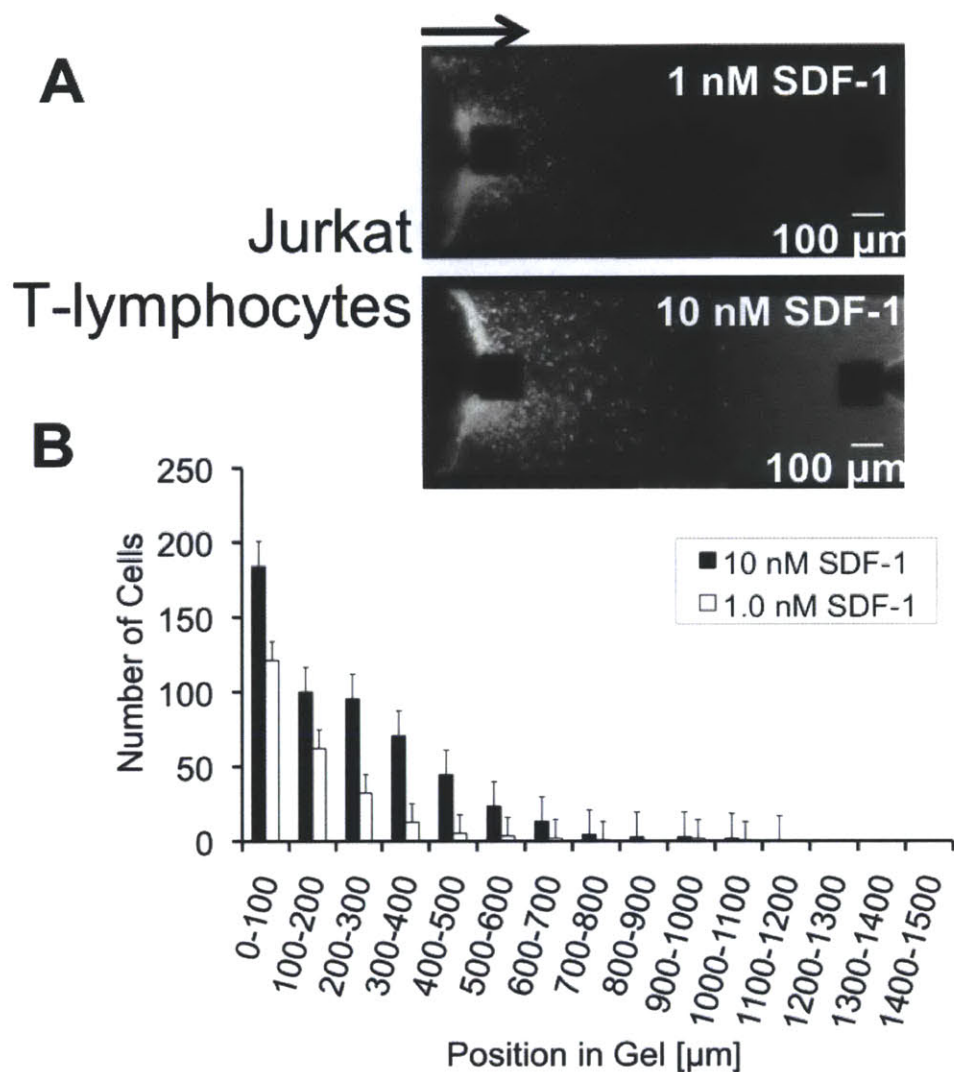
Figure 3.4.2 – Dose Dependent Migration of Jurkat T-Lymphocytes in RC-Bioreactor
(A) Migration of Jurkat T lymphocytes from left to right toward a 1 nM solution of SDF-1 and a 10 nM solution of SDF-1. (B) Dose response of Jurkat T lymphocyte migration toward SDF-1 concentrations. 10X. White = DAPI, Arrows indicate direction of migration.
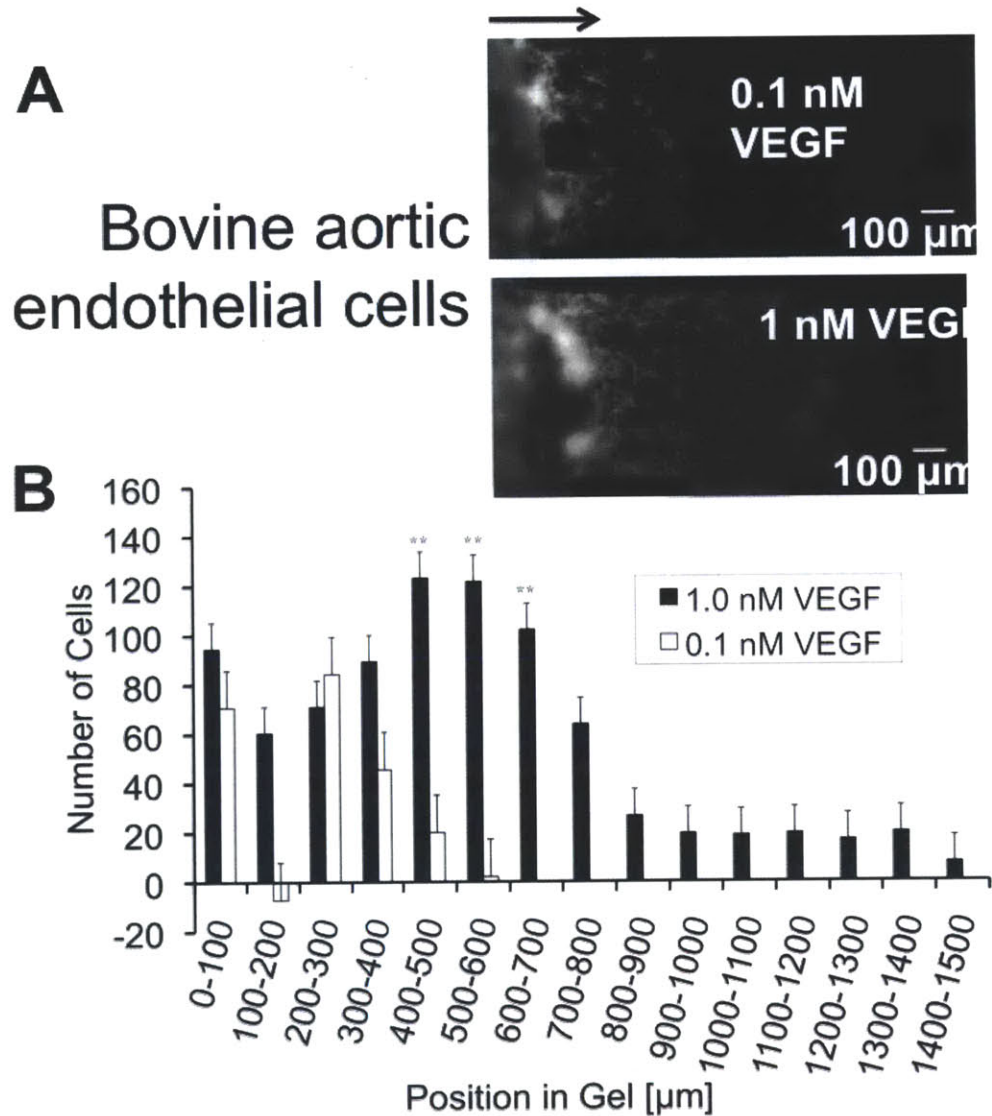
Figure 3.4.3 - Dose Dependent Migration of Bovine Aortic Endothelial Cells in RC-Bioreactor

(A) Migration of bovine aortic endothelial cells from left to right toward a 0.1 nM solution of VEGF and a 1 nM solution of VEGF. (B) Dose response of migration of bovine aortic endothelial cells toward VEGF concentrations. 10X. White = DAPI. ** P < 0.01, arrows indicate direction of migration.
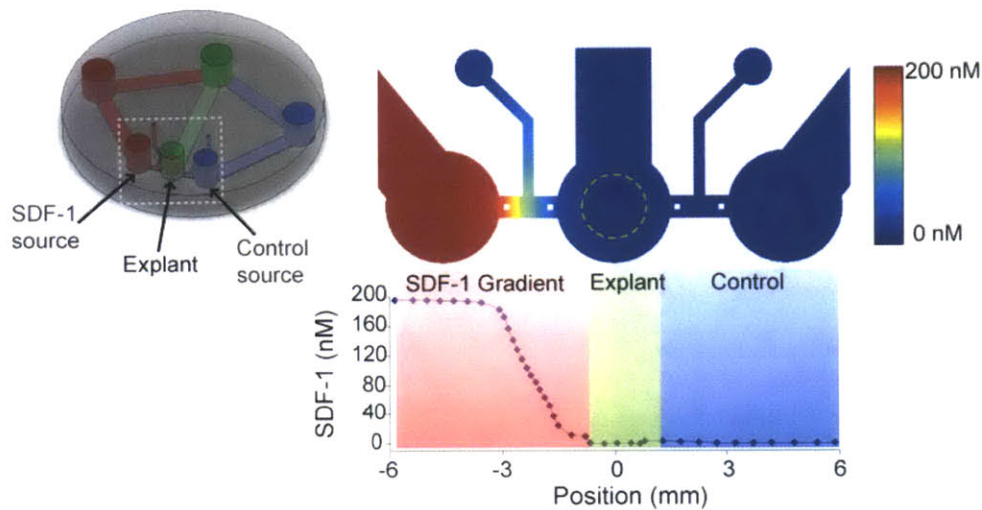
Figure 3.4.4 – Concentration Gradients in Explant Migration RC-Bioreactor
(Left) – The skeletal muscle explant, approximately 1-1.5mm in diameter, is placed in the cell/sink well of the modified RC-Bioreactor. The red shaded channels represent the presence of chemoattractant, while the blue channels serve as an internal control. (Right) – A finite element model of diffusion in the modified RC-Bioreactor (magnified diagram of boxed region on the left). The explant is located within a continuous gel spanning both the experimental and control gel channels. The modeled SDF-1 gradient decays from the source well to a shallow slope adjacent to the explant (dashed circle). Opposite the SDF-1 gradient, the control gel has a nearly uniform and zero chemoattractant concentration.
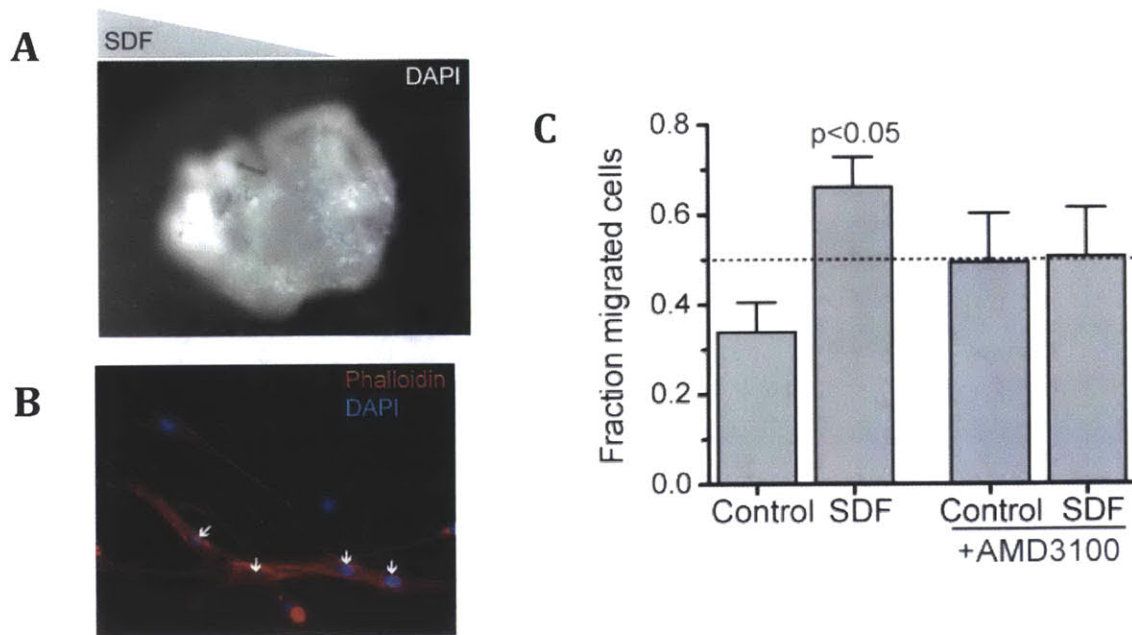
Figure 3.4.5 – Satellite Cell Migration to SDF-1 in RC-Bioreactor
(A) Skeletal muscle explant in the RC-Bioreactor sink well with an increasing SDF-1 gradient to its left. Nuclear staining reveals an abundance of cells to the left of the explant indicating migration toward the SDF-1 source. (B) Actin staining suggests cells emanating from the explant may be fusing into multinuclear aggregates, a process that is known to occur in differentiating myoblasts. (C) Quantification of migrating cell preferences in the modified RC-Bioreactor. Cells preferentially migrate toward SDF-1 as opposed to control wells when explants are exposed to a 200nM SDF-1 source gradient. AMD3100 abolishes this preferential migration confirming an SDF-1/CXCR4 dependent mechanism.

CHAPTER FOUR: 2D GRADIENT BIOREACTOR

4.1 - Introduction

Microfluidic technology and the dissemination of soft lithography fabrication have ushered in a new wave of approaches. These techniques feature chemotaxis in two and three dimensions, under continuous fluid flow, in the presence of linear and non-linear gradients, and spanning time lengths from hours to days at a time (Lin and Butcher 2006; Li, Chen et al. 2007; Keenan and Folch 2008; Zervantonakis, Chung et al. 2010). More recently competing and moving gradients have been created to study the integration of and adaptation to multiple signals (Brett, DeFlorio et al. 2012).

Morphogenesis, however, primarily in the context of development, has been primarily studied through *in vivo* genetic models while few *in vitro* models of gradient induced patterning have been developed (Park, Kim et al. 2009; Amadi, Steinhauser et al. 2010). While exposing cells to a single gradient might demonstrate concentration dependent gene expression in response to a single molecule, understanding how additional molecules might influence this behavior demands a more sophisticated approach. To this end, a new microfluidic system is described and characterized - capable of maintaining concentration gradients along orthogonal vectors in a single plane. In the 2D Gradient (2Dg) Bioreactor device, cells are exposed to combinatorial gradients, mutually superimposed and perpendicularly aligned.

The gradients exist in 2.5 dimensions, where the concentration field is uniform in a limited "third" dimension, but cell growth occurs in a three dimensional matrix of extracellular matrix components. This device enables two broad classes of experimental approaches. First, two morphogen gradients may be orthogonally

situated in a uniform or heterogeneous field of cells. As an enhanced surrogate to a high-throughput multi-well plate approach, multiple combinations of two morphogens exist in a single chip. Furthermore, each individual sub-region, as defined by the unique combination of molecular concentrations, is physically juxtaposed to and chemically communicating with adjacent sub-regions enabling emergent paracrine signaling and/or migration. In the second class, chemotaxis, stimulated by competing gradients may be induced on a localized or diffuse population of cells.

4.2 – Methods

4.2.1 – Device Fabrication

The 2Dg-Bioreacor was fabricated in a manner similar to the RC-Bioreactor described in Sections 2.2.2 and 2.2.3. A few departures from this established protocol, however, were necessary. First, wafers (Stanford Microfluidics Foundry, Palo Alto, CA) featured etching depths of approximately 250μm which produced taller channels in the 2Dg-Bioreactors. 2Dg devices were also thicker, approximately 15mm, in order to accommodate various connections between the device and plastic tubing necessary for continuous flow. Following plasma treatment, devices were bound to Corning® plain glass microslides, 50 x 75mm, and then coated with poly-d-lysine. Collagen hydrogels were introduced into the 2Dg-Bioreactor through each for four gel filling ports. The pre-polymer solution was injected sequentially through each port until fluid entered the central square region and the entire gel region was contiguously filled.

4.2.2 – Gradient and Flow Characterization

After collagen polymerization, 2Dg devices were filled with approximately 200μl of phosphate-buffered saline (PBS, pH 7.4) by wedging a pipette into the output well

and back-filling the four input wells. In order to prevent evaporation or convection through the gel filling ports, four sterile 5mm diameter glass cover slips (Warner Instruments, Hamden, CT) were plasma treated and bound to the top surface of each device, sealing each port from ambient communication. Flow was established using positive pressure or negative pressure. In the positive pressure setup, four 25ml glass gastight syringes (Model 1025 TLL, Hamilton Company, Reno, NV) were filled with appropriate solutions and loaded into a standard PHD Ultra infuse/withdraw syringe pump (Model 703006, Harvard Apparatus, Hollistion, MA). Tygon PVC tubing, 1/16" inner diameter, (McMaster-Carr Supply Company, Elmhurst, IL) with 14 gauge Type 304 stainless steel blunt needles (McMaster-Carr) as interconnects were connected to syringes and forward filled to dispel air form the tubing. Male luer lock plastic was removed from 14 gauge blunt needles in order to mate the tubing with the four 2Dg inlet wells. The same tubing and interconnects were used to connect the outlet well to a plunger-less 25ml plastic syringe collection reservoir (BD Biosciences, Franklin Lakes, NJ). Syringe pump infusion drove fluid through the tubing and device and into the collection reservoir.

In the negative pressure protocol, 3ml plastic syringes (BD Biosciences, Franklin Lakes, NJ) were connected directly to the four inlet wells with 14 gauge blunt needles. A single, large plastic syringe was filled with PBS, loaded into the syringe pump, and connected to Tygon tubing. After discharging air from the tubing, it was attached to the 2Dg outlet well. Each inlet syringe was filled with the appropriate solutions, which were then drawn through the device and into the syringe by operating the syringe pump in withdraw mode.

Fluid profiles were observed in devices by suspending fluorescent 1μm polystyrene microspheres (Life Technologies, Carlsbad, CA) in PBS and imaging channels with a high shutter rate camera. Gradients were visualized by loading appropriate inlet syringes with 50mg/ml fluorescein isothiocyanate or rhodamine B isothiocyanate conjugated dextran, average molecular weight 10kDa, (Sigma Aldrich, St. Louis, MO).

After initiating flow within the device, images were acquired at 1.25X magnification and analyzed with MATLAB software (Mathworks, Natick, MA).

4.3 - Results & Discussion

4.3.1 – Design and Operation

The design of the 2Dg-Bioreactor is shown in Figure 4.4.1. Four channels with separate inlets and a common outlet surround a cross-shaped gel region, bounded by support posts. Depending on the fluid composition in each of the four channels, gradients are formed across the gel region as shown in the finite element model in Figure 4.4.2. Fluid within each channel specifies the concentration boundary conditions in the North, South, East and West wings of the gel via direct physical communication. The gradients or non-gradients in each of the four wings determine the four boundary conditions along the edges of the square central gel region. Thus a horizontal gradient in species A is formed by placing a high concentration of species A in channels 1 and 3 and a low concentration in channels 2 and 4. The North and South wings develop species A gradients while the West wing features a uniform, high concentration profile and the East wing is uniformly low. The western border of the central square is thus given a high concentration boundary condition and the eastern border a low concentration boundary condition. Diffusion from the West wing to the East wing produces a horizontal gradient within the central square. Simultaneously, the gradients within the North and South Wings establish a linear gradient boundary condition along the north and south borders of the central square preventing the vertical skewing of the horizontal west-to-east flux.

In order to create a superimposed gradient in species B in the central square, high and low concentrations of species B are included in channels 1 & 2 and channels 3 & 4, respectively. B gradients, decreasing from north to south, form in the West and East wings, the North wing is uniformly high, and the South wing is uniformly low. As with species A, the boundary conditions along the central square are

66

appropriately specified such that a uni-directional flux of B occurs from north to south with the concomitant production of a gradient perpendicular to the species A gradient. In addition the orthogonal gradients within the central square, the four wings also exhibit unique combinations of the two soluble compounds. In the North and South wings, species A gradients are superimposed on uniform high and low backgrounds of species B, respectively. Similarly, in the West and East wings, species B gradients are superimposed on uniform high and low concentrations of species A, respectively. Thus five different experiments may be observed in a single 2Dg-Bioreactor.

The fluid velocity within the device was calculated to balance the convective transport of solute through the channels with diffusion through the gels and between the channels. At a very high velocity, very little diffusion would occur, gradients would develop slowly, and cellular metabolic demands would not be met. Alternatively, at a very low velocity diffusion between the gel would deplete solute from the high concentration solutions before exiting the device, equilibrating the high and low concentration solutions and producing shallow gradients. The Peclet number, Pe, is a dimensionless parameter that compares the relative magnitude of advection in the presence of bulk fluid flow to diffusion in the presence of concentration gradients. A control volume entering the 2Dg-Bioreactor experiences a transit time, τ_{adv}, due to advection of

$$\tau_{adv} = \frac{L_{channel}}{v_{fluid}},$$

where $L_{channel}$ is the length of the channel and v_{fluid} is the linear fluid velocity. The time-scale for diffusion between two channels, τ_{diff}, is given by:

$$\tau_{diff} = \frac{W_{gel}^2}{D},$$

where W_{gel} is the width of the gel region normal to the fluid flow and D is the diffusion constant of the solute. A suitable Peclet number, where advection occurs 10 to 100 times more rapidly than diffusion, is then defined as:

$$Pe = \frac{\tau_{adv}}{\tau_{diff}} = \frac{L_{channel}D}{v_{fluid}W^2} \approx \frac{1}{10} \rightarrow \frac{1}{100},$$

$$v_{fluid} = \frac{L_{channel}D}{W^2Pe}$$

where the fluid velocity is a function of the appropriate Peclet number.

4.3.2 - Convective Diffusion Characterization

The pressure gradient issues that were addressed in the RC-Bioreactor were also relevant in the 2Dg-Bioreactor. Pressure differences between parallel channels would induce interstitial flow through the gel region, which, when a concentration gradient existed between channels, would disrupt the linear gradient in the gel wing and incorrectly specify the corresponding boundary condition along the central square. Merging the outlets of each channel into a single outlet imposes a single outlet pressure for each of the four channels. Identical flow rates caused by identically driven syringes and positive pressure flow, or uniform inlet pressure and negative pressure flow should create roughly identical pressure distributions within each channel. Figure 4.4.3 illustrates the fluid streamlines at the convergence of two channels in a positive pressure-driven device. A pressure difference between the two channels would tilt streamlines toward the low pressure region as the two flows meet. In Figure 4.4.3, streamlines remain parallel after merging of flows, suggesting that the two channel pressures are identical upstream.

Fluorescently labeled dextrans allowed visualization of concentration gradients in the 2Dg Bioreactor. Both positive and negative pressure driven flows produced two perpendicular sets of symmetric, linear concentration regions within the central square and four wings Figures 4.4.4-6. The gradients span only an intermediate range of concentrations within the central square due to local depletion/accumulation at the "uniform" high and low concentration boundaries, respectively. These local changes may diminished by creating a device in which the channels and wing regions are three times taller than the central square. In this

case, the flux across the central square produces smaller changes in the concentration at the adjacent wing sections due to their increased volume. Nonetheless, these experimentally derived gradients confirm the ability to create perpendicular gradients in the 2Dg-Bioreactor.

4.4 Figures
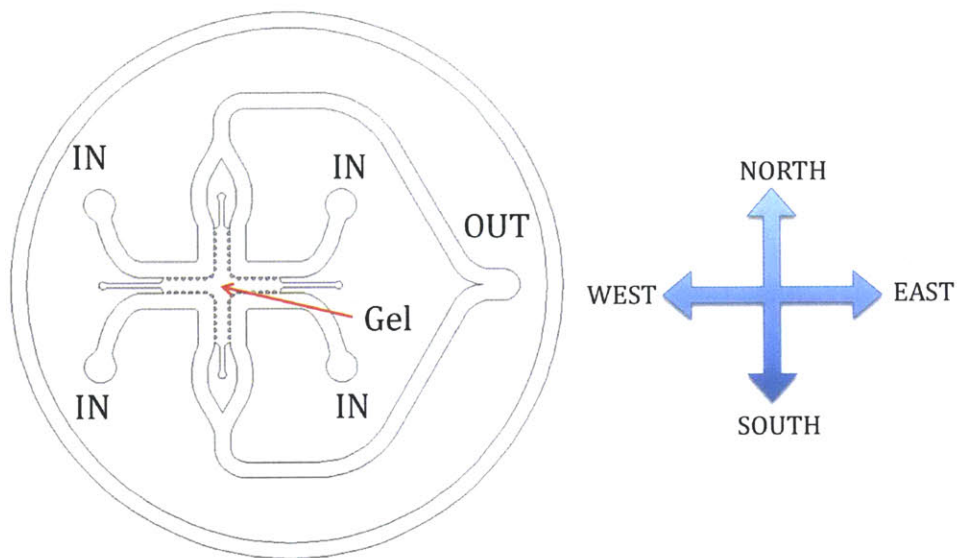
Figure 4.4.1 – 2D Gradient Bioreactor Design
Schematic of 2Dg-Bioreactor showing four inlets that converge in a single outlet. The gel region is bounded by the channels and can be divided into North, South, West, and East wings according to the compass as well as a central square region where the four wings converge. Channels are 1mm in width and the gel region wings were either 1.0 or 1.5mm in width. Channel height was typically 250µm.
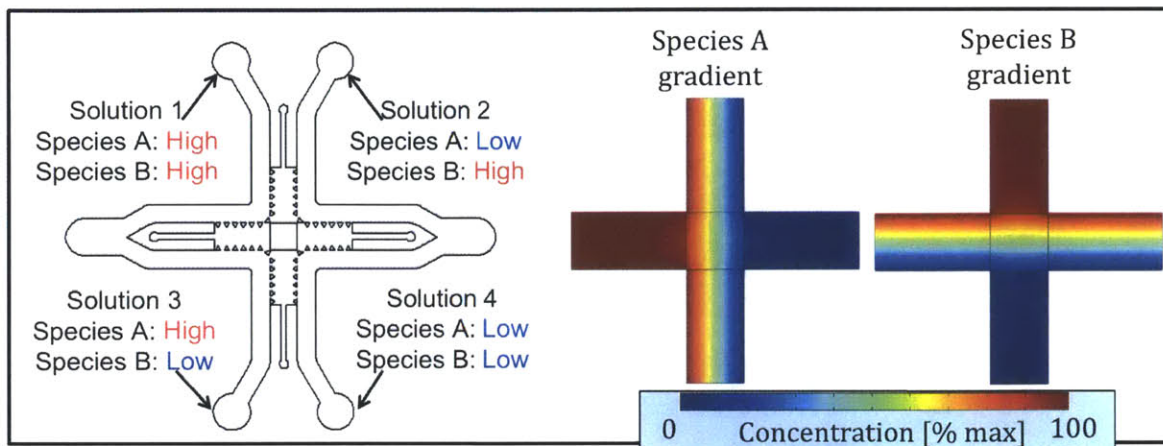
Figure 4.4.2 – Finite Element Model of 2D Gradient Formation
The combination of four different input solutions into the 2Dg-Bioreactor produces two orthogonal gradients – a horizontal gradient in species A and a vertical gradient in species B. In addition to the two overlapping gradients in the central square, single species gradients in the North, South, West, and East wings are superimposed on high or low backgrounds of the second species. Simulation was performed for 6 hours with constant concentration boundary conditions along the cross-shaped gel region.

Figure 4.4.3 – Fluid Streamlines in 2Dg Bioreactor
Fluorescent beads 1μm in diameter were suspended in the 2Dg-Bioreactor channels with a flow velocity of 1μl/min (A) and 5μl/min (B). To fluid streams converge and streamlines remain parallel to the direction of bulk fluid flow indicating that the pressures just upstream to the convergence point are appropriately matched.
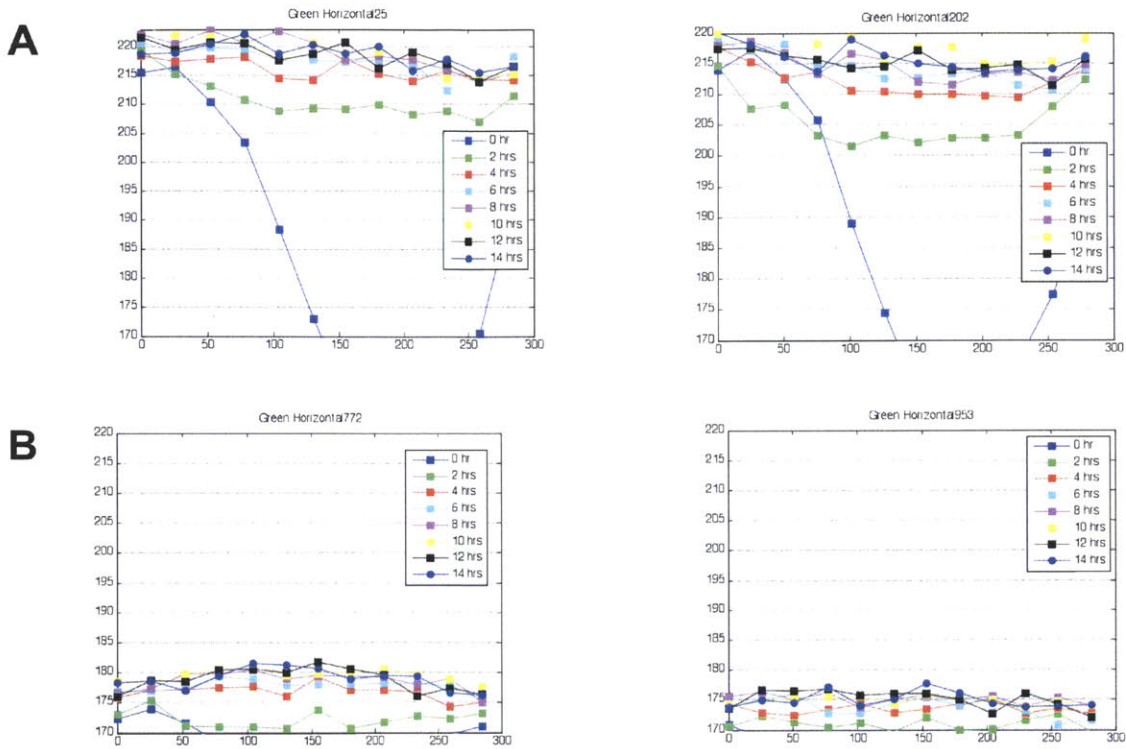
Figure 4.4.4 – North and South Wing Horizontal Concentration Gradients Formed in 2Dg Bioreactor

A north-to-south descending gradient of FITC-Dextran was generated in the 2Dg-Bioreactor. (A) Horizontal gradients at two points in the North wing exhibit uniformly high concentrations as compared to (B) horizontal gradients at two points in South wing at uniformly low concentrations.

A

Green Vertical 151

Green Vertical 414

B

Green Vertical 992

Green Vertical 1249

Figure 4.4.5 – West and East Wing Vertical Concentration Gradients in 2Dg Bioreactor

A north-to-south descending gradient of FITC-Dextran was generated in the 2Dg-Bioreactor. Thus vertical gradients are present in the West (A) and East (B) wings. At two points in either wing, the concentration gradient decreases linearly from north to south, achieving and maintaining a linear profile for several hours.

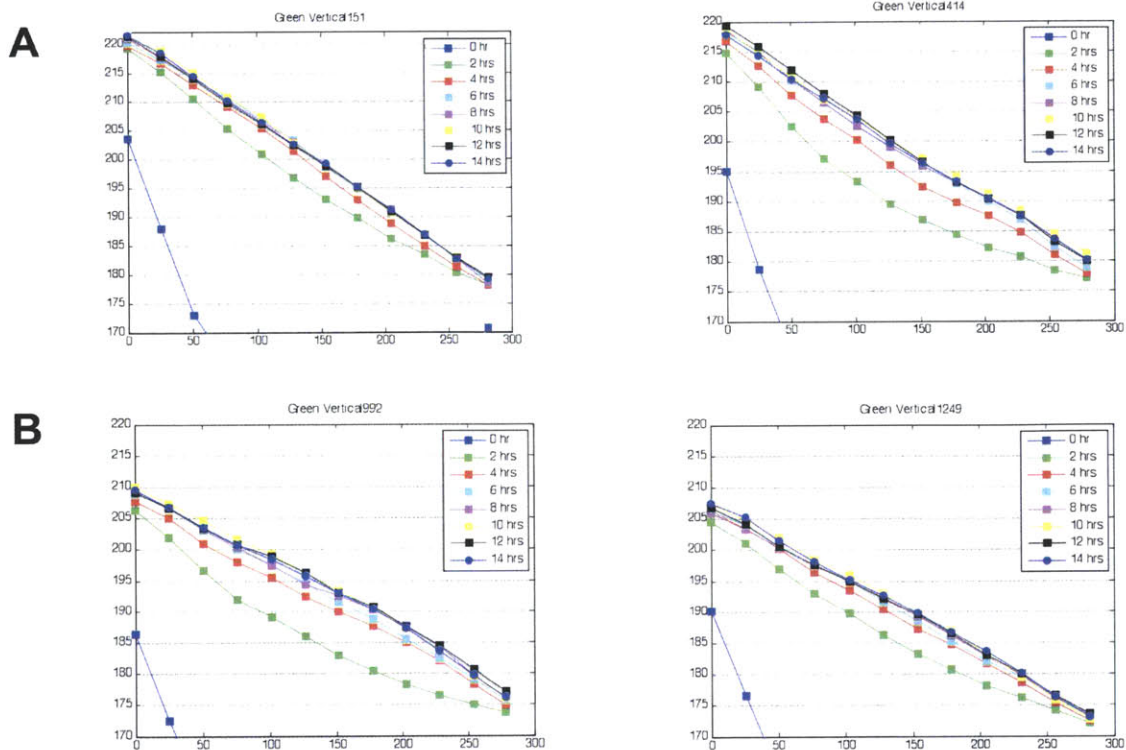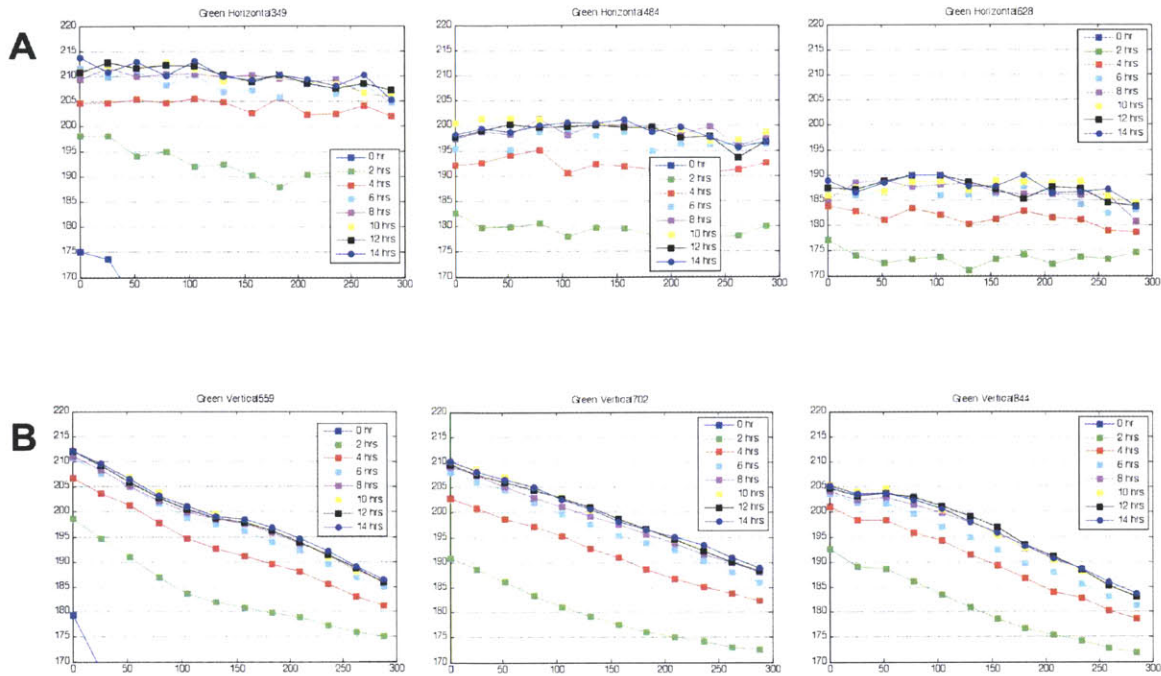**Figure 4.4.6 – Central Square Concentration Gradients in 2Dg Bioreactor**

A north-to-south descending gradient of FITC-Dextran was generated in the 2Dg-Bioreactor. (A) Horizontal gradients at three locations in the central square demonstrate uniform, constant concentration profiles. (B) Vertical gradients at three locations are linearly decreasing from North to South.

CHAPTER FIVE: VENTRAL NEURAL TUBE MORPHOGENESIS

5.1 – Introduction

The roles of Wnt signaling in the developing vertebrate ventral neural tube have been suggested previously, but a holistic reconciliation of seemingly contradictory functions has not yet been demonstrated (Ulloa and Marti 2010). While it may be clear that Wnt signaling is active in the ventral neural tube, whether it functions to promote or suppress the expression Shh induced genes remains contextually unclear, Figure 5.4.3. Wnt functions in two distinct roles via its Tcf effectors. In the first instance, Tcf repression strongly inhibits the expression of Nkx2.2 in the p3 domain, thus setting a threshold of Shh/Gli activity beyond which Nkx2.2 may be expressed (Wang, Lei et al. 2011). Conversely, in the second instance Tcf repression inhibits Gli3R activity, an inhibition that is reversed when Tcf becomes an activator in the presence of Wnt stimulation.

It has been shown that Wnt expression is limited to the dorsal midline in the developing neural tube. Thus, of the ventral progenitor domains, the p3 domain is farthest from the region of high Wnt expression and hence an ideal region to be dependent on the absence of Wnt activation for the proper initiation of its genetic program. Tcf-repression would be most resilient in a regulatory scheme where its critical function is employed at the farthest distance from its own repressor, namely Wnt activity. Indeed a *cis*-regulatory enhancer region containing Tcf and Gli consensus binding sites has been identified upstream of the Nkx2.2 promoter (Lei, Jeong et al. 2006). Gli activation must overcome Tcf repression in order to initiate Nkx2.2 expression (Wang, Lei et al. 2011). Outside of the p3 domain, Nkx2.2 expression, must also be restricted from other more dorsal regions in the neural tube where increased Wnt activity, and hence decreased Tcf-repression of Nkx2.2, is present. Such inhibition is augmented by the presence of Wnt antagonists such as

sFRP2 (Lei, Jeong et al. 2006). Additionally, the stimulus of Nkx2.2 expression, Shh/Gli activity, decreases dorsal to the p3 domain. Together, a ventral to dorsal decrease in Shh/Gli activity, a dorsal to ventral decrease in Wnt activity, Tcf *cis*-regulatory inhibition of Nkx2.2, and sFRP2 antagonism of Wnt signaling present a potent barrier to Nkx2.2 expression throughout the neural tube.

Although Gli3 is known to have both activator and repressor functions (Jacob and Briscoe 2003), it is thought to function primarily as a repressor (Gli3R) in the neural tube (Persson, Stamataki et al. 2002). Gli3R activity is most prevalent in the dorsal aspects of the neural tube, and mouse Gli3$^{-/-}$ mutants show no defects in the expression of ventral genes (Stamataki, Ulloa et al. 2005). Intermediate and dorsal regions, however, exhibit a ventralized phenotype – as if a higher concentration of Shh had been present. Thus Gli3 represses Shh induced genes in regions of moderate to low Shh activity. These regions are also closer to the roof plate where Wnt proteins are produced. Evidence suggests that Wnts antagonize Shh signaling by inducing Gli3R expression by relieving Tcf-repression of Gli3R (Lei, Jeong et al. 2006). In the absence of Wnt signaling, Tcf represses Gli3R expression and Tcf consensus binding sites have been identified in the Gli3 enhancer region. Positive Wnt signaling converts Tcf to its activator form which allows Gli3R expression to increase, reducing Gli activator function.

Herein lies the potential conflict in which Tcf represses Shh induced Nkx2.2 expression while also repressing Gli3R and effectively promoting Shh activity, Figure 5.4.3. Wnt signaling should then simultaneously promote Nkx2.2 expression while inducing Gli3R and suppressing Shh activity. Novel microfluidic technology enabled the simultaneous creation of Shh and Wnt gradients in the context of neural gene induction. By combining these two signals the conditions where Wnt might function as a positive or negative regulator of Nkx2.2 may be elucidated.

5.2 – Methods

5.2.1 - Embryonic stem cell culture and differentiation

The Olig2-GFP reporter ES cell line was developed as described previously (Hai-Qing, Elizabeth et al. 2003). An Nkx2.2-tdTomato reporter line was created by electroporating the construct in cells with a wild-type or Rosa26-Gli1-FLAG background (Vokes SA, Ji H et al. 2007). Cells were cultured separately on 0.1% gelatin coated flasks in Gasglow Minimum Essential Media supplemented with 15% KnockOut™ Serum, 1X Non-essential amino acids, 1X sodium pyruvate, 0.1 mM 2-mercaptoethanol, 1% penicillin-streptomycin, and 1000 units/ml leukemia inhibitory factor.

To induce differentiation the Olig2-GFP and Nkx2.2-tdTomato cell lines were mixed in a 1:1 ratio in DFNB medium: DMEM-High glucose, F-12 Medium, and Neurobasal Medium in a 1:1:2 ratio supplemented with 1% penicillin-streptomycin, 1% L-glutamine, 10% KnockOut™ Serum, and 55μM 2-mercaptoethanol. Hanging drops were formed with 500 cells per 12 μl droplet and embryoid bodies were allowed to form for 2 days.

5.2.2 - Sonic Hedgehog Morphogen Gradient Validation

A collagen prepolymer solution was used to seed embryoid bodies in the RC devices. The solution was prepared on ice by combining 10X DMEM, deionized water and Rat Tail Collagen Type I to produce a final collagen concentration of 2 mg/ml at pH 7. Day 2 embryoid bodies were collected in a pellet, and approximately 6500 embryoid bodies were added to 35 μl of the collagen pre-polymer solution. Approximately 4 μl of the suspension was injected into each gel region of the devices and the collagen was allowed to polymerize at 37 °C for 30 minutes. Devices were then filled with DFNB medium supplemented with retinoic acid at a concentration of 500 mM. The source and source reservoir wells of each device were loaded with retinoic acid

supplemented DFNB and recombinant Sonic Hedgehog protein (R&D Systems, Minneapolis, MN) at concentrations of 12.5 nM, 25 nM, 50 nM, and 125 nM. Media in the devices were changed every 24 hours and images of the gel regions were acquired daily. The cells remained in the devices for 4 days.

5.2.3 – p3 Differentiation Assay: 2-Dimensional Perpendicular Gradients

Nkx2.2-tdtomato reporter ES cells were suspended in 2mg/ml collagen type I gels at a density of 5×10^6 cells/ml. Devices were incubated at 37°C in humidity chambers for 30 minutes to allow the collagen gels to polymerize. Each device was then filled with DFNB medium by firmly inserting a pipette tip into the outlet port and back-filling the device. Devices were returned to humidity chambers at 37°C for 48 hours, and media was changed every 12-24 hours. Devices were then connected to syringe pumps and media reservoirs as described above. To create Shh/Wnt-3a gradients the 4 input solutions were: (1) DFNB-RA + 0.1nM mouse recombinant Wnt-3a (R&D Systems), (2) DFNB-RA + 12.5nM mouse recombinant Shh-C25Il (R&D Systems) + 0.1nM mouse recombinant Wnt-3a (R&D Systems), (3) DFNB-RA + 12.5nM Shh-C25Il+ 1.0nM Wnt-3a, and (4) DFNB-RA + 1.0nM Wnt-3a. Media was withdrawn from each device at a rate of 6µl/min for 4 days, with reservoir replenishment as necessary. Cells were imaged with ImageJ software which were analyzed with MATLAB (Mathworks).

5.2.4 – p3 Differentiation Assay: 1-Dimensional Superimposed Gradient

RC-Bioreactor devices were fabricated and seeded with Nkx2.2-tdtomato reporter ES cells in a 1mg/ml collagen gel at a density of 50×10^6 cells/ml. After collagen polymerization, devices were filled with DFNB media and incubated at 37°C in humidity chambers for 48 hours. Then, media was aspirated from each device and new media, containing DFNB-RA supplemented with either 0.1nM or 1.0nM Wnt-3a, was added to each device. The source well was additionally supplemented with

12.5nM Shh-C25Il to create the Shh gradient. Media was changed daily. After 4 days, devices were imaged and the fluorescent intensity in each gel region was quantified.

5.2.5 - Gene regulatory network modeling

The system of ordinary differential equations was solved in the MATLAB program (Mathworks, Natick, MA) using the ode23 solver. System parameters were chosen such that a tripartite expression pattern between transcription factors Nkx2.2, Olig2, and Pax6 was observed in response to an increasing Shh input with a concomitantly low Wnt input. The effect of an increasing Wnt input was observed in the setting of the highest Shh input.

5.2.6 - Western blots

Nkx2.2-tdtomato reporter ES cells were seeded at a density of 2×10^5 cells in 1 ml of DFNB media in Corning Ultra-Low Attachment 24 well plates. After 48 hours, media was replaced with fresh DFNB medium containing retinoic acid (500nM), recombinant mouse Shh-C25II (R&D Systems, Minneapolis, MN) and recombinant mouse Wnt-3a (R&D Systems, Minneapolis, MN). After 72 additional hours, cells were lysed in RIPA buffer and transferred to a polyvinylidene difluoride membrane. Western blot analysis was performed using primary antibodies targeting: dsRed 1:8000 (Abcam, Cambridge, UK); Nkx2.2 0.5 µg/ml (Developmental Studies Hybridoma Bank [DSHB], Iowa City, IA); Gli3 1 µg/ml (R&D Systems, Minneapolis, MN); Pax6 0.5 µg/ml (DSHB); Tubulin 1:1000 (Sigma Aldrich, St. Louis, MO) and HRP-conjugated secondary antibodies 1:2000 (Bio-Rad, Hercules, CA).

5.2.7 – Quantitative RT-PCR

RNA was isolated with Trizol Reagent and reverse transcription was performed using random hexamer primers. For qPCR, technical samples were performed in duplicate using SYBR Green master mix on an ABI Prism 7900HT machine. Data was normalized to GAPDH expression and the following primers were used: Pax6-F-TACCAGTGTCTACCAGCCAAT; Pax6-R-TGCACGAGTATGAGGAGGTCT; Olig2-F-TCCCCAGAACCCGATGATCTT; Olig2-R-CGTGGACGAGGACACAGTC; Nkx2.2-F-AAGCATTTCAAAACCGACGGA; Nkx2.2-R-CCTCAAATCCACAGATGACCAGA; Gapdh-F-AGGTCGGTGTGAACGGATTTG; Gapdh-R-TGTAGACCATGTAGTTGAGGTCA.

5.3 - Results & Discussions

5.3.1 - Sonic hedgehog induced Olig2 and Nkx2.2 expression

Embryonic stem cells seeded in the collagen gel regions continued to proliferate, eventually merging into one large continuous mass covering the entire gel volume, Figure 5.4.1. On day 0 a Shh gradient was formed in the gel regions containing the differentiating cells. Shh stimulates the expression of the transcription factors Olig2 and Nkx2.2 (Dessaud, Yang et al. 2007), and initially Olig2 or Nkx2.2 expression was undetectable by fluorescent microscopy. On day 3, both Olig2 and Nkx2.2 expression became evident at the edge of the gel closest to the Shh source and by day 4 the expression had spread farther into the gel. The cells farther from the Shh source were exposed to lower Shh concentrations and required more Shh exposure time before activating expression of Olig2 and Nkx2.2, illustrating the interplay between Shh dosing concentration and dosing time in neural tube development. As shown in Figure 5.4.1, the expression levels in the untreated control gels were uniform at baseline levels. In the gels with the Shh gradient both Olig2 and Nkx2.2 expression levels were highest closest to the Shh source and decayed to the baseline untreated level approximately halfway between the Shh source and sink. This is consistent with the notion that in the portion of the gel where the Shh concentration exceeded some critical threshold, expression of Olig2 and Nkx2.2 was stimulated; in

the remainder of the gel, where the Shh concentration was below the threshold, no such stimulation occurred.

In response to steeper concentration gradients created by increasing the concentration of Shh in the source well the concentration at each point in the gel increased. Accordingly with increasing Shh source concentration the extent of Olig2 and Nkx2.2 expression into the gel region increased as well, Figure 5.4.2.

5.3.2 - Nkx2.2 Reporter Exhibits a Biphasic Expression Pattern

To investigate the opposing mechanisms (Figure 5.4.3) of Wnt on Shh induced expression of the p3 domain transcription factor Nkx2.2, embryonic stem cells transgenically expressing tdtomato fluorescent protein driven by the presumptive Nkx2.2 enhancer (Lei, Jeong et al. 2006; Vokes, Ji et al. 2007) were exposed to combinatorial gradients of Shh (increasing from South to North) and Wnt-3a (increasing from West to East) in the 2Dg-Bioreactor, Figure 5.4.4. Compared to the control scenario lacking a Wnt-3a gradient, tdtomato expression was diminished in the West wing where the Wnt-3a concentration is only 0.1nM. In the Central region and East wing where Wnt-3a increases to 1nM, tdtomato expression was increased to or beyond the level of expression in the control device.

To confirm this result, and isolate the role of Wnt-3a stimulation, Nkx2.2 expression was stimulated in the RC-Bioreactor where a single, linear Shh gradient was superimposed on a uniform background of Wnt-3a at either 0.1 or 1.0 nM, Figure 5.4.5. Quantifying the tdtomato fluorescent signal, confirmed that increasing the Wnt-3a signal from 0 to 0.1nM decreased gene expression while increasing it further to 1.0 nM reversed this effect.

This Nkx2.2 reporter model is consistent with a regulatory model governed by the following 3 relationships,

$$Gli^{Nkx2.2-Threshold} = f_1(Wnt) \qquad (1)$$

$$GliA = f_2(Shh, Wnt) \qquad (2)$$

$$Shh^{Nkx2.2-Threshold} = f_3(Wnt) \qquad (3)$$

where f_1, f_2, and f_3 are generalized functions that describe the following relationships: Equation 1 indicates that the Gli signal required to induced Nkx2.2 expression is a function of the Wnt signal strength, Figure 5.4.6a As the Wnt signal increases, less Gli stimulation is required to compensate for the diminished repression of Nkx2.2 by Tcf. Equation 2 indicates that the strength of Gli activation signaling is directly proportional to Shh and inversely proportional to Wnt, Figure 5.4.6b. Wnt signaling increases the expression of Gli3R which suppresses Gli activator function. Combining equations 1 and 2 yields equation 3 - the magnitude of the Shh signal required to induce Nkx2.2 is a function of Wnt, Figure 5.4.6c. Under certain constraints, equation 3 describes the biphasic role of Wnt, in which slight Wnt stimulation increases the Shh signal necessary for Nkx2.2 expression and further stimulation reduces this threshold back toward the Shh threshold present in the absence of Wnt.

5.3.3 - Nkx2.2 protein expression is down-regulated by Wnt-3a

Protein-protein interactions between Olig2 and Nkx2.2 transcription factors have been demonstrated (Sun, Dong et al. 2003) and represent a mechanism by which neural tube gene regulatory network components exert mutual cross-repressive influences. The effect of such interactions would be undetectable in a transgenic reporter model in which tdtomato expression is driven by the presumptive Nkx2.2 enhancer. To investigate this possibility we measured tdtomato and Nkx2.2 protein expression semi-quantitatively in the presence of Shh and Wnt-3a, Figure 5.4.7.

Similarly to the 2Dg-Bioreactor fluorescent patterns, compared to stimulation with 10nM Shh alone, tdtomato was down-regulated with the addition of 0.1nM Wnt-3a but remained unchanged/increased with the addition of 1.0nM Wnt-3a. Nkx2.2 was also suppressed in the presence of 0.1nM Wnt-3a, however, it was further suppressed in the presence of 1.0nM Wnt-3a. Wnt suppression of Nkx2.2 is mediated by an up-regulation of Gli3 which increased in a dose dependent manner with increasing Wnt-3a stimulation. An increase in Gli3, in its repressor role, would inhibit Shh signaling and promote the expression of more dorsally expressed neural tube homeodomain proteins. Indeed Pax6, which is expressed dorsal to Nkx2.2 in the neural tube, and thus maintained by a weaker Shh signal, is concomitantly increased with Wnt-3a stimulation and Gli3 expression.

5.3.4 – Gene Regulatory Network and Expression

A post-transcription or post-translation intervention on Nkx2.2 gene expression could account for the difference between Nkx2.2 and tdtomato protein expression even if the tdtomato reporter accurately reflects Nkx2.2 transcription. However, differences between Nkx2.2 and tdtomato transcript levels would imply differential cis-regulatory behavior at the endogenous and transgenic enhancer regions. Pax6, Olig2, and Nkx2.2 gene expression in response to Shh and Wnt-3a is shown in Figure 5.4.8. In the presence of Shh, Nkx2.2 expression decreases with increasing Wnt-3a, while Pax6 expression increases. Thus the Nkx2.2 protein expression data accurately reflects Nkx2.2 transcription suggesting a discrepancy between the putatively identified Nkx2.2 enhancer and the true combination of Nkx2.2 regulatory elements.

To understand this monophasic down-regulation of Nkx2.2 protein expression in the context of a biphasic interaction described by Wnt and the Nkx2.2 enhancer the Balaskas-Briscoe cross-repressive gene regulatory network model (see Figure 5.4.9) (Balaskas, Ribeiro et al. 2012) was appropriately modified. The new model included Wnt and Shh as inputs and included both the induction of Nkx2.2 by Wnt via the

Nkx2.2 enhancer as well as the Wnt mediated suppression of Shh induced Gli activity, Figure 5.4.10. The resulting differential equations describe the kinetics of gene expression:

$$\frac{dP}{dt} = \frac{\alpha}{1 + \left(\frac{N}{N_P}\right)^{h_1} + \left(\frac{O}{O_P}\right)^{h_2}} - k_P P$$

$$\frac{dO}{dt} = \left(\frac{\beta G}{1+G}\right)\left[\frac{1}{1 + \left(\frac{N}{N_O}\right)^{h_3}}\right] - k_O O$$

$$\frac{dN}{dt} = \left[\frac{\kappa G W}{(1+G)(1+W)}\right]\left[\frac{1}{1 + \left(\frac{O}{O_N}\right)^{h_4} + \left(\frac{P}{P_N}\right)^{h_5}}\right] - k_N N$$

$$\frac{dG}{dt} = \left(\frac{\varepsilon S}{1+S}\right)\left[\frac{1}{1 + \left(\frac{W}{W_G}\right)^{h_6}}\right] - k_G G$$

This model accurately predicted a tri-stable system dominated by the expression of single transcription factors as the degree of Shh stimulation increased in the presence of a minimal Wnt input. The progression from P[High] to O[High] to N[High] corresponded to progressively ventral positions in the neural tube with progressively larger stimulation within the Shh gradient. In agreement with experimental data, when the Wnt signal was increased in the presence of an Shh input of sufficient magnitude to induce Nkx2.2 expression in the absence of Wnt, Nkx2.2 expression was down-regulated and Pax6 expression is increased.

These results indicate that the presumptive Nkx2.2 enhancer incompletely determines the expression pattern of Nkx2.2 in response to Shh and Wnt. While protein-protein interactions between Nkx2.2 and Olig2 or other factors are possible, there may also be additional genetic regulatory elements in non-coding DNA regions

that create additional regulatory opportunities. Identification of this mechanism is the proximal step in further understanding the role of Wnt proteins in the neural tube gene regulatory network.
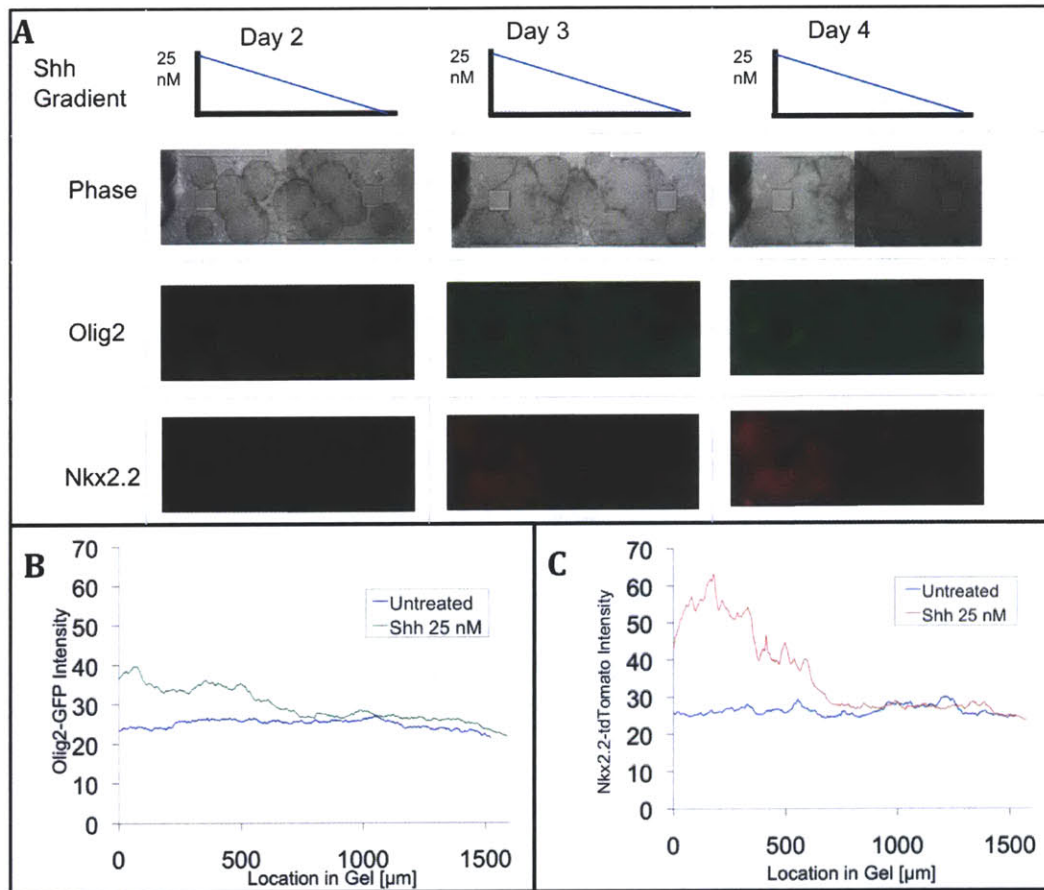
5.4 – Figures

Figure 5.4.1 – Shh Gradients Induce Olig2 and Nkx2.2 Expression
(A) ES cell reporter lines (Olig2-GFP and NKX2.2-tdTomato) were mixed and differentiated in hanging drops. Two days later (day 0 of Shh exposure), embryoid bodies we seeded in collagen gels and exposed to a concentration gradient ranging from 25 nM to 0 nM along the length of the gel. On day 3, Olig2 and Nkx2.2 expression were evident by fluorescent signal at the higher concentration region in the gel. On day 4 this expression had increased in intensity and penetration into the gel as regions of lower Shh concentration received sufficient temporal exposure to induce a response. Measured day 4 expression for Olig2 (B) and Nkx2.2 (C) compared to untreated gels shows the extent of differentiation at different points in the gradient by plotting reporter fluorescent intensity vs. distance from the Shh source. Expression is highest at the locations in the gel closest to the Shh source and eventually falls to the baseline level present in the gels that contained embryoid bodies that were not simulated with Shh. This indicates the location in the gel where the Shh concentration is equal to the threshold level necessary to induce Olig2 and Nkx2.2 expression.
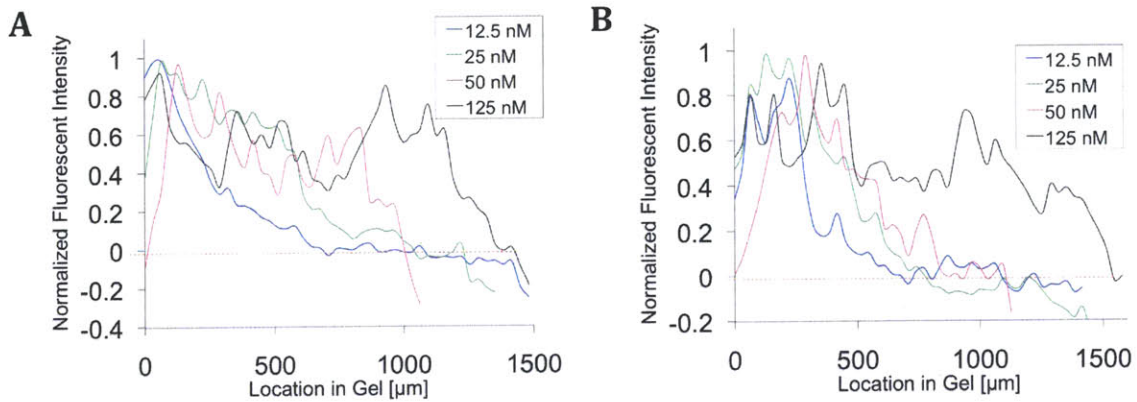
Figure 5.4.2 – Concentration Dependence of Olig2 and Nkx2.2 Expression Penetration

2 day old embryoid bodies were seeded in the gel regions of the RC device and exposed to Shh gradients produced by 12.5 nM (blue), 25 nM (green), 50 nM (pink), and 125 nM (black) Shh concentrations in the source well. After 4 days of Shh exposure Olig2 (A) and Nkx2.2 (B) expression in the gel region as judged by fluorescent reporter intensity was plotted against distance from the source well. The expression levels at all four of the Shh doses were highest in the in the regions adjacent to the source wells and decreased to the baseline levels present in the gels with untreated embryoid bodies (red dashed line). Increasing Shh doses increased the Shh concentration at each location in the gel. Thus at higher concentrations the location of the expression threshold moves farther form the source well and the Olig2 and Nkx2.2 expression extends farther into the gel.
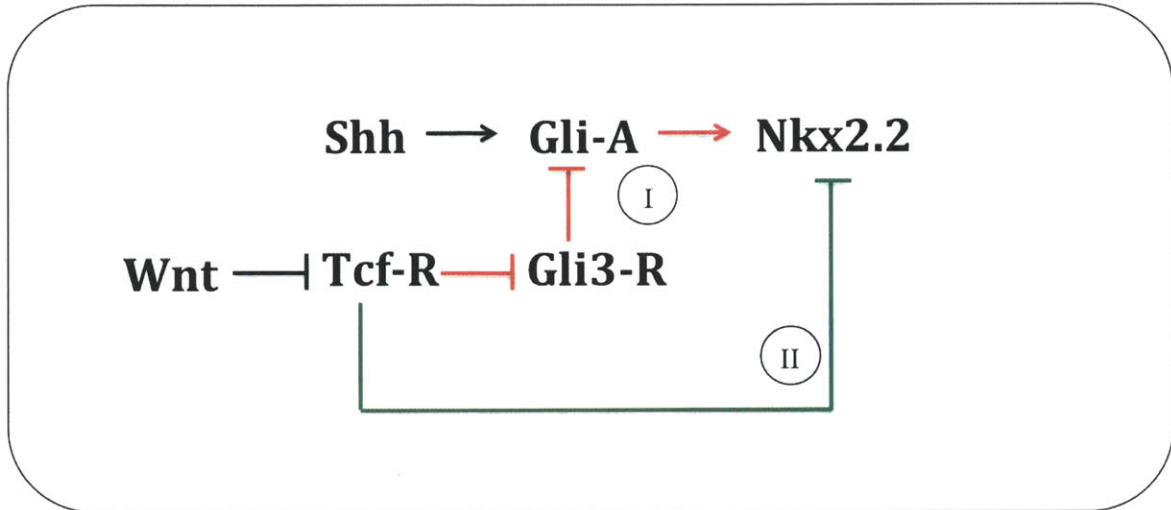
Figure 5.4.3 – Opposing Influences of Wnt Signaling on Nkx2.2 Expression

Nkx2.2 expression is dependent on Shh induction of Gli activator function. Wnt intersects with this pathway to differentially regulate Nkx2.2 expression in response to Shh induction. In pathway I, Wnt turns off the repressive actions of Tcf. In the absence of Wnt signaling, Tcf represses Gli3 which primarily functions to repress Gli activator activity and hence suppresses Nkx2.2 expression. Positive Wnt signaling then increase Gli3R allowing increased Nkx2.2 down-regulation. In pathway II, in the absence of Wnt signaling, Tcf represses Nkx2.2 expression. Positive Wnt signaling suppresses Tcf repression of Nkx2.2 leading to Nkx2.2 up-regulation.
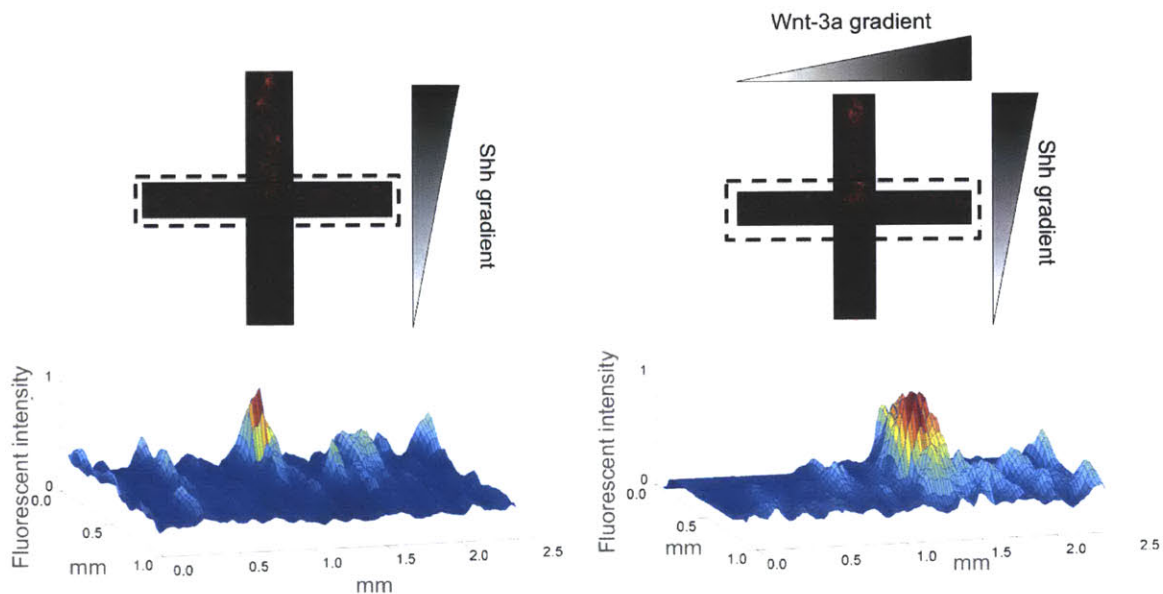
Figure 5.4.4 – Biphasic Expression of Nkx2.2 in the Presence of Shh and Wnt-3a 2Dg Bioreactor Gradients

(Top-Left) A north-south gradient created by 12.5nM of Shh induces Nkx2.2 gene expression uniformly in the North wing and non-uniformly in the West wing, East wing, and central square. Boxed region - (Bottom-Left) Graphical representation of Nkx2.2 driven expression tdtomato fluorescence – height and color correspond to fluorescent intensity. (Top-Right) A west to east 0.0 to 1.0nM Wnt-3a gradient is oriented perpendicular to the Shh gradient. (Bottom-Right) – Compared to the control case with a single Shh gradient, Nkx2.2-tdtomato expression is decreased in the West wing at low Wnt-3a concentrations, and increased in the central square and East wing at intermediate and high Wnt-3a concentrations.
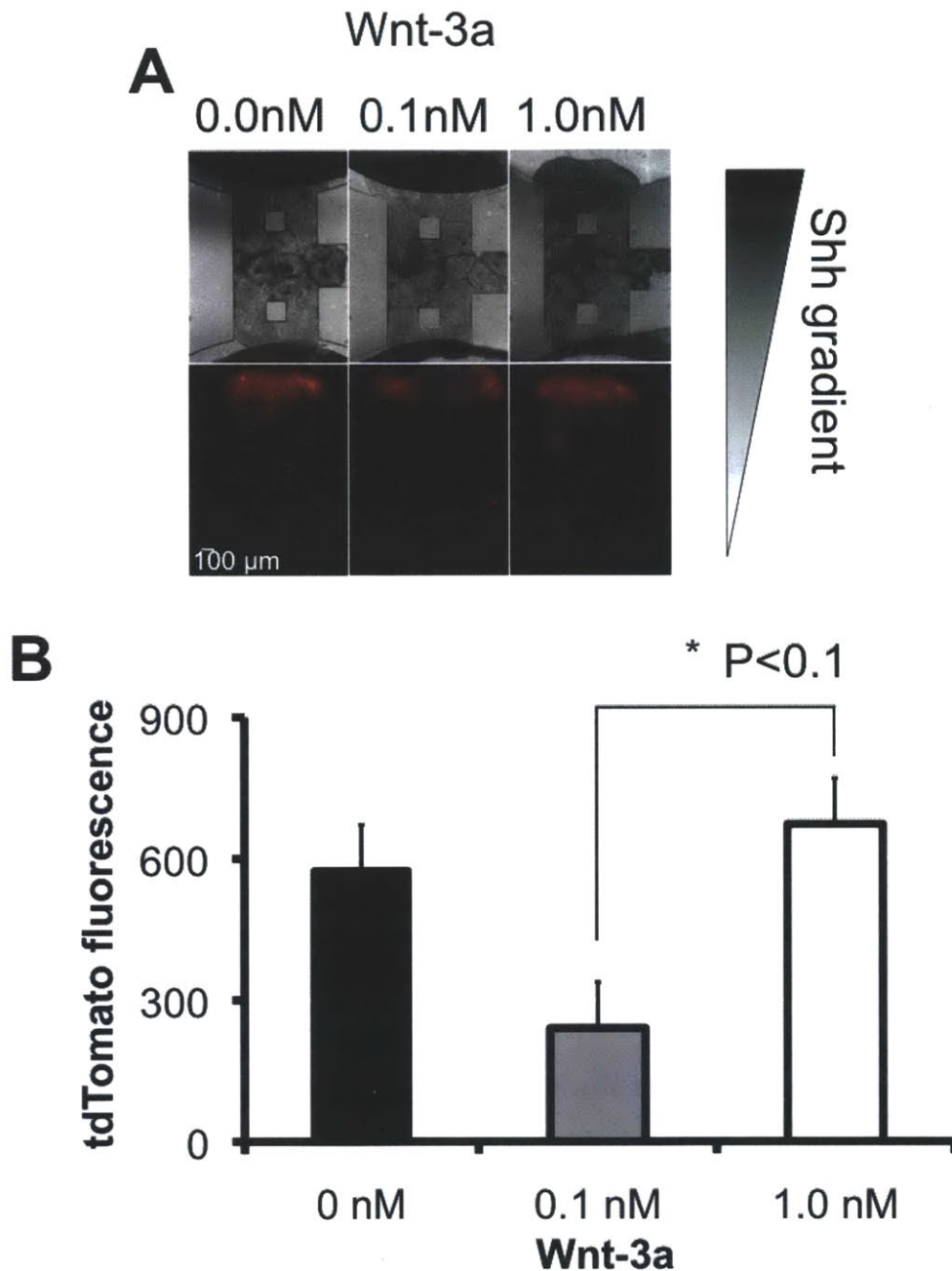
Figure 5.4.5 – Biphasic Expression of Nkx2.2 in RC-Bioreactor
(A) Nkx2.2-tdtomato expressing ES cell line was seeded in the RC-Bioreactor and media was supplemented with 0.0, 0.1, or 1.0nM Wnt-3a. A 12.5nM Shh gradient was then created in the experimental gel. Phase and tdtomato fluorescent images are shown (6X magnification). (B) Quantification of tdtomato expression in the gel regions shows a biphasic response to Wnt-3a, first decreasing at 0.1nM and then increasing at 1.0nM.
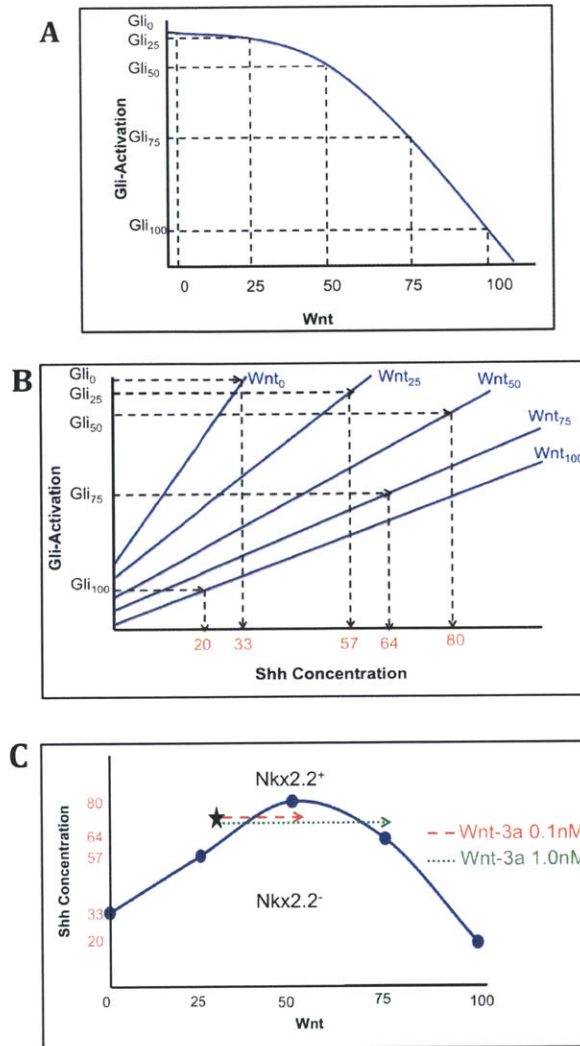
Figure 5.4.6 – Biphasic Model of Nkx2.2 Enhancer
(A) Model describing inverse relationship between Gli signal strength required to induce Nkx2.2 expression and the magnitude of Wnt stimulation. (B) Shh concentration is directly proportional to intracellular Gli activity at any arbitrary level of Wnt signaling. As the Wnt strength increases, intracellular Gli activity decreases at each level of Shh signaling. (C) The Shh concentrations corresponding to the magnitude of Gli activity required to induce Nkx2.2 expression in the presence of Wnt stimulation produces a biphasic curve. The star represents a cell in which the local Shh concentration exceeds the threshold for Nkx2.2 expression. A slight increase in Wnt concentration (0.1 nM), at a constant Shh concentration, displaces the cell to a state where the Shh threshold for Nkx2.2 expression exceeds the local Shh concentration. Further increases in Wnt concentration (1.0 nM) displace to cell to a state where Nkx2.2 expression is again permissible.
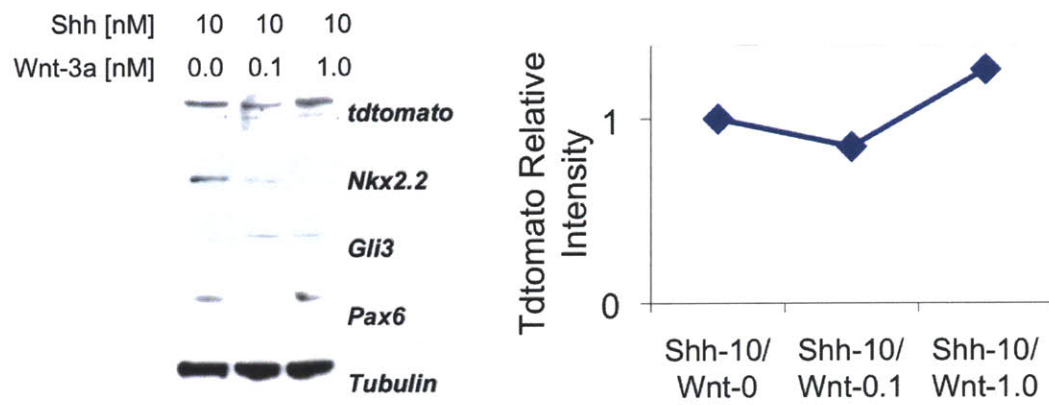
Figure 5.4.7 – Protein Expression in Response to Shh and Wnt-3a
(Left) Protein expression in neural progenitor cells treated with 10nM
Shh and 0, 0.1, or 1.0 nM Wnt-3a. (Right) Quantification of tdtomato
protein expression as a function of Wnt-3a. The biphasic behavior of
tdtomato is not mirrored by the Nkx2.2 protein expression.
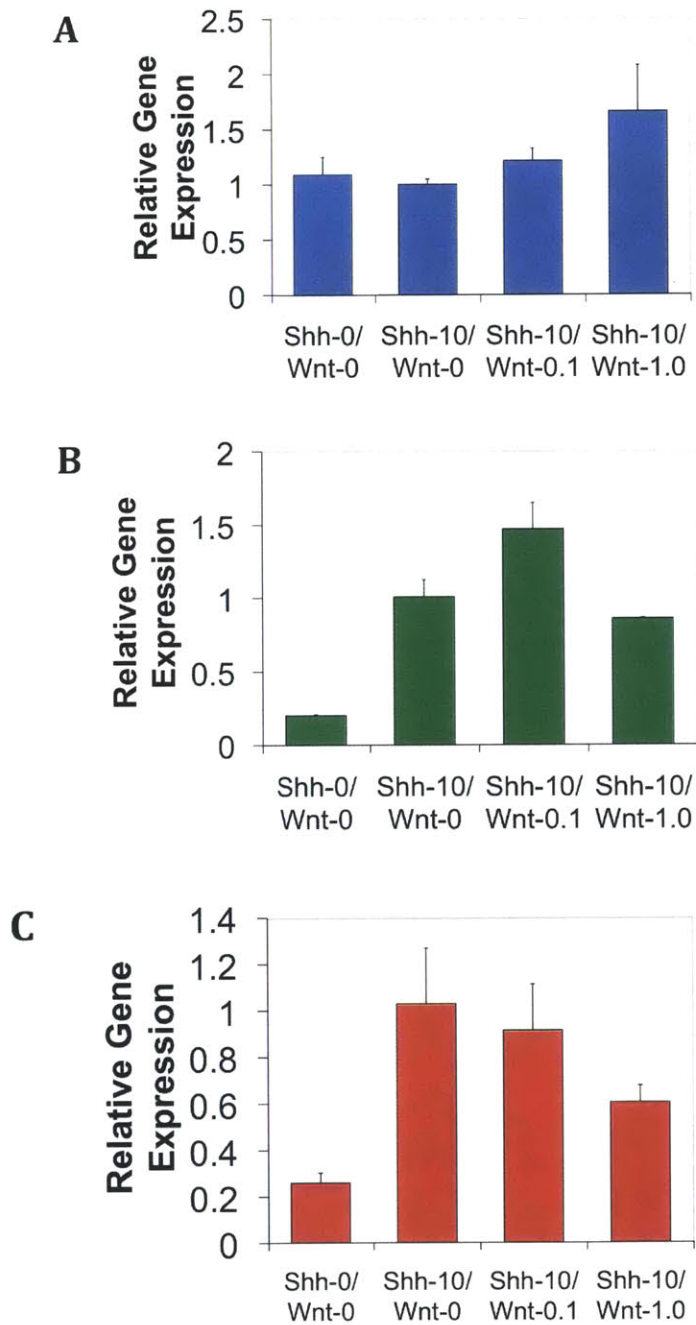
Figure 5.4.8 – Transcription Factor Gene Expression
(A) Pax6 gene expression increases in response to Wnt-3a stimulation. (B) Olig2 gene expression is absent in the absence of Shh and is responsive to Wnt-3a signaling. (C) Nkx2.2 expression is also absent in the absence of Shh and decreases monotonically in response to increasing levels of Wnt-3a.
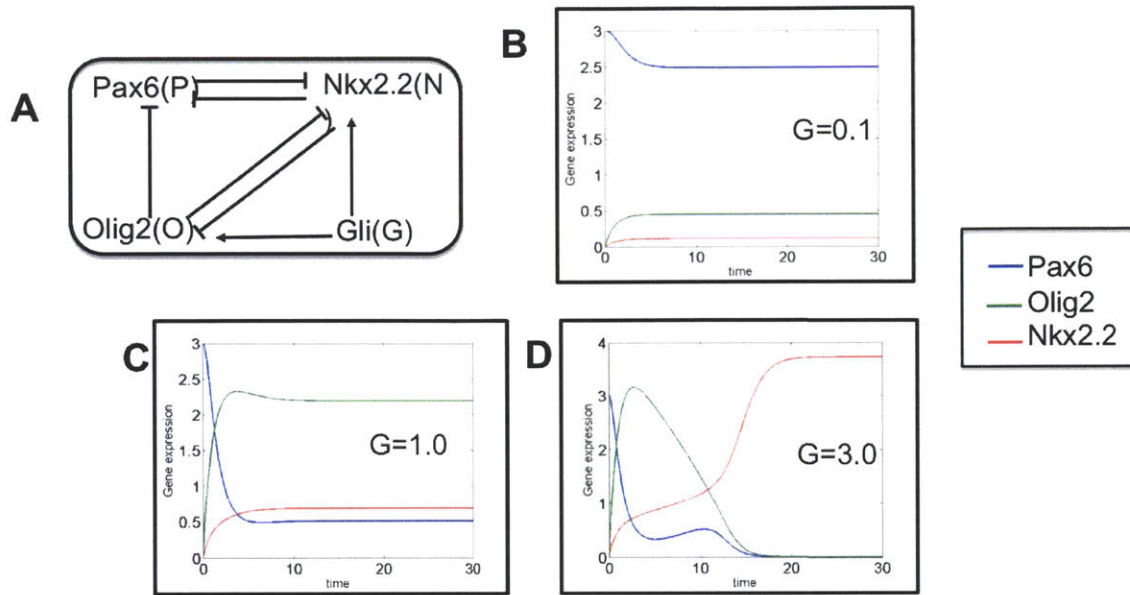
Figure 5.4.9 – Single Input Shh Driven Gene Regulatory Network
(A) Cross-repression between neural tube transcription factors as described by the Balaskas-Briscoe model. (B) At the lowest level of Gli, Pax6 expression is highest. (C) A moderate increase in Gli signaling switches the network output to Olig2 expression. (D) Further increases in Gli signaling switch the system to maximal Nkx2.2 expression. This model functions as a tristable switch in response to increasing levels of Gli activator function.
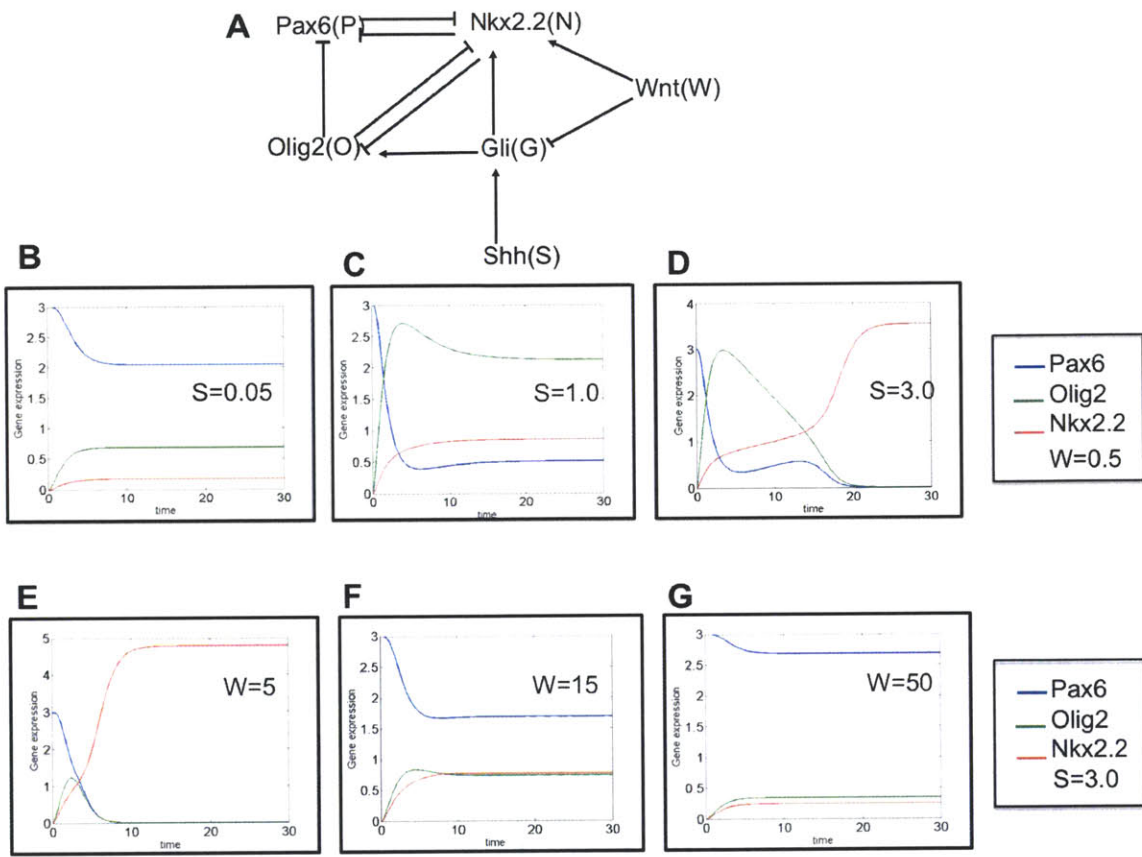
Figure 5.4.10 – Dual Input - Shh and Wnt – Gene Regulatory Network

(A) Cross repressive gene regulatory network in which Wnt (W) and Shh (S) are the primary inputs. Tristable simulation of GRN, at a minimum Wnt signal strength, in which increasing levels of Shh transition the model from Pax6 dominant (B) to Olig2 dominant (C) to Nkx2.2 dominant (D). Increasing Wnt at a high level of Shh suppresses Nkx2.2 expression and increases Pax6 expression (E-G).

CHAPTER SIX: CONCLUSIONS AND FUTURE DIRECTIONS

Two novel devices capable of maintaining stable linear concentration gradients for the study of cell behavior in a 3-dimensional environment have been presented. This work presents a significant advance over previously reported techniques because the RC-Bioreactor device does not require continuous fluid flow and allows stable concentration gradients to be formed in a 3-dimensional environment for a period of days (Li Jeon, Baskaran et al. 2002; Mao, Cremer et al. 2003; Lin, Saadi et al. 2004; Zhu, Chu et al. 2004; Biddiss and Li 2005; Chung, Flanagan et al. 2005; Chung, Lin et al. 2006; Diao, Young et al. 2006; Irimia, Geba et al. 2006; Lin and Butcher 2006; Saadi, Wang et al. 2006; Amarie, Glazier et al. 2007; Cheng, Heilman et al. 2007; Herzmark, Campbell et al. 2007; Li, Chen et al. 2007; Park, Hwang et al. 2007; Yang, Pi et al. 2007; Cheng JY, Yen MH et al. 2008; Fok, Domachuk et al. 2008; Kang, Han et al. 2008; Li, Liu et al. 2008; Liu, Sai et al. 2008; Motoo, Toda et al. 2008; Shamloo, Ma et al. 2008; Sun, Wang et al. 2008; Atencia, Morrow et al. 2009; Cooksey, Sip et al. 2009; Englert, Manson et al. 2009; Glawdel, Elbuken et al. 2009; Haessler, Kalinin et al. 2009; Hattori, Sugiura et al. 2009; Jeon, Lee et al. 2009; Joong Yull, Suel-Kee et al. 2009; Kalinin, Jiang et al. 2009; Kim, Pinelis et al. 2009; Park, Yoo et al. 2009; Siyan, Feng et al. 2009; Yusuf, Baldock et al. 2009; Zhou, Wang et al. 2009). Other devices produce gradients without continuous flow but are still limited to 2-dimensional geometries (with limited degrees of gradient stability) (Abhyankar, Lokuta et al. 2006; Frevert, Boggy et al. 2006; Wu, Huang et al. 2006; Du, Shim et al. 2009; Kim, Lokuta et al. 2009), while others establish gradients in 3-dimensional environments but are dependent on fluid flow (Mosadegh, Huang et al. 2007; Saadi, Rhee et al. 2007; Tingjiao, Chunyu et al. 2009; He, Du et al. 2010; Zervantonakis, Chung et al. 2010). The incorporation of low resistance reservoir paths prevents convective transport of soluble factors through the hydrogel region and the disruption of the concentration profile by pressure gradients. This result is achieved without the incorporation of multilayered microfluidic chips, specialized

pressure regulators, valves, or continuous fluid flow. The simple design coupled with the device's resistance to perturbations during handling make the RC-Bioreactor optimal for cell biology applications, with no prerequisite expertise in microfluidic technology required.

Chemotaxis assays were performed with 3 different cell types, which each behave differently in culture. Vascular smooth muscle cells attach to flat substrates and grow in a 2-dimensional monolayer whereas endothelial cells have the ability to form a monolayer on 3-dimensional surfaces (Chung, Sudo et al. 2009). Jurkat T lymphocytes that are normally cultured in suspension were also able to adhere to and invade the collagen gel. In addition to these and other cell types, the versatility of the RC-Bioreactor also lends itself to the study of explant biology and other 3-dimensional cellular aggregates such as embryoid bodies. Results indicate that cells are induced to migrate from skeletal muscle tissue explants in response to SDF-1. Additionally, differentiating embryonic stem cells as 3-dimensional aggregates in the gel region with superimposed a Shh morphogen gradient to show, for the first time, differential expression of neural tube transcription factors in a Shh concentration gradient in 3-dimensional differentiation cultures. These results confirm the accepted paradigm governing the role of Shh in neural development and motivated future studies with more complex gradients to elucidate the role of additional signaling gradients, such as Wnts, that affect the spatiotemporal patterning in the neural tube (Joong Yull, Suel-Kee et al. 2009; Ulloa and Martì 2010).

Finally the RC-Bioreactor design is amenable to simple modifications to enhance its performance for specific applications. Chemotaxis occurring over 1-2 days and differentiation occurring over the course of 3-4 days have been observed in the RC-Bioreactor, but some processes might require longer observation periods. By increasing the sizes of the source and sink wells relative to that of the gel region a steep gradient can be maintained for longer periods of time as the flux of solute now occurs between two larger volumes. Additionally, the integration of larger wells

increases the availability of media and nutrients, slows the accumulation of waste products, and eliminates the need for frequent media changes. Although increasing the well volumes would also reduce pressure gradients caused by volume imbalances, this would not eliminate the need for the low resistance bypass channels unless the wells were increased dramatically. Using Darcy's Law the Peclet number, Pe, for mass transport through the gel can be written as a function of a volume imbalance ΔV and the diameter of the wells, (Lek, Dias et al. 2010)

$$Pe = \frac{4K\rho g \Delta V}{D\pi D_w^2 \mu}$$

For convection and diffusion to balance ($Pe=1$) in the presence of a 10 μl bolus and for a molecule with a diffusivity of 1.6×10^{-6} cm^2/s, the diameter of the wells would need to be 2.8 cm which is nearly 10 times the size of the wells in this paper.

Together, the simplicity of the design that eliminates solute convection through the gel, the variety of biological systems that can be incorporated into the device, and the adaptability of the device to new designs that can modulate gradient formation create an effective tool for interrogating the behavior of cells within a defined 3D microenvironment and under the influence of a stable concentration gradient.

The 2Dg-Bioreactor enabled the elucidation of the role of Wnt on Shh induction of Nkx2.2. Wnt effectively suppressed Nkx2.2 expression as confirmed by protein and gene analysis as well as by modeling the gene regulatory model. The differential expression of Nkx2.2 and the Nkx2.2-tdtomato reporter suggest that additional, unidentified, regulatory components exist that govern Nkx2.2 expression but are not included in the putative Nkx2.2 enhancer. Identification of these regulatory events will provide mechanistic insight into the observations described here.

The gene regulatory model in which cross-repression between Pax6, Olig2, and Nkx2.2 result in a tri-stable switch generally exhibits stable transitions from Pax6 to Olig2 to Nkx2.2 as the Shh input increases. However, there exist conditions where the transition from Olig2 to Nkx2.2 expression exhibits oscillations. Initially, in

response to an increasing Shh concentration, Olig2 and Nkx2.2 expressions increase and together they inhibit Pax6 expression. Olig2 becomes the most highly expressed gene while Nkx2.2 increases mores slowly. Eventually Nkx2.2 reaches a level capable of inhibiting Olig2 expression, however, upon the elimination of Olig2 expression, Nkx2.2 inhibits Pax6 alone. This creates a transient increase in Pax6 expression which inhibits Nkx2.2 and allows Olig2 expression to increase. Olig2 eliminates Pax6 expression and the pattern continues, oscillating between Olig2 and Nkx2.2 dominance (Panovska-Griffiths, Page et al. 2013), Figure 6.1.

A key step in the evolution of this oscillatory behavior is inhibition of Nkx2.2 by Pax6. There exists evidence to suggest that some or all of this inhibition may be dependent on Pax6 dependent expression of sFRP2 (Lei, Jeong et al. 2006). This soluble Wnt inhibitor could then increase Tcf repression of Nkx2.2. This presents an interesting rationale for the functionally silent role of Wnt as a positive regulator of Nkx2.2. If Pax6 inhibition of Nkx2.2 requires antagonizing an extracellular field of Wnt ligands, a single oscillating cell may not be capable of producing quantities of sFRP2 sufficient to neutralize the Wnt signal, Figure 6.1. Instead, multiple contiguous cells would be required to locally concentrate sFRP2 to the level required to abrogate intracellular Wnt signaling. In the neural tube, prior to Shh production, Pax6 is widely expressed allowing multiple cells to participate in pan-inhibition of Nkx2.2. However, after Pax6 expression has been eliminated in some ventral regions, a few cells at the p3/pMN boundary where Nkx2.2 is just barely induced might lack the coordinated sFRP2 production necessary to re-inhibit Nkx2.2. Further elucidation of this theory may reveal its role in stabilizing Olig2/Nkx2.2 oscillations at the p3/pMN boundary.
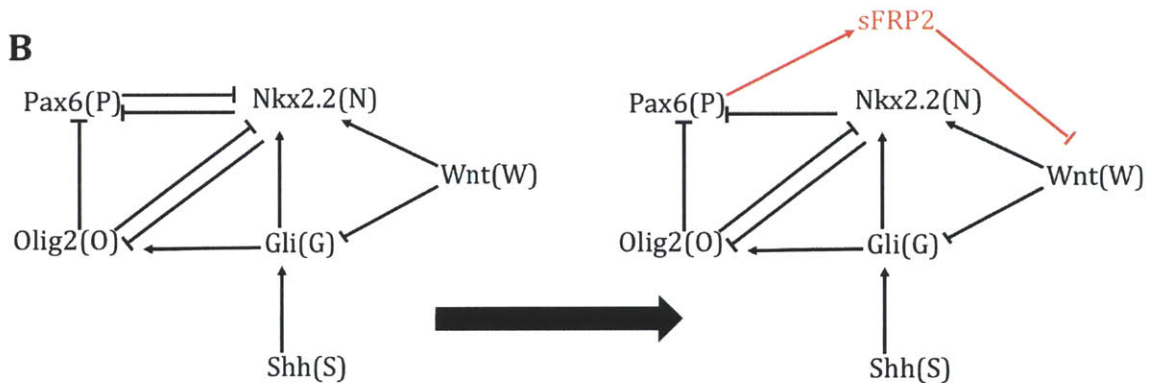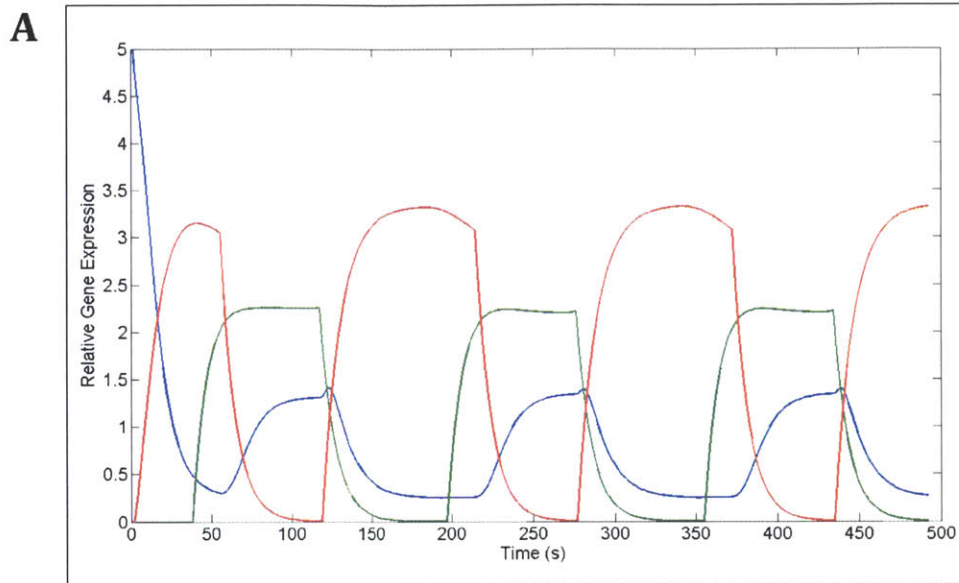
Figure 6.1 – Gene Regulatory Network Instability and sFRP2 Mediated Inhibition of Nkx2.2.

(A) A time delay model in which at intermediate Shh levels, Nkx2.2 (red) induction is periodic alternating a dominant expression pattern with Olig2 (green) as a result of insufficient Pax6 (blue) inhibition. As it is the inhibition of Nkx2.2 by Pax6 that induces Nkx2.2 expression to decline, (B) if this mechanism were dependent on the sFRP2 mediated inhibition of Wnt signaling, the lack of coordinated action between multiple cells might prevent the oscillatory behavior seen in (A).

REFERENCES

Abbott, A. (2003). "Cell culture: Biology's new dimension." Nature **424**(6951): 870-872.

Abhyankar, V. V., M. A. Lokuta, et al. (2006). "Characterization of a membrane-based gradient generator for use in cell-signaling studies." Lab on a Chip **6**(3): 389-393.

Abhyankar, V. V., M. W. Toepke, et al. (2008). "A platform for assessing chemotactic migration within a spatiotemporally defined 3D microenvironment." Lab on a Chip **8**(9): 1507-1515.

Allen, B. L., T. Tenzen, et al. (2007). "The Hedgehog-binding proteins Gas1 and Cdo cooperate to positively regulate Shh signaling during mouse development." Genes Dev **21**(10): 1244-1257.

Amadi, O. C., M. L. Steinhauser, et al. (2010). "A low resistance microfluidic system for the creation of stable concentration gradients in a defined 3D microenvironment." Biomed Microdevices **12**(6): 1027-1041.

Amarie, D., J. A. Glazier, et al. (2007). "Compact Microfluidic Structures for Generating Spatial and Temporal Gradients." Analytical Chemistry **79**(24): 9471-9477.

Ashe, H. L. and J. Briscoe (2006). "The interpretation of morphogen gradients." Development **133**(3): 385-394.

Atencia, J., J. Morrow, et al. (2009). "The microfluidic palette: A diffusive gradient generator with spatio-temporal control." Lab on a Chip **9**(18): 2707-2714.

Babcock, G. T. and M. Wikstrom (1992). "Oxygen activation and the conservation of energy in cell respiration." Nature **356**(6367): 301-309.

Bahat, A. and M. Eisenbach (2006). "Sperm thermotaxis." Molecular and Cellular Endocrinology **252**(1,Äì2): 115-119.

Bahat, A., I. Tur-Kaspa, et al. (2003). "Thermotaxis of mammalian sperm cells: A potential navigation mechanism in the female genital tract." Nat Med **9**(2): 149-150.

Balaskas, N., A. Ribeiro, et al. (2012). "Gene regulatory logic for reading the Sonic Hedgehog signaling gradient in the vertebrate neural tube." Cell **148**(1-2): 273-284.

Baldauf, S. L., A. J. Roger, et al. (2000). "A kingdom-level phylogeny of eukaryotes based on combined protein data." Science **290**(5493): 972-977.

Ben-Zvi, D. and N. Barkai (2010). "Scaling of morphogen gradients by an expansion-repression integral feedback control." Proc Natl Acad Sci U S A **107**(15): 6924-6929.

Ben-Zvi, D., B. Z. Shilo, et al. (2008). "Scaling of the BMP activation gradient in Xenopus embryos." Nature **453**(7199): 1205-1211.

Benazet, J. D. and R. Zeller (2009). "Vertebrate limb development: moving from classical morphogen gradients to an integrated 4-dimensional patterning system." Cold Spring Harb Perspect Biol **1**(4): a001339.

Berg, H. C. (1988). "A Physicist Looks at Bacterial Chemotaxis." Cold Spring Harbor Symposia on Quantitative Biology **53**: 1-9.

Biddiss, E. and D. Li (2005). "Electrokinetic generation of temporally and spatially stable concentration gradients in microchannels." Journal of Colloid and Interface Science **288**(2): 606-615.

Bonner, J. T., W. W. Clarke, et al. (1950). "The orientation to light and the extermely sensitive orientation to temperature gradients in the slime mold Dictyostelium discoideum." Journal of Cellular and Comparative Physiology **36**(2): 149-158.

Bornfeldt KE, R. E., Nakano T, Graves LM, Krebs EG, and Ross R (1994). "Insulin-like growth factor-I and platelet-derived growth factor-BB induce directed migration of human arterial smooth muscle cells via signaling pathways that are distinct from those of proliferation." Journal of Clinical Investigations **93**(3): 1266-1274.

Boyden, S. (1962). "The chemotactic effect of mixtures of antibody and antigen on polymorphonuclear leucocytes." J Exp Med **113**(3): 453-466.

Brett, M. E., R. DeFlorio, et al. (2012). "A microfluidic device that forms and redirects pheromone gradients to study chemotropism in yeast." Lab Chip **12**(17): 3127-3134.

Capers, C. R. (1960). "Multinucleation of skeletal muscle in vitro." J Biophys Biochem Cytol **7**: 559-566.

Chamberlain, C. E., J. Jeong, et al. (2008). "Notochord-derived Shh concentrates in close association with the apically positioned basal body in neural target cells and forms a dynamic gradient during neural patterning." Development **135**(6): 1097-1106.

Chen, M. H., Y. J. Li, et al. (2004). "Palmitoylation is required for the production of a soluble multimeric Hedgehog protein complex and long-range signaling in vertebrates." Genes Dev **18**(6): 641-659.

Chen, Y. and A. F. Schier (2002). "Lefty proteins are long-range inhibitors of squint-mediated nodal signaling." Curr Biol **12**(24): 2124-2128.

Cheng JY, Yen MH, et al. (2008). "A transparent cell-culture microchamber with a variably controlled concentration gradient generator and flow field rectifier." Biomicrofluidics **2**(2): 24105.

Cheng, S.-Y., S. Heilman, et al. (2007). "A hydrogel-based microfluidic device for the studies of directed cell migration." Lab on a Chip **7**(6): 763-769.

Chung, B. G., L. A. Flanagan, et al. (2005). "Human neural stem cell growth and differentiation in a gradient-generating microfluidic device." Lab on a Chip **5**(4): 401-406.

Chung, B. G., F. Lin, et al. (2006). "A microfluidic multi-injector for gradient generation." Lab on a Chip **6**(6): 764-768.

Chung, S., R. Sudo, et al. (2009). "Cell migration into scaffolds under co-culture conditions in a microfluidic platform." Lab on a Chip **9**(2): 269-275.

Cooksey, G. A., C. G. Sip, et al. (2009). "A multi-purpose microfluidic perfusion system with combinatorial choice of inputs, mixtures, gradient patterns, and flow rates." Lab on a Chip **9**(3): 417-426.

Crick, F. (1970). "Diffusion in embryogenesis." Nature **225**(5231): 420-422.

Cukierman, E., R. Pankov, et al. (2001). "Taking Cell-Matrix Adhesions to the Third Dimension." Science 294(5547): 1708-1712.

Dai, P., H. Akimaru, et al. (1999). "Sonic Hedgehog-induced activation of the Gli1 promoter is mediated by GLI3." J Biol Chem 274(12): 8143-8152.

Dessaud, E., A. P. McMahon, et al. (2008). "Pattern formation in the vertebrate neural tube: a sonic hedgehog morphogen-regulated transcriptional network." Development 135(15): 2489-2503.

Dessaud, E., L. L. Yang, et al. (2007). "Interpretation of the sonic hedgehog morphogen gradient by a temporal adaptation mechanism." Nature 450(7170): 717-720.

Dessaud, E., L. L. Yang, et al. (2007). "Interpretation of the sonic hedgehog morphogen gradient by a temporal adaptation mechanism." Nature 450(7170): 717-720.

Diao, J., L. Young, et al. (2006). "A three-channel microfluidic device for generating static linear gradients and its application to the quantitative analysis of bacterial chemotaxis." Lab on a Chip 6(3): 381-388.

Driever, W. and C. Nusslein-Volhard (1988). "The bicoid protein determines position in the Drosophila embryo in a concentration-dependent manner." Cell 54(1): 95-104.

Driever, W. and C. Nusslein-Volhard (1988). "A gradient of bicoid protein in Drosophila embryos." Cell 54(1): 83-93.

Driever, W., G. Thoma, et al. (1989). "Determination of spatial domains of zygotic gene expression in the Drosophila embryo by the affinity of binding sites for the bicoid morphogen." Nature 340(6232): 363-367.

Du, Y., J. Shim, et al. (2009). "Rapid generation of spatially and temporally controllable long-range concentration gradients in a microfluidic device." Lab on a Chip 9(6): 761-767.

Dubrulle, J. and O. Pourquie (2004). "fgf8 mRNA decay establishes a gradient that couples axial elongation to patterning in the vertebrate embryo." Nature 427(6973): 419-422.

Dyson, S. and J. B. Gurdon (1998). "The interpretation of position in a morphogen gradient as revealed by occupancy of activin receptors." Cell 93(4): 557-568.

Eaton, S. (2008). "Multiple roles for lipids in the Hedgehog signalling pathway." Nat Rev Mol Cell Biol 9(6): 437-445.

Echelard, Y., D. J. Epstein, et al. (1993). "Sonic hedgehog, a member of a family of putative signaling molecules, is implicated in the regulation of CNS polarity." Cell 75(7): 1417-1430.

Eldar, A., R. Dorfman, et al. (2002). "Robustness of the BMP morphogen gradient in Drosophila embryonic patterning." Nature 419(6904): 304-308.

Elsdale, T. and J. Bard (1972). "COLLAGEN SUBSTRATA FOR STUDIES ON CELL BEHAVIOR." The Journal of Cell Biology 54(3): 626-637.

Englert, D. L., M. D. Manson, et al. (2009). "Flow-Based Microfluidic Device for Quantifying Bacterial Chemotaxis in Stable, Competing Gradients." Appl. Environ. Microbiol. 75(13): 4557-4564.

Entchev, E. V., A. Schwabedissen, et al. (2000). "Gradient formation of the TGF-beta homolog Dpp." Cell 103(6): 981-991.

Even-Ram, S. and K. M. Yamada (2005). "Cell migration in 3D matrix." Current Opinion in Cell Biology 17(5): 524-532.

Fabiato, A. (1983). "Calcium-induced release of calcium from the cardiac sarcoplasmic reticulum." American Journal of Physiology - Cell Physiology 245(1): C1-C14.

Ferguson, E. L. and K. V. Anderson (1992). "Decapentaplegic acts as a morphogen to organize dorsal-ventral pattern in the Drosophila embryo." Cell 71(3): 451-461.

Fok, S., P. Domachuk, et al. (2008). "Planar Microfluidic Chamber for Generation of Stable and Steep Chemoattractant Gradients." Biophysical Journal 95(3): 1523-1530.

Frank-Kamenetsky, M., X. M. Zhang, et al. (2002). "Small-molecule modulators of Hedgehog signaling: identification and characterization of Smoothened agonists and antagonists." J Biol 1(2): 10.

Frevert, C. W., G. Boggy, et al. (2006). "Measurement of cell migration in response to an evolving radial chemokine gradient triggered by a microvalve." Lab on a Chip 6(7): 849-856.

Friedl, P. and D. Gilmour (2009). "Collective cell migration in morphogenesis, regeneration and cancer." Nat Rev Mol Cell Biol 10(7): 445-457.

Friedl, P., E. Sahai, et al. (2012). "New dimensions in cell migration." Nat Rev Mol Cell Biol 13(11): 743-747.

Friedl, P. and B. Weigelin (2008). "Interstitial leukocyte migration and immune function." Nat Immunol 9(9): 960-969.

Gabriel, G. M. and K. John (2006). "Endothelial cell protrusion and migration in three-dimensional collagen matrices." Cell Motility and the Cytoskeleton 63(2): 101-115.

Gallet, A., L. Ruel, et al. (2006). "Cholesterol modification is necessary for controlled planar long-range activity of Hedgehog in Drosophila epithelia." Development 133(3): 407-418.

Garanich, J. S., M. Pahakis, et al. (2005). "Shear stress inhibits smooth muscle cell migration via nitric oxide-mediated downregulation of matrix metalloproteinase-2 activity." Am J Physiol Heart Circ Physiol 288(5): H2244-2252.

Ghibaudo, M., L. Trichet, et al. (2009). "Substrate Topography Induces a Crossover from 2D to 3D Behavior in Fibroblast Migration." Biophysical Journal 97(1): 357-368.

Gilbert, S. (2000). Developmental Biology. Sunderland, MA, Sinauer Associates.

Glawdel, T., C. Elbuken, et al. (2009). "Microfluidic system with integrated electroosmotic pumps, concentration gradient generator and fish cell line (RTgill-W1)-towards water toxicity testing." Lab on a Chip 9(22): 3243-3250.

Grinnell, F. and W. M. Petroll (2010). "Cell Motility and Mechanics in Three-Dimensional Collagen Matrices." Annual Review of Cell and Developmental Biology 26(1): 335-361.

Haessler, U., Y. Kalinin, et al. (2009). "An agarose-based microfluidic platform with a gradient buffer for 3D chemotaxis studies." Biomedical Microdevices 11(4): 827-835.

Hai-Qing, X., M. Elizabeth, et al. (2003). "A Subset of ES-Cell-Derived Neural Cells Marked by Gene Targeting." Stem Cells 21(1): 41-49.

Harunaga, J. S. and K. M. Yamada (2011). "Cell-matrix adhesions in 3D." Matrix Biol 30(7-8): 363-368.

Hattori, K., S. Sugiura, et al. (2009). "Generation of arbitrary monotonic concentration profiles by a serial dilution microfluidic network composed of microchannels with a high fluidic-resistance ratio." Lab on a Chip 9(12): 1763-1772.

He, J., Y. Du, et al. (2010). "Rapid generation of biologically relevant hydrogels containing long-range chemical gradients." Adv. Funct. Mater 20(1): 131-137.

Hedgecock, E. M. and R. L. Russell (1975). "Normal and mutant thermotaxis in the nematode Caenorhabditis elegans." Proceedings of the National Academy of Sciences 72(10): 4061-4065.

Herzmark, P., K. Campbell, et al. (2007). "Bound attractant at the leading vs. the trailing edge determines chemotactic prowess." PNAS 104(33): 13349-13354.

Hesselgesser, J., M. Liang, et al. (1998). "Identification and Characterization of the CXCR4 Chemokine Receptor in Human T Cell Lines: Ligand Binding, Biological Activity, and HIV-1 Infectivity." J Immunol 160(2): 877-883.

Hodgkin, A. L. and A. F. Huxley (1952). "A quantitative description of membrane current and its application to conduction and excitation in nerve." The Journal of Physiology 117(4): 500-544.

Huang, Y. E., M. Iijima, et al. (2003). "Receptor-mediated regulation of PI3Ks confines PI(3,4,5)P3 to the leading edge of chemotaxing cells." Mol Biol Cell 14(5): 1913-1922.

Humphries, J. D., A. Byron, et al. (2006). "Integrin ligands at a glance." Journal of Cell Science 119(19): 3901-3903.

Hynes, M., W. Ye, et al. (2000). "The seven-transmembrane receptor smoothened cell-autonomously induces multiple ventral cell types." Nat Neurosci 3(1): 41-46.

Incardona, J. P., J. Gruenberg, et al. (2002). "Sonic hedgehog induces the segregation of patched and smoothened in endosomes." Curr Biol 12(12): 983-995.

Incardona, J. P., J. H. Lee, et al. (2000). "Receptor-mediated endocytosis of soluble and membrane-tethered Sonic hedgehog by Patched-1." Proc Natl Acad Sci U S A 97(22): 12044-12049.

Irimia, D., D. A. Geba, et al. (2006). "Universal Microfluidic Gradient Generator." Analytical Chemistry 78(10): 3472-3477.

Jacob, J. and J. Briscoe (2003). "Gli proteins and the control of spinal-cord patterning." EMBO Rep 4(8): 761-765.

Jacob, J. and J. Briscoe (2003). "Gli proteins and the control of spinal-cord patterning." EMBO Rep. 4(8): 761-765.

Jeon, H., Y. Lee, et al. (2009). "Quantitative analysis of single bacterial chemotaxis using a linear concentration gradient microchannel." Biomedical Microdevices 11(5): 1135-1143.

Jeong, J. and A. P. McMahon (2005). "Growth and pattern of the mammalian neural tube are governed by partially overlapping feedback activities of the hedgehog antagonists patched 1 and Hhip1." Development 132(1): 143-154.

Jessell, T. M. (2000). "Neuronal specification in the spinal cord: inductive signals and transcriptional codes." Nat Rev Genet 1(1): 20-29.

Joong Yull, P., K. Suel-Kee, et al. (2009). "Differentiation of Neural Progenitor Cells in a Microfluidic Chip-Generated Cytokine Gradient." Stem Cells 27(11): 2646-2654.

Kalinin, Y. V., L. Jiang, et al. (2009). "Logarithmic Sensing in Escherichia coli Bacterial Chemotaxis." Biophysical Journal 96(6): 2439-2448.

Kang, T., J. Han, et al. (2008). "Concentration gradient generator using a convective-diffusive balance." Lab on a Chip 8(7): 1220-1222.

Keenan, T. M. and A. Folch (2008). "Biomolecular gradients in cell culture systems." Lab on a Chip 8(1): 34-57.

Keenan, T. M. and A. Folch (2008). "Biomolecular gradients in cell culture systems." Lab Chip 8(1): 34-57.

Kessler, J. O., L. F. Jarvik, et al. (1979). "Thermotaxis, chemotaxis and age." AGE 2(1): 5-11.

Kicheva, A., P. Pantazis, et al. (2007). "Kinetics of morphogen gradient formation." Science 315(5811): 521-525.

Kim, D., M. A. Lokuta, et al. (2009). "Selective and tunable gradient device for cell culture and chemotaxis study." Lab on a Chip 9(12): 1797-1800.

Kim, T., M. Pinelis, et al. (2009). "Generating steep, shear-free gradients of small molecules for cell culture." Biomedical Microdevices 11(1): 65-73.

Laird, D. J., U. H. von Andrian, et al. (2008). "Stem Cell Trafficking in Tissue Development,†Growth, and Disease." 132(4): 612-630.

Lauffenburger, D. A. and A. F. Horwitz (1996). "Cell Migration: A Physically Integrated Molecular Process." Cell 84(3): 359-369.

Lecuit, T., W. J. Brook, et al. (1996). "Two distinct mechanisms for long-range patterning by Decapentaplegic in the Drosophila wing." Nature 381(6581): 387-393.

Lee, J., M. J. Cuddihy, et al. (2008). "Three-Dimensional Cell Culture Matrices: State of the Art." Tissue Engineering Part B: Reviews 14(1): 61-86.

Lei, Q., Y. Jeong, et al. (2006). "Wnt signaling inhibitors regulate the transcriptional response to morphogenetic Shh-Gli signaling in the neural tube." Dev Cell 11(3): 325-337.

Lek, M., J. M. Dias, et al. (2010). "A homeodomain feedback circuit underlies step-function interpretation of a Shh morphogen gradient during ventral neural patterning." Development 137(23): 4051-4060.

Li, C.-W., R. Chen, et al. (2007). "Generation of linear and non-linear concentration gradients along microfluidic channel by microtunnel controlled stepwise addition of sample solution." Lab on a Chip 7(10): 1371-1373.

Li, G., J. Liu, et al. (2008). "Multi-Molecular Gradients of Permissive and Inhibitory Cues Direct Neurite Outgrowth." Annals of Biomedical Engineering 36(6): 889-904.

Li Jeon, N., H. Baskaran, et al. (2002). "Neutrophil chemotaxis in linear and complex gradients of interleukin-8 formed in a microfabricated device." Nat Biotech **20**(8): 826-830.

Lin, F. and E. C. Butcher (2006). "T cell chemotaxis in a simple microfluidic device." Lab Chip **6**(11): 1462-1469.

Lin, F. and E. C. Butcher (2006). "T-cell chemotaxis in a simple microfluidic device." Lab on a Chip **6**(11): 1462-1469.

Lin, F. and E. C. Butcher (2006). "T†cell chemotaxis in a simple microfluidic device." Lab on a Chip **6**(11): 1462-1469.

Lin, F., W. Saadi, et al. (2004). "Generation of dynamic temporal and spatial concentration gradients using microfluidic devices." Lab on a Chip **4**(3): 164-167.

Liu, A. and L. A. Niswander (2005). "Bone morphogenetic protein signalling and vertebrate nervous system development." Nat Rev Neurosci **6**(12): 945-954.

Liu, Y., J. Sai, et al. (2008). "Microfluidic switching system for analyzing chemotaxis responses of wortmannin-inhibited HL-60 cells." Biomedical Microdevices **10**(4): 499-507.

Mack, P. J., Y. Zhang, et al. (2009). "Biomechanical Regulation of Endothelium-dependent Events Critical for Adaptive Remodeling." J. Biol. Chem. **284**(13): 8412-8420.

Maeda, K., Y. Imae, et al. (1976). "Effect of temperature on motility and chemotaxis of Escherichia coli." Journal of Bacteriology **127**(3): 1039-1046.

Mao, H., P. S. Cremer, et al. (2003). "A sensitive, versatile microfluidic assay for bacterial chemotaxis." Proceedings of the National Academy of Sciences of the United States of America **100**(9): 5449-5454.

Marti, E., D. A. Bumcrot, et al. (1995). "Requirement of 19K form of Sonic hedgehog for induction of distinct ventral cell types in CNS explants." Nature **375**(6529): 322-325.

Matise, M. P. and A. L. Joyner (1999). "Gli genes in development and cancer." Oncogene **18**(55): 7852-7859.

Mercader, N., E. Leonardo, et al. (2000). "Opposing RA and FGF signals control proximodistal vertebrate limb development through regulation of Meis genes." Development **127**(18): 3961-3970.

Meyer, N. P. and H. Roelink (2003). "The amino-terminal region of Gli3 antagonizes the Shh response and acts in dorsoventral fate specification in the developing spinal cord." Dev Biol **257**(2): 343-355.

Miller, R. J., G. Banisadr, et al. (2008). "CXCR4 signaling in the regulation of stem cell migration and development." J Neuroimmunol **198**(1-2): 31-38.

Mizuno, T., K. Kawasaki, et al. (1992). "Construction of a thermotaxis chamber providing spatial or temporal thermal gradients monitored by an infrared video camera system." Analytical Biochemistry **207**(2): 208-213.

Montero, J.-A. and C.-P. Heisenberg (2004). "Gastrulation dynamics: cells move into focus." Trends in Cell Biology **14**(11): 620-627.

Mosadegh, B., C. Huang, et al. (2007). "Generation of Stable Complex Gradients Across Two-Dimensional Surfaces and Three-Dimensional Gels." Langmuir **23**(22): 10910-10912.

Motoo, K., N. Toda, et al. (2008). "Generation of concentration gradient from a wave-like pattern by high frequency vibration of liquid–liquid interface." Biomedical Microdevices **10**(3): 329-335.

Murone, M., A. Rosenthal, et al. (1999). "Sonic hedgehog signaling by the patched-smoothened receptor complex." Curr Biol **9**(2): 76-84.

Namba, R., T. M. Pazdera, et al. (1997). "Drosophila embryonic pattern repair: how embryos respond to bicoid dosage alteration." Development **124**(7): 1393-1403.

Nelson, R. D., P. G. Quie, et al. (1975). "Chemotaxis Under Agarose: A New and Simple Method for Measuring Chemotaxis and Spontaneous Migration of Human Polymorphonuclear Leukocytes and Monocytes." J Immunol **115**(6): 1650-1656.

Niswander, L., C. Tickle, et al. (1993). "FGF-4 replaces the apical ectodermal ridge and directs outgrowth and patterning of the limb." Cell **75**(3): 579-587.

O'Hayre, M., C. L. Salanga, et al. (2008). "Chemokines and cancer: migration, intracellular signalling and intercellular communication in the microenvironment." Biochem J **409**(3): 635-649.

Palecek, S. P., J. C. Loftus, et al. (1997). "Integrin-ligand binding properties govern cell migration speed through cell-substratum adhesiveness." Nature **385**(6616): 537-540.

Pan, Y., C. B. Bai, et al. (2006). "Sonic hedgehog signaling regulates Gli2 transcriptional activity by suppressing its processing and degradation." Mol Cell Biol **26**(9): 3365-3377.

Panovska-Griffiths, J., K. M. Page, et al. (2013). "A gene regulatory motif that generates oscillatory or multiway switch outputs." J R Soc Interface **10**(79): 20120826.

Parent, C. A. and P. N. Devreotes (1999). "A Cell's Sense of Direction." Science **284**(5415): 765-770.

Park, J. Y., C. M. Hwang, et al. (2007). "Gradient generation by an osmotic pump and the behavior of human mesenchymal stem cells under the fetal bovine serum concentration gradient." Lab on a Chip **7**(12): 1673-1680.

Park, J. Y., S.-K. Kim, et al. (2009). "Differentiation of Neural Progenitor Cells in a Microfluidic Chip-Generated Cytokine Gradient." STEM CELLS **27**(11): 2646-2654.

Park, J. Y., S. J. Yoo, et al. (2009). "Simultaneous generation of chemical concentration and mechanical shear stress gradients using microfluidic osmotic flow comparable to interstitial flow." Lab on a Chip **9**(15): 2194-2202.

Pasut, A., A. E. Jones, et al. (2013). "Isolation and culture of individual myofibers and their satellite cells from adult skeletal muscle." J Vis Exp(73): e50074.

Pepinsky, R. B., C. Zeng, et al. (1998). "Identification of a palmitic acid-modified form of human Sonic hedgehog." J Biol Chem **273**(22): 14037-14045.

Persson, M., D. Stamataki, et al. (2002). "Dorsal-ventral patterning of the spinal cord requires Gli3 transcriptional repressor activity." Genes & Development **16**(22): 2865-2878.

Persson, M., D. Stamataki, et al. (2002). "Dorsal-ventral patterning of the spinal cord requires Gli3 transcriptional repressor activity." Genes Dev 16(22): 2865-2878.

Petrie, R. J., N. Gavara, et al. (2012). "Nonpolarized signaling reveals two distinct modes of 3D cell migration." J Cell Biol 197(3): 439-455.

Porter, J. A., K. E. Young, et al. (1996). "Cholesterol modification of hedgehog signaling proteins in animal development." Science 274(5285): 255-259.

Proudfoot, D. and C. Shanahan (2012). "Human vascular smooth muscle cell culture." Methods Mol Biol 806: 251-263.

Ratajczak, M. Z., M. Majka, et al. (2003). "Expression of Functional CXCR4 by Muscle Satellite Cells and Secretion of SDF-1 by Muscle-Derived Fibroblasts is Associated with the Presence of Both Muscle Progenitors in Bone Marrow and Hematopoietic Stem/Progenitor Cells in Muscles." STEM CELLS 21(3): 363-371.

Ribes, V. and J. Briscoe (2009). "Establishing and interpreting graded Sonic Hedgehog signaling during vertebrate neural tube patterning: the role of negative feedback." Cold Spring Harb Perspect Biol 1(2): a002014.

Riddle, R. D., R. L. Johnson, et al. (1993). "Sonic hedgehog mediates the polarizing activity of the ZPA." Cell 75(7): 1401-1416.

Roelink, H., J. A. Porter, et al. (1995). "Floor plate and motor neuron induction by different concentrations of the amino-terminal cleavage product of sonic hedgehog autoproteolysis." Cell 81(3): 445-455.

Rogers, K. W. and A. F. Schier (2011). "Morphogen Gradients: From Generation to Interpretation." Annual Review of Cell and Developmental Biology 27(1): 377-407.

Roth, S., D. Stein, et al. (1989). "A gradient of nuclear localization of the dorsal protein determines dorsoventral pattern in the Drosophila embryo." Cell 59(6): 1189-1202.

Rubin, J. B., Y. Choi, et al. (2002). "Cerebellar proteoglycans regulate sonic hedgehog responses during development." Development 129(9): 2223-2232.

Saadi, W., S. Rhee, et al. (2007). "Generation of stable concentration gradients in 2D and 3D environments using a microfluidic ladder chamber." Biomedical Microdevices 9(5): 627-635.

Saadi, W., S.-J. Wang, et al. (2006). "A parallel-gradient microfluidic chamber for quantitative analysis of breast cancer cell chemotaxis." Biomedical Microdevices 8(2): 109-118.

Schneider, I. C. and J. M. Haugh (2006). "Mechanisms of gradient sensing and chemotaxis: conserved pathways, diverse regulation." Cell Cycle 5(11): 1130-1134.

Shamloo, A., N. Ma, et al. (2008). "Endothelial cell polarization and chemotaxis in a microfluidic device." Lab on a Chip 8(8): 1292-1299.

Shimizu, K. and J. B. Gurdon (1999). "A quantitative analysis of signal transduction from activin receptor to nucleus and its relevance to morphogen gradient interpretation." Proc Natl Acad Sci U S A 96(12): 6791-6796.

Siyan, W., Y. Feng, et al. (2009). "Application of microfluidic gradient chip in the analysis of lung cancer chemotherapy resistance." Journal of Pharmaceutical and Biomedical Analysis **49**(3): 806-810.

Smalley, K. S. M., M. Lioni, et al. (2006). "LIFE ISN'T FLAT: TAKING CANCER BIOLOGY TO THE NEXT DIMENSION." In Vitro Cellular & Developmental Biology - Animal **42**(8): 242-247.

Smalley, K. S. M., M. Lioni, et al. (2006). "Life isn't flat: taking cancer biology to the next dimension." In Vitro Cellular & Developmental Biology - Animal **42**(8 & 9): 242-247.

Stamataki, D., F. Ulloa, et al. (2005). "A gradient of Gli activity mediates graded Sonic Hedgehog signaling in the neural tube." Genes & Development **19**(5): 626-641.

Stamataki, D., F. Ulloa, et al. (2005). "A gradient of Gli activity mediates graded Sonic Hedgehog signaling in the neural tube." Genes Dev **19**(5): 626-641.

Standley, H. J., A. M. Zorn, et al. (2001). "eFGF and its mode of action in the community effect during Xenopus myogenesis." Development **128**(8): 1347-1357.

Steimle, P. A., S. Yumura, et al. (2001). "Recruitment of a myosin heavy chain kinase to actin-rich protrusions in Dictyostelium." Curr Biol **11**(9): 708-713.

Sudo, R., S. Chung, et al. (2009). "Transport-mediated angiogenesis in 3D epithelial coculture." FASEB J. **23**(7): 2155-2164.

Sun, K., Z. Wang, et al. (2008). "Modular microfluidics for gradient generation." Lab on a Chip **8**(9): 1536-1543.

Sun, S., J. Wise, et al. (2004). "Human Fibroblast Migration in Three-Dimensional Collagen Gel in Response to Noninvasive Electrical Stimulus. I. Characterization of Induced Three-Dimensional Cell Movement." Tissue Engineering **10**(9-10): 1548-1557.

Sun, T., H. Dong, et al. (2003). "Cross-repressive interaction of the Olig2 and Nkx2.2 transcription factors in developing neural tube associated with formation of a specific physical complex." J Neurosci **23**(29): 9547-9556.

Swaney, K. F., C.-H. Huang, et al. (2010). "Eukaryotic Chemotaxis: A Network of Signaling Pathways Controls Motility, Directional Sensing, and Polarity." Annual Review of Biophysics **39**(1): 265-289.

Tabebordbar, M., E. T. Wang, et al. (2013). "Skeletal Muscle Degenerative Diseases and Strategies for Therapeutic Muscle Repair." Annual Review of Pathology: Mechanisms of Disease **8**(1): 441-475.

Tenzen, T., B. L. Allen, et al. (2006). "The cell surface membrane proteins Cdo and Boc are components and targets of the Hedgehog signaling pathway and feedback network in mice." Dev Cell **10**(5): 647-656.

Tingjiao, L., L. Chunyu, et al. (2009). "A microfluidic device for characterizing the invasion of cancer cells in 3-D matrix." ELECTROPHORESIS **30**(24): 4285-4291.

Tsuda, M., K. Kamimura, et al. (1999). "The cell-surface proteoglycan Dally regulates Wingless signalling in Drosophila." Nature **400**(6741): 276-280.

Ulloa, F. and E. Marti (2010). "Wnt won the war: antagonistic role of Wnt over Shh controls dorso-ventral patterning of the vertebrate neural tube." Dev Dyn 239(1): 69-76.

Ulloa, F. and E. Martì (2010). "Wnt won the war: Antagonistic role of Wnt over Shh controls dorso-ventral patterning of the vertebrate neural tube." Developmental Dynamics 239(1): 69-76.

Van Haastert, P. J. M. and P. N. Devreotes (2004). "Chemotaxis: signalling the way forward." Nat Rev Mol Cell Biol 5(8): 626-634.

Veldkamp, C. T., C. Seibert, et al. (2008). "Structural Basis of CXCR4 Sulfotyrosine Recognition by the Chemokine SDF-1/CXCL12." Sci. Signal. 1(37): ra4-.

Vernon, R. B. and E. H. Sage (1999). "A Novel, Quantitative Model for Study of Endothelial Cell Migration and Sprout Formation within Three-Dimensional Collagen Matrices." Microvascular Research 57(2): 118-133.

Vickerman, V., J. Blundo, et al. (2008). "Design, fabrication and implementation of a novel multi-parameter control microfluidic platform for three-dimensional cell culture and real-time imaging." Lab on a Chip 8(9): 1468-1477.

Vokes SA, M. S. Ji H, et al. (2007). "Genomic characterization of Gli-activator targets in sonic hedgehog-mediated neural patterning." Development 134: 1977-1989.

Vokes, S. A., H. Ji, et al. (2007). "Genomic characterization of Gli-activator targets in sonic hedgehog-mediated neural patterning." Development 134(10): 1977-1989.

Vyas, N., D. Goswami, et al. (2008). "Nanoscale organization of hedgehog is essential for long-range signaling." Cell 133(7): 1214-1227.

Wallingford, J. B., L. A. Niswander, et al. (2013). "The Continuing Challenge of Understanding, Preventing, and Treating Neural Tube Defects." Science 339(6123).

Wang, H., Q. Lei, et al. (2011). "Tcf/Lef repressors differentially regulate Shh-Gli target gene activation thresholds to generate progenitor patterning in the developing CNS." Development 138(17): 3711-3721.

Wang, P. H., D. Moller, et al. (1989). "Coordinate regulation of glucose transporter function, number, and gene expression by insulin and sulfonylureas in L6 rat skeletal muscle cells." The Journal of Clinical Investigation 84(1): 62-67.

Wang, S. and J. M. Tarbell (2000). "Effect of Fluid Flow on Smooth Muscle Cells in a 3-Dimensional Collagen Gel Model." Arterioscler Thromb Vasc Biol 20(10): 2220-2225.

White, R. J., Q. Nie, et al. (2007). "Complex regulation of cyp26a1 creates a robust retinoic acid gradient in the zebrafish embryo." PLoS Biol 5(11): e304.

Wijgerde, M., J. A. McMahon, et al. (2002). "A direct requirement for Hedgehog signaling for normal specification of all ventral progenitor domains in the presumptive mammalian spinal cord." Genes Dev 16(22): 2849-2864.

Wolpert, L. (1969). "Positional information and the spatial pattern of cellular differentiation." J Theor Biol 25(1): 1-47.

Wu, H., B. Huang, et al. (2006). "Generation of Complex, Static Solution Gradients in Microfluidic Channels." Journal of the American Chemical Society 128(13): 4194-4195.

Xu, J., F. Wang, et al. (2003). "Divergent signals and cytoskeletal assemblies regulate self-organizing polarity in neutrophils." Cell **114**(2): 201-214.

Yan, D. and X. Lin (2009). "Shaping morphogen gradients by proteoglycans." Cold Spring Harb Perspect Biol **1**(3): a002493.

Yang, J., X. Pi, et al. (2007). "Diffusion Characteristics of a T-type Microchannel with Different Configurations and Inlet Angles." Analytical Sciences **23**(6): 697-703.

Yu, S. R., M. Burkhardt, et al. (2009). "Fgf8 morphogen gradient forms by a source-sink mechanism with freely diffusing molecules." Nature **461**(7263): 533-536.

Yusuf, H. A., S. J. Baldock, et al. (2009). "Optimisation and analysis of microreactor designs for microfluidic gradient generation using a purpose built optical detection system for entire chip imaging." Lab on a Chip **9**(13): 1882-1889.

Zaman, M. H., R. D. Kamm, et al. (2005). "Computational Model for Cell Migration in Three-Dimensional Matrices." Biophysical Journal **89**(2): 1389-1397.

Zaman, M. H., L. M. Trapani, et al. (2006). "Migration of tumor cells in 3D matrices is governed by matrix stiffness along with cell-matrix adhesion and proteolysis." Proceedings of the National Academy of Sciences **103**(29): 10889-10894.

Zervantonakis, I., S. Chung, et al. (2010). "Concentration gradients in microfluidic 3D matrix cell culture systems." International Journal of Micro-Nano Scale Transport **1**(1): 27-36.

Zhang, S., P. G. Charest, et al. (2008). "Spatiotemporal regulation of Ras activity provides directional sensing." Curr Biol **18**(20): 1587-1593.

Zhang, S., F. V. W. George, et al. (2008). Designer Self-Assembling Peptide Nanofiber Scaffolds for Study of 3-D Cell Biology and Beyond. Advances in Cancer Research, Academic Press. **Volume 99:** 335-362.

Zhou, Y., Y. Wang, et al. (2009). "Generation of complex concentration profiles by partial diffusive mixing in multi-stream laminar flow." Lab on a Chip **9**(10): 1439-1448.

Zhu, X., L. Y. Chu, et al. (2004). "Arrays of horizontally-oriented mini-reservoirs generate steady microfluidic flows for continuous perfusion cell culture and gradient generation." The Analyst **129**(11): 1026-1031.

Zicha, D., G. A. Dunn, et al. (1991). "A new direct-viewing chemotaxis chamber." J Cell Sci **99**(4): 769-775.

Zigmond, S. H. (1977). "Ability of polymorphonuclear leukocytes to orient in gradients of chemotactic factors." J. Cell Biol. **75**(2): 606-616.